THERMOBAROMETRY, $^{40}Ar/^{39}Ar$ GEOCHRONOLOGY, AND STRUCTURE OF THE MAIN CENTRAL THRUST ZONE AND TIBETAN SLAB, EASTERN NEPAL HIMALAYA

by

MARY SYNDONIA HUBBARD

B.A. University of Colorado, Boulder
(1981)

Submitted to the Department of
Earth, Atmospheric and Planetary Sciences
in Partial Fulfillment of the Requirements
for the Degree of

DOCTOR OF PHILOSOPHY

at the

MASSACHUSETTS INSTITUTE OF TECHNOLOGY

September 1988

Signature of Author_____
Department of Earth, Atmospheric and
Planetary Sciences, June 28, 1988

Certified by_____
Kip Hodges
Thesis Supervisor

Accepted by_____
William Brace
Chairman, Departmental Committee

THERMOBAROMETRY, $^{40}Ar/^{39}Ar$ GEOCHRONOLOGY, AND STRUCTURE OF THE MAIN CENTRAL THRUST ZONE AND TIBETAN SLAB, EASTERN NEPAL HIMALAYA

by

Mary Syndonia Hubbard

Submitted to the Department of Earth, Atmospheric , and Planetary Sciences
in partial fulfillment of the requirements for the
Degree of Doctor of Philosophy
June, 1988

ABSTRACT

The Main Central Thrust (MCT) is a major north-dipping intraplate subduction zone which parallels the trend of the Himalaya and separates unmetamorphosed to medium-grade rocks of the physiographic Lesser Himalaya from the overlying high-grade rocks of the Tibetan Slab. The MCT has been studied in different parts of the Himalaya (e.g. Heim and Gansser, 1939; LeFort, 1975, 1981; Pêcher, 1978; Valdiya, 1980; Arita, 1983) and though the timing of this structure has been uncertain and there has been some disagreement as to the structural nature and exact location of the MCT, there is one feature that has been recognized by all workers: the association of the MCT and an inverted sequence of metamorphic isograds where the apparently higher grade rocks appear at structurally higher levels. This study was aimed at characterizing the structural style and location of the MCT in a region south of Mt. Everest in eastern Nepal and obtaining thermobarometric and geochronologic data in order to constrain the timing and thermal effects of this major structure.

In the area surrounding the Dudh Kosi, Hinku, and Hongu drainages in eastern Nepal the MCT is a north-dipping, 3-5 km-thick shear zone. The zone consists of a sequence of augen gneiss, marble, amphibolite, psammitic schist, and pelitic schist. Throughout the zone high strain is concentrated along bands that are parallel to the dominant schistosity, lithologic contacts, and the metamorphic isograds.

Samples with assemblages suitable for the application of the garnet-

biotite geothermometer (Ferry and Spear, 1978) and 3 geobarometers (gt-pg-AlSi-qtz, gt-mu-pg-bi, gt-mu-bi-AlSi-qtz (see Hodges and Crowley, 1985)) were collected from a wide range of structural levels along several cross-strike transects across the MCT zone and the Tibetan Slab. Thirty samples were analyzed, with the results showing a significant decrease in pressures towards higher structural levels from 685±160 MPa to 385±96 MPa across the MCT zone and to 328±102 MPa in the middle of the Tibetan Slab. Temperatures across the same section show an increase up-section across the MCT zone and lower Tibetan Slab from 793±42 K to 998±96 K. From the lower Tibetan Slab to the middle Tibetan Slab temperature decrease to 866±50 K. These pressure and temperature profiles across the MCT zone and lower Tibetan Slab are consistent with a model of heat conduction following "hot over cold" thrust emplacement. The thermobarometric data, together with metamorphic textures suggest that metamorphism was syn-deformational

$^{40}Ar/^{39}Ar$ mineral ages from the MCT zone include a hornblende age of 20.9±0.2 Ma. The hornblende closure temperature (500±50°C) falls within the range of recorded metamorphic temperatures and thus dates the metamorphism and deformation along the MCT at ~21 Ma.

Leucogranite and pegmatite within the upper Tibetan Slab yield biotite and muscovite cooling ages of ~15-16 Ma. A hornblende from an amphibolite in the upper Tibetan Slab yielded a 22.7±4.4 Ma age. The hornblende age suggests that the upper Tibetan Slab was hot (~500°C) at roughly the same time that the MCT was active. High temperatures in the upper Tibetan Slab may have been due to the advection of heat during leucogranitic intrusion.

Young ages (3.6±0.2 to 9.1±0.2 Ma) were recorded in a small shear zone in the lower Tibetan Slab suggesting that there may have been some amount of post-MCT deformation within the Tibetan Slab.

Thesis supervisor: Dr. Kip V. Hodges
Title: Associate Professor of Geology

ACKNOWLEDGMENTS

Before you read further, you should be aware of others who have contributed in some way to the work which is discussed on the following pages.

There is a group of people who worked many long, hard hours on a job for which they probably never understood a purpose - in fact, I'm sure they thought I was crazy (no Kip, you are not supposed to fall in this category!) I am very grateful to Mangabahadur, Rambahadur, Wonbahadur, Dhanbahadur, Mindu, Mingmar, Pasey, Mani Dam Rai, Balbahadur, Tanka Rai, Babu, Dillisher, Gomba and Pemba for their honesty, dedication and hard work while carrying loads of rocks, food, and equipment all over eastern Nepal.

There are four other people who helped me and this project immeasurably and, in addition, became great friends: Sange Dorje Sherpa, Nima Rinza Sherpa, Dorje Sherpa, and Pasang Sherpa. Mountain Travel Nepal generously provided logistical support and introduced me to Sange.

Sara Neustadtl, Andrew Harvard, Patrick LeFort, Thekla Von Hagke, Brad Washburn, and Dan Schelling provided useful information about living and working in Nepal, which greatly eased my first field season. Henry Heyburn, Liz Schermer, and Barb Sheffels were wonderful companions and assistants in the field. In addition to putting up with me they had to leave their scenic workplace in the States and deal with early mornings that started with tea in bed, treacherous outcrops, high altitude and my frequent outings in the night, carrots cooked in sugar when our Sherpa friends thought we needed "Western food," Buddhist religious festivals, and the occasional cup or two of raksi.

Mark Harrison and Matt Heizler generously shared their lab at SUNY Albany and their time, thus enabling me to obtain $^{40}Ar/^{39}Ar$ ages. Matt, Lynn and Ashley Heizler also shared their home, which greatly enhanced visits to Albany.

One of the most important and accessible sources of support (scientific and moral) at MIT is the group of other graduate students. My thanks go to Doug Walker, Dave Klepacki, Peter Crowley, Peter Tilke, Jane Selverstone, Brian Taras, Don Hickmott, Liz Schermer, Barb Sheffels, Jim Knapp, Zhang Pei-Zhen, David Silverberg, Laurence Page, Larry McKenna, Allison McFarlane, Dave Dinter, Joann Stock, Cindy Ebinger, Peter Wilcock, Cathy Summa, and Tanya Furman for their help and for the exposure to their research. It was a

pleasure to get to know Olaf Svenningson and Eveline Herren during the last six months. Eveline has shared the Swiss perspective on Himalayan geology, a post-doctoral perspective on thesis writing, help with my reference list, German-language instruction, and inspiration for next year in Zürich.

The hockey team provided a marvelous distraction plus the much-needed exercise. I have been happy to have a few non-MIT activities and friends around Boston. Without Andy Harvard's private resort with the loons in Deering, New Hampshire I would not have survived four Boston Summers. The real reason I finished my thesis is that he sold the place! Sara Neustadtl has been a great help with her support, encouragement, and friendship, which have been known to appear all over the world including Kathmandu, Grenoble, London, Panamint Springs, and Boston. Another refreshing distraction from the routine of grad student life have been visits to and from Larky and Rachel Hodges. These two have a real knack for putting life back in a proper perspective. Tom Slocum has been a true friend, sharing his family and favorite New England activities, and being patient through thesis angst.

Of course the greatest inspiration for my career as a graduate student and geologist has come from Kip Hodges. Kip's enthusiasm, knowledge, patience, generosity, and sense of humor work together to make a great advisor and friend. Wiki Royden has provided a valuable introduction to the pros and cons of thermal modeling. Clark Burchfiel has convinced me that there are other interesting mountain belts in the world in addition to the Himalaya. Peter Molnar has shown me that, if you think hard you can always find a good excuse to get to those mountain belts, all of them! Roger Burns has taught me that mineralogy has practical and interesting applications. He has also provided financial support for me during this last year. Valerie Wood has made long probe hours seem short.

My deepest thanks go to my parents who really introduced me to science, geology, world travel, and life in general. Thanks also to David, Janice, and Christopher for their love and support and for adding some real joy to the last four months.

This project received financial support from The American Alpine Club, The Explorer's Club, The Geological Society of America and U.S. National Science Foundation grant EAR-8414417. Thanks to Mr. Shrestha and the Department of Mines and Geology for allowing us to take rock samples from Nepal.

TABLE OF CONTENTS

LIST OF FIGURES

LIST OF TABLES

LIST OF PLATES

Chapter 1: INTRODUCTION AND GEOLOGIC BACKGROUND

INTRODUCTION

The Himalaya, the world's highest mountain range, owes its existence to the collision and continued converge between the Indian subcontinent and the Eurasian continent. The Eocene collision followed the ~ 80 Ma long northward journey of the Indian land mass after the break-up of Gondwanaland (Norton and Sclater, 1979). Convergence between India and Asia has resulted in a variety of deformation styles over a broad area from the Ganges plain to central Asia. Within the Himalaya itself much of the major compression has been accommodated along north-dipping thrust faults (Fig. 1.1). The northernmost of the major faults, the Main Central Thrust (MCT) is a shear zone of possibly great displacement (>100 km), which has always been found together with an inverted metamorphic sequence (Gansser, 1964; Bordet, 1973; LeFort, 1975). In many places the hanging wall to the MCT has been intruded by Tertiary leucogranites. The goal of this thesis was to gain a better understanding of the MCT: its structure, age, and relation to metamorphism and intrusion. Toward this goal, an area in eastern Nepal (Dudh Kosi, Hinku and Hongu drainages) was chosen and a variety of techniques were applied to these problems. The techniques include field mapping, thermobarometric analysis, and $^{40}Ar/^{39}Ar$ geochronology.

GENERAL GEOLOGY

The Himalaya, which now separate the Asian continent from the Indian subcontinent, are an orogenic belt of collisional origin, which, like the Alps, resulted from the closing of the Tethyan ocean basin (Sengör, 1984). This

Figure 1.1 Simplified geologic map of the Himalaya (after Gansser, 1981). The major north-dipping faults are shown separating the four physiographic/tectonic zones. The Main Boundary Thrust (MBT) and the Main Central Thrust (MCT) are identified as is the approximate location of the study area in eastern Nepal.

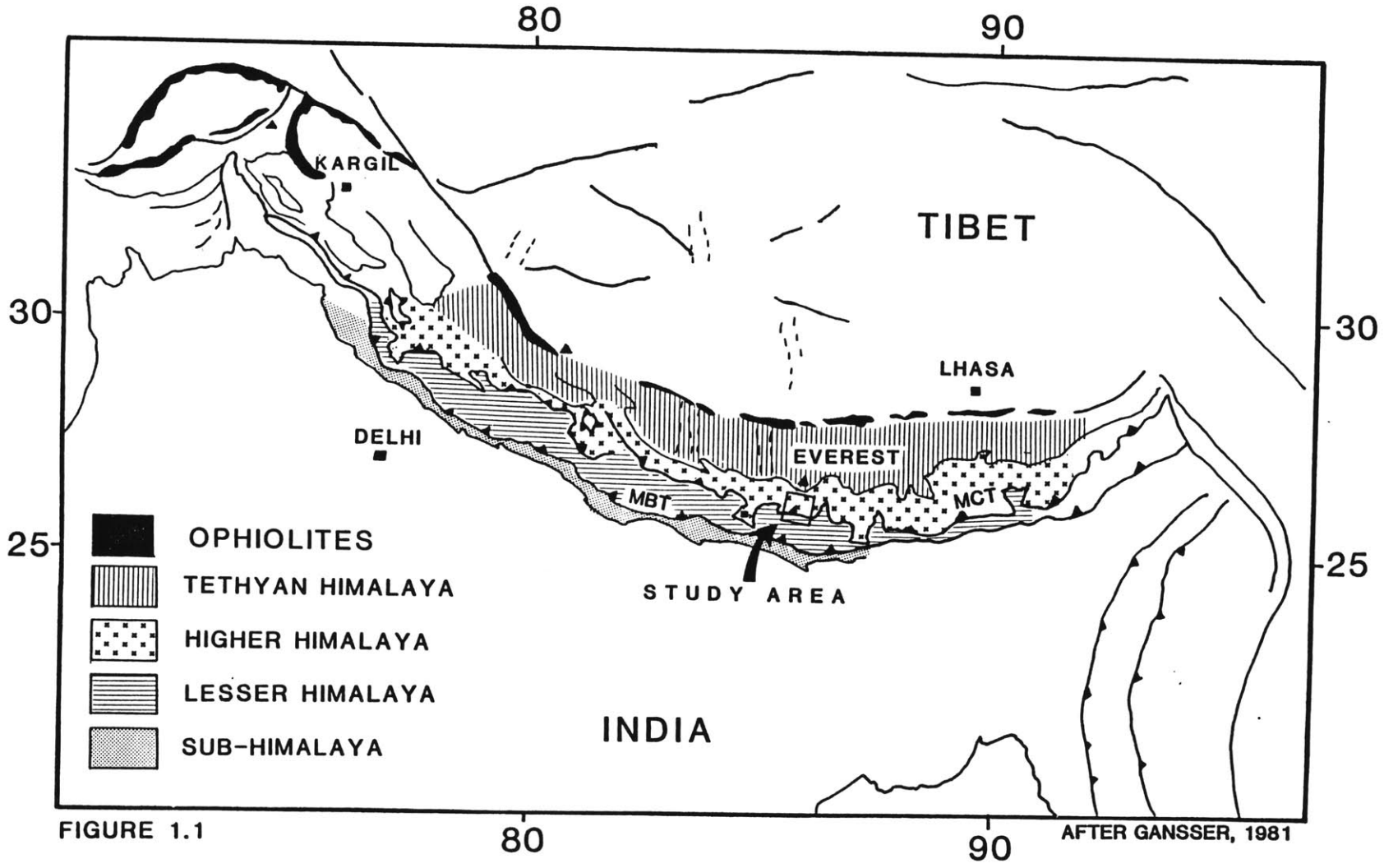

FIGURE 1.1

AFTER GANSSER, 1981

arcuate mountain belt extends over 2500 km from Pakistan in the northwest to northern Burma in the east (Fig. 1.1). Geographically, the highlands of the Tibetan Plateau border the Himalaya to the north while the lowlands of northern India and southern Nepal form the southern border. Traditionally the range has been divided into four major physiographic/tectonic zones (LeFort, 1975; Gansser, 1964). These zones are fault-bounded and continuous along the length of the range (Fig. 1.1). From south to north the zones are: 1) the Sub-Himalaya; 2) the Lesser Himalaya; 3) the Higher Himalaya; and 4) the Tibetan or Tethyan Himalaya. Local names for these zones vary somewhat in the literature, but the general characteristics for each zone are relatively consistent along the range.

Sub-Himalaya

Topographically the Sub-Himalaya form the lowermost foothills of the Himalaya. The predominant lithologic units in this zone are the Kasauli and Dagshai Formations of Upper Oligocene-Lower Miocene age and the Siwalik molassic deposits which include shaly layers, sandstones, and conglomerates of Middle Miocene-Pleistocene age (Bhattacharya and Niyogi, 1971: LeFort, 1975). The Kasauli/Dagshai sequence may represent a littoral marine / deltaic / fluvial transition, but the Siwalik series is terrestrial in origin and relates to erosion during early Himalayan uplift (LeFort, 1975; Hashimoto et al., 1973). Conglomerate clasts within the Siwalik series include not only reworked syndepositional facies and identifiable components from various Sub-Himalayan and Lesser Himalayan formations, but also schistose and gneissic rocks from Higher Himalayan units (Gansser, 1964). The combined Sub-

Himalayan sequence is several kilometers thick.

The Sub-Himalayan zone is probably thrust-bounded in most places. The southern boundary is problematic in many localities and where not marked by a frontal fold belt, is characterized by the laterally discontinuous Main Frontal Thrust in northern India and Nepal (Gansser, 1981). Lack of continuity of this structure may be due to the scarcity of outcrop in this densely vegetated region. In Nepal, Japanese workers refer to this thrust as the Kamla thrust (Hashimoto et al., 1973).

The northern boundary of the Sub-Himalaya is the Main Boundary Thrust (MBT). Along this north-dipping thrust fault upper plate rocks override parts of the Siwalik series dating the thrust as Middle Miocene or younger. The MBT is steeply dipping, but to the north, windows of Sub-Himalayan units indicate the flattening of this fault at depth. These windows also provide a minimum estimate for the displacement at 35 km (Gansser, 1964). Structures within the Sub-Himalaya of India and Nepalconsist of faulted folds with WNW-ESE trending fold axes. The intensity of internal deformation increases toward the north (Gansser, 1981).

Lesser Himalaya

North of the Main Boundary Thrust is the Lesser Himalaya. The hills of this zone are topographically higher than the Sub-Himalaya, but are still dwarfed by the snow-capped peaks of the Higher Himalaya further to the north. Rock units of this zone are made up mostly of clastic shallow marine shelf sediments with some associated carbonate horizons. These sediments

probably constitute the northern continental shelf and slope of the Indian portion of northern Gondwana and strike parallel or subparallel to the present Himalayan range (Gansser, 1981). Some rocks are unmetamorphosed, but many have been metamorphosed to low-grade slate, phyllite, quartzite, and marble. In Nepal the Lesser Himalaya has been divided into two parallel, east-west trending belts. The southern belt is characterized by intense deformation with tight overturned folds. The northern or Midland sedimentary belt exhibits undisturbed clastic sedimentary sequences and broad open folds. In some areas the two belts are separated geographically by high-grade gneisses which may represent klippen of the Higher Himalayan crystalline rocks (Stöcklin, 1980). The Lesser Himalaya of the Kumaun area of northern India also includes klippen of crystalline rocks (Valdiya, 1981). The fossil record is poor throughout the Lesser Himalaya so the stratigraphy is not well-documented, especially in tectonized zones. Based on scarce fossils, depositional ages probably are late Precambrian-lower Paleozoic and Mesozoic, with a sedimentary gap in between (LeFort, 1975).

The Main Central Thrust (MCT) zone forms the northern boundary to the Lesser Himalaya. This structure, like the MBT, is laterally continuous at least from Kashmir to Sikkim and possibly still further east. The MCT has been studied in several locations by a variety of workers (Heim and Gansser, 1939; LeFort, 1975; Valdiya,1980; Maruo et al., 1979), but there is disagreement as to the structural nature of this thrust and its relation to metamorphism in the hanging wall. These problems will be discussed in a later section.

Higher Himalaya

The hanging wall of the MCT consists of high-grade metamorphic rocks and Tertiary leucogranites of the Higher Himalayan crystalline complex. Immediately above the Lesser Himalayan formations is a sequence of augen gneiss, mica schist, phyllite, graphitic schist, quartzite, amphibolite, and calc schist. The lithologic units are 50-500m thick, strongly deformed, and metamorphosed to greenschist - lower amphibolite facies. This sequence is 3-5 km thick and has been called an MCT zone by several authors in Nepal (Bordet et al., 1981; Arita, 1983; and Hubbard, in press). In the Kumaun area of northern India, Valdiya (1980) bounds this sequence by two thrusts and refers to the rocks in the middle as the Munsiari Formation. He actually equates his upper thrust, or Vaikrita Thrust, to the MCT. Gansser (1964) places this section above the MCT, as do Fuchs and Frank (1970), and they call it the Lower Crystalline Nappe.

The true Higher Himalaya lies above the Munsiari Formation, Lower Crystalline Nappe, or MCT zone. This zone includes the highest peaks of the range. A number of different names have been given to the rocks of this zone. In an effort to be consistent with French workers in central Nepal the term Tibetan Slab will be used in this thesis.

The Tibetan Slab consists of a thick section (5-20 km) of high-grade crystalline rocks, migmatites and granites. Lithologies include: garnet-biotite gneiss, augen gneiss, calc-silicate rock and amphibolite. Tertiary granitic bodies, which vary in size, have intruded the upper levels of the Tibetan Slab along the range from Pakistan in the west to eastern Bhutan in the east. These granites are mostly tourmaline-bearing or two-mica leucogranites. Cooling ages of the granites range from ~14 to~25 Ma from Rb/Sr whole rock-mineral pairs and the $^{40}Ar/^{39}Ar$ dating techniques (Bordet et al., 1981; Copeland, 1987;

Maluski et al., 1988; Hubbard et al., 1988).

The origin of the melt that produced these granites is uncertain. Relict zircons and monazites from the granite yield Paleozoic and Precambrian U/Pb ages (Schärer et al., 1986; Copeland et al.,in press), which qualify any of the Tibetan Slab and most of the Lesser Himalayan units to have been a possible source. Initial $^{87}Sr/^{86}Sr$ ratios are consistently high (0.7433-0.7874), thus supporting a crustal origin (Vidal et al., 1984). LeFort (1981) has suggested that emplacement of the hot Tibetan Slab over the cooler Lesser Himalaya along the MCT caused de-watering of Lesser Himalayan units. The introduction of Lesser Himalayan fluids into the hot Tibetan Slab could have lowered the melting temperature sufficiently to allow melting of the Tibetan Slab rocks. France-Lanord (1987) presents oxygen isotope data which suggests Formation I, the lowest unit in the Tibetan Slab in Central Nepal, as a possible source for the Manaslu leucogranite. Other authors have suggested that granitic melt may have come from below the MCT (Andrieux et al., 1977; Molnar et al., 1983).

The upper contact of the Tibetan Slab is now believed to be a normal fault (Caby et al,. 1983; Burg et al., 1984; Herren, 1987; Royden and Burchfiel, 1987;). This structure was originally recognized as a normal fault by Shah and Sinha(1974) in Kumaun, but until more recently most workers have considered the contact to be a thrust or conformable sequence. The upper plate to this north-dipping normal fault is the Tethyan sedimentary series. The mechanics of a normal fault of possibly considerable displacement (tens of kilometers) in a convergent zone are not yet clearly understood. Burchfiel and Royden (1985) and Searle (1986) have suggested some sort of gravity driven "collapse" of an area of extreme elevation.

Tethyan Himalaya

The Tethyan Himalaya consists of a ~10 km-thick stack of fossiliferous marine sedimentary rocks that range in age from Cambrian to mid-Eocene (Gansser, 1964; LeFort, 1975). The section is nearly continuous with the exception of a Carboniferous gap in sedimentation. The entire sequence represents a shallow-water shelf environment with a paleontologic record suggesting a Gondwanan affinity (Gansser, 1981).

The northern edge of the Tethyan Himalaya is marked by the Indus-Tsangpo suture zone. Here, deep-sea pelitic and flyschoid sedimentary rocks of mid-Triassic to early Tertiary age are found together with Cretaceous volcanic rocks (Gansser, 1964). Tectonic slices of ophiolites represent remnants of former Tethyan oceanic crust (Nicolas et al., 1981). It is generally thought that this suture zone was the site of northward oceanic subduction prior to the collision of India and Asia(Gansser, 1966; Dewey and Bird, 1970).

MAIN CENTRAL THRUST

After the Eocene continental collision, ongoing convergence was partly accomodated along the Main Central Thrust (MCT). Traditionally, (during the last ~25 years!) this thrust has been mapped as continuous along the Himalaya, at least from Kashmir to Bhutan. Estimates on the timing of thrust movement vary from Oligocene (Mattauer, 1975), to Miocene (LeFort, 1975), and even to Recent (Krummenacher et al., 1978). It is generally believed that the MCT pre-dates movement on the next major thrust system to the south, the Main

Boundary Thrust (MBT).

There is lack of agreement on the structural style and position of the MCT. Originally Heim and Gansser (1939) designated the MCT in Kumaun as the break between the non-metamorphic to low-grade rocks of the Lesser Himalaya and medium- to high-grade rocks of the Higher Himalaya. Many Indian geologists follow this convention (Sinha, 1981; Thakur and Choudhury, 1983). French and Japanese workers in Nepal (Bordet, 1973; Hashimoto et al., 1973; LeFort, 1975; Pêcher, 1977) however, place the MCT at a higher structural level where medium-grade rocks are in contact with high-grade kyanite/sillimanite-bearing gneiss. Valdiya (1980), on the other hand, recognizes two major structural discontinuities in Kumaun. He calls the lower fault (the MCT of Heim and Gansser, 1939) the Munsiari Thrust and the higher tectonic break (~ the MCT of the French) the Vaikrita Thrust. In Kumaun, the rocks between these two thrusts are the low- to medium-grade metamorphic rocks of Valdiya's Munsiari unit, which correlate with the Lower Crystalline Nappe of Fuchs (1981) and Honegger (1983) or the MCT zone in eastern Nepal (Hubbard, in press). Gansser (1981) now interprets the Munsiari unit as a tectonic slice of the Higher Himalaya. Conversely, Valdiya (1980) believes that the Vaikrita Thrust marks the lower tectonic boundary of the Higher Himalaya or Tibetan Slab.

In Nepal Arita (1983) and Maruo et al., (1979) have made a similar interpretation to that of Valdiya. Arita recognizes two thrusts, the MCT I and the MCT II, which bound a package of rocks he calls the Main Central Thrust zone. Maruo et al. also identified two thrusts, but whereas Arita calls the structurally lower thrust MCT I, Maruo et al. call this thrust the MCT II and vice versa for the structurally higher thrust.

Generally workers from different parts of the Himalaya agree that the "zone" between the sedimentary rocks of the Lesser Himalaya and the gneissic rocks of the Higher Himalaya is, to some degree, a schuppen zone or "zone des écaille" (Bordet, 1973; Hashimoto et al., 1973; Maruo et al., 1979; Valdiya, 1980; Hodges and Silverberg, 1988). The lack of consistency in placement of the MCT is partly the result of various interpretations of the location of maximum displacement within this zone. Those who see one discrete plane of maximum tectonic displacement locate the MCT accordingly. Those who recognize a distribution of displacement throughout the zone adhere to the MCT schuppen zone interpretation. Because this thrust is continuous over such a great distance (>1600 km), and because the thrust involves different lithologies in different locations it is very likely that the structural style and position of the MCT varies from place to place.

An important feature associated with the MCT is the so-called inverted metamorphism. This feature was first recognized in India by H.B. Medlicott (1864) and it consists of isograds of successively higher metamorphic grade appearing at successively shallower structural levels. The nature of the relationship between the inverted metamorphism and the MCT depends somewhat on the structural characteristics of the MCT itself. As previously mentioned there have been a variety of structural interpretations so, consequently, there have been a variety of theories proposed to explain the inverted metamorphism. These theories include: 1) large-scale, post-metamorphic recumbent folding (Heim and Gansser, 1939); 2) a multiplicity of post-metamorphic thrust faults sequentially placing higher grade rocks over lower grade rocks (Bordet, 1961; Hashimoto et al., 1973); 3) the consequences of thermal conduction following the overthrusting of "hot" rocks onto "cold" rocks

(LeFort, 1975); 4) shear heating along the thrust plane (Graham and England, 1976; Scholz, 1980); and 5) differences in bulk composition causing an apparent inversion.

The biggest obstacle in understanding the structural and thermal history of the Main Central Thrust is a lack of basic petrologic, geochronologic, and structural data. This thesis project was dedicated to the aquisition and analysis of such data using a variety of techniques for an area in eastern Nepal including the MCT zone and overlying Tibetan Slab. Field work was done in order to understand the structural nature of the MCT in this area and to collect samples for petrology and geochronology. Thermobarometric techniques were applied in an effort to quantify the metamorphism across the MCT zone and Tibetan Slab. The $^{40}Ar/^{39}Ar$ method of age dating was used to obtain cooling ages for several minerals from locations across the study area. Chapter 2 includes a description of the general geology, stratigraphy, petrography and structure of this area. Chapter 3 is a thermobarometric study of pelitic samples collected along several cross-strike transects across the MCT zone and Tibetan Slab. This chapter has been accepted by the Journal of Metamorphic Geology. Chapter 4, which was also written in manuscript form and will be co-authored with Mark Harrison, covers $^{40}Ar/^{39}Ar$ dates of mineral separates from the area.

It is necessary at this point to make one remark. The trend in current scientific literature is toward the use of SI units. With the subtle encouragement of my advisor (K.V.H.), chapter 3 was written with this trend in mind. The use of Kelvin for metamorphic temperatures has created a painful reaction during talks as people have had to subtract 273° in public without the use of a calculator (I confess the use of a calculator in the privacy of my own office). So chapter 4 was written with temperatures in the traditional units of Centigrade. I apologize

for this inconsistency; however, all changes in custom need a transition period and this thesis is clearly a product of that transition.

Chapter 2: GEOLOGY AND STRUCTURE OF THE DUDH KOSI, HINKU AND HONGU DRAINAGES

INTRODUCTION

In the Himalayan literature, there is substantial disagreement as to the structural styles and characteristics of the Main Central Thrust (MCT) zone (e.g. Heim and Gansser, 1939; Pêcher, 1978; Maruo et al., 1979; Brunel and Kienast, 1986). Much of this disagreement probably reflects the extreme length (~2000 km) of this structure and the fact that only a few areas have been studied in detail. It is probable that future studies will demonstrate significant variations in the style and timing of deformation over the length of the thrust zone. Clearly, the only way to improve our general understanding of this thrust zone is through more and better detailed studies of this zone. In this light, I present here the results of my efforts to examine the the tectonostratigraphy and structure of an area of eastern Nepal.

STUDY AREA

The study area lies south of Mt. Everest (Sagarmatha) in eastern Nepal and includes the Dudh Kosi, Hinku and Hongu drainages (Figs. 1.1 & 2.1). This region covers the uppermost Lesser Himalayan unit, the MCT zone, and a nearly complete section of the Tibetan Slab. The southern limit of the area is approximately the confluence of the Hongu Khola and the Dudh Kosi. The northern limit was in the northern end of the Gokyo valley at Ngozumba.

The steep terrain in this area limited travel to existing trails in most places. Moreover, elevations below ~3500m are densely vegetated, while higher elevations are often glaciated. Structural data on Plate 1 outlines the path actually followed. Regions in between were reached only with binoculars and an imagination! Field work was done during three 6-8 week field seasons.

Figure 2.1 Simplified geologic map of the study area in eastern Nepal. The three major tectonic zones that are focused on in this study are identified: the Lesser Himalaya, the Main Central Thrust (MCT) zone, and the Tibetan Slab. Leucogranitic intrusives occur throughout the Tibetan Slab, but only the region of the largest leucogranitic bodies is outlined and labeled "granite." All of the geographic names that are refered to in this study are identified.

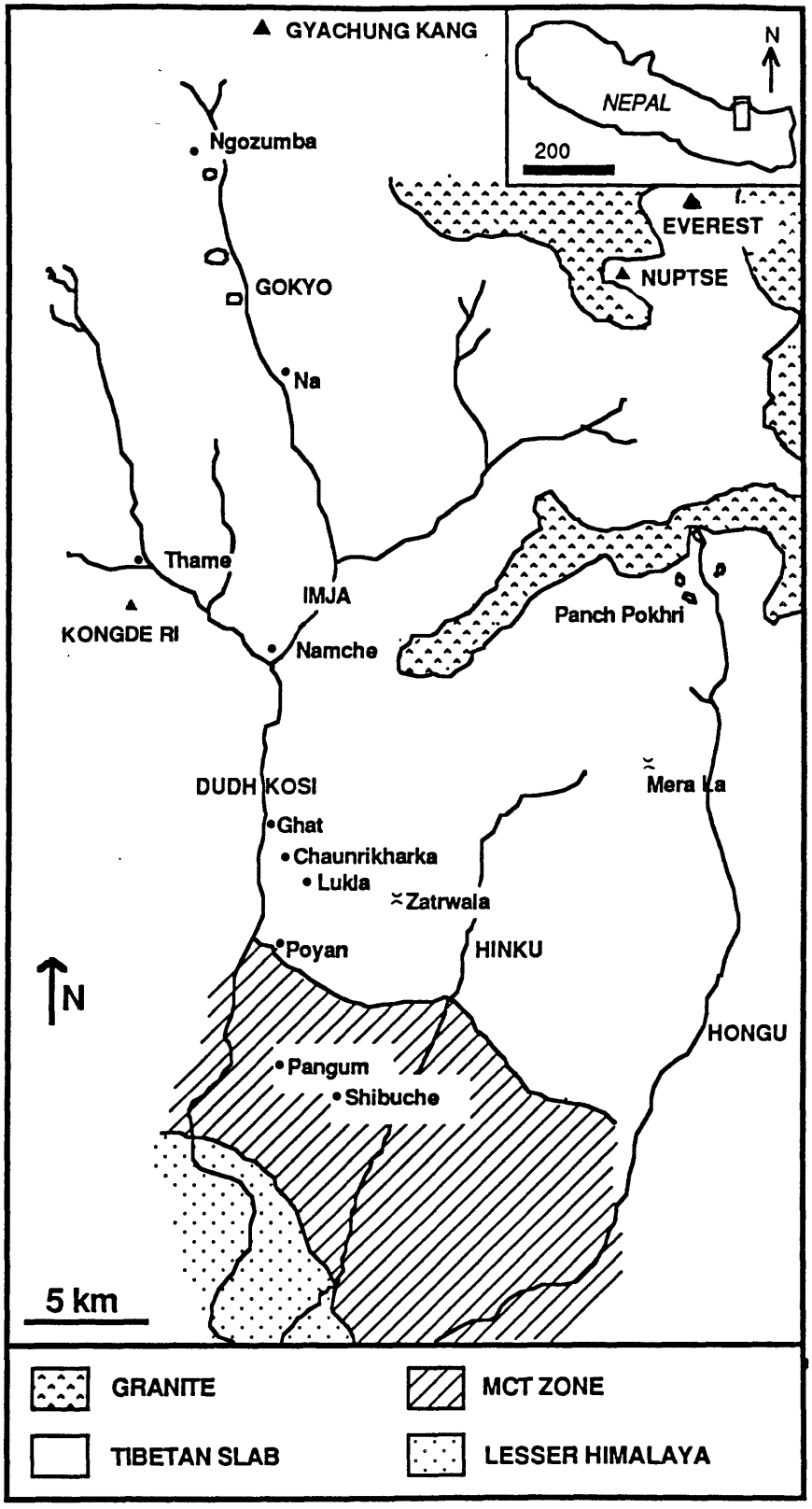
GYACHUNG KANG
N
NEPAL
200
Ngozumba
EVEREST
NUPTSE
GOKYO
Na
Thame
IMJA
KONGDE RI
Namche
Panch Pokhri
DUDH KOSI
Mera La
Ghat
Chaunrikharka
Lukla
Zatrwala
Poyan
HINKU
N
HONGU
Pangum
Shibuche
5 km
GRANITE
MCT ZONE
TIBETAN SLAB
LESSER HIMALAYA

Figure 2.1

PREVIOUS WORK

The first published geologic account of the region south of Mt. Everest was the product of a Swiss expedition in 1952 (Lombard, 1953). Lombard (1958) provides very detailed observations and numerous geologic sketches. Bordet accompanied expeditions to this area in 1954 and 1955 and he, too, has prepared a detailed volume (Bordet, 1961). Krummenacher published petrographic accounts of samples from the Everest region in the 1950's, and his more recent work reports K-Ar dates from the area (Krummenacher, 1956a&b; Krummenacher et al., 1978). Hagen also visited the area in the 1950's and he published a general volume on the geology of Nepal (1969).

Japanese groups have worked in eastern Nepal in the Tamba Kosi, Dudh Kosi and Arun river valleys and adjacent areas (Ishida, 1969; Hashimoto, 1973; Maruo et al., 1979). Schelling (1987) has also been working in recent years in the Tamba Kosi- Rolwaling area. For his thesis Brunel made a number of N-S transects in eastern Nepal between the Tamba Kosi and the Arun valleys (Brunel, 1983). A Czechoslovakian group has done a geologic and petrologic study in the Makalu area (Palivcová et al., 1982; Jaros and Kalvoda, 1976). Vuichard (pers. comm.) has recently mapped the Khumbu region (high peak area drained by the Dudh Kosi), but I have not yet seen this map. Italian workers have concentrated on the leucogranites in the Khumbu, and Rb/Sr dating of them (Bortolami et al., 1983; Ferrara et al., 1983). Each group seems to have made a different interpretation of the tectonic stratigraphy. A summary of these interpretations and that which is followed in this study are shown in Figure 2.2. Though I have made a different structural interpretation, I have

Figure 2.2 Correlation of tectonostratigraphic nomenclature used by workers in the Everest region of eastern Nepal. The column labeled "this study" identifies the sequence of lithologies found along the Dudh Kosi and Gokyo valleys and the tectonic zones discussed in this paper. The other columns correlate the nomenclature used by previous workers in the same region. The contacts shown with barbs reflect thrust fault interpretations made by the respective authors. The section labeled "MCT zone" in the "this study" column is interpreted to be a thrust zone.

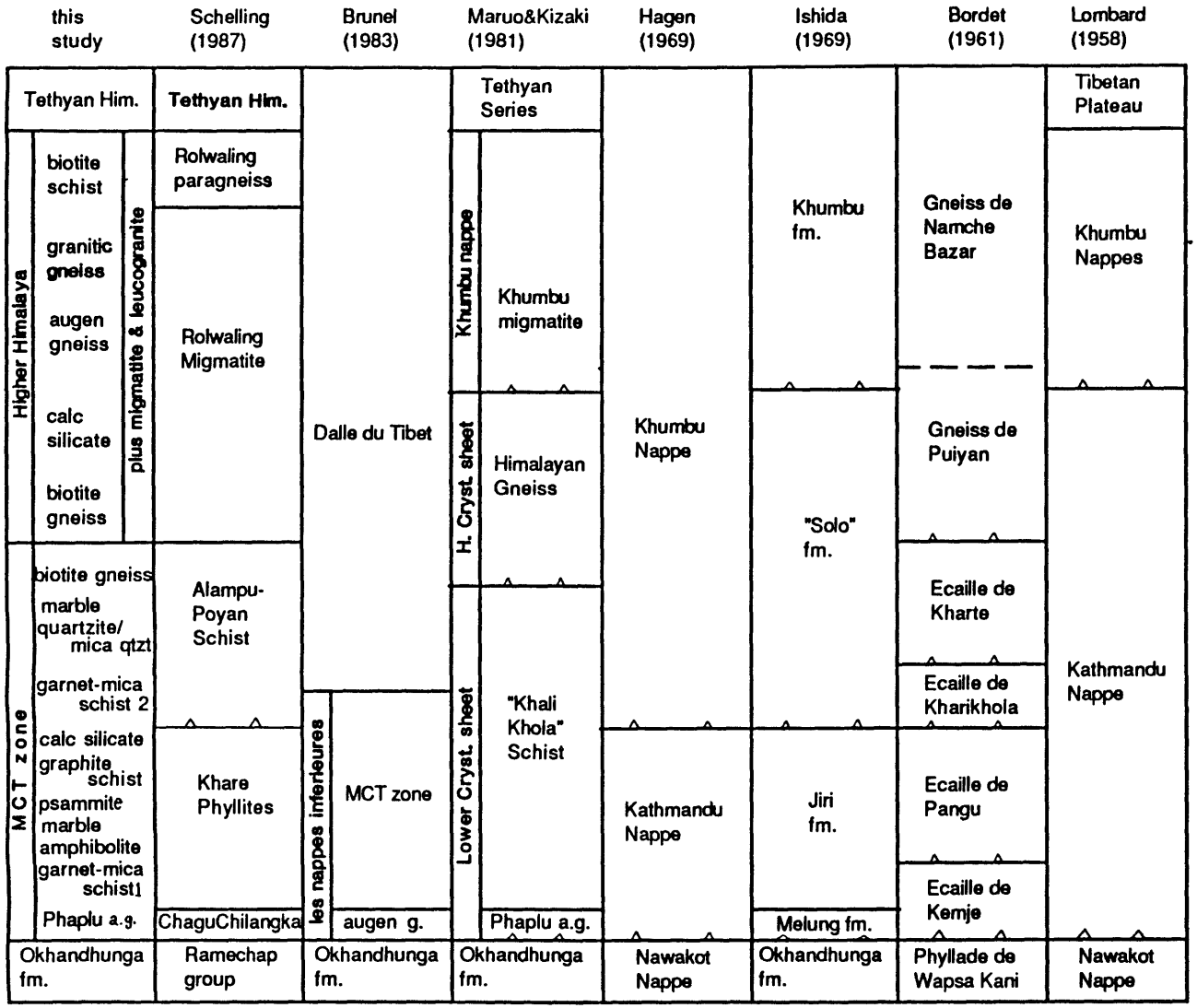
this study
Schelling (1987)
Brunel (1983)
Maruo&Kizaki (1981)
Hagen (1969)
Ishida (1969)
Bordet (1961)
Lombard (1958)
Tethyan Him.
Tethyan Him.
Tethyan Series
Tibetan Plateau
Higher Himalaya
biotite schist
granitic gneiss
augen gneiss
calc silicate
biotite gneiss
plus migmatite & leucogranite
Rolwaling paragneiss
Rolwaling Migmatite
Dalle du Tibet
Khumbu nappe
Khumbu migmatite
Khumbu fm.
Gneiss de Namche Bazar
Khumbu Nappes
H. Cryst. sheet
Himalayan Gneiss
Khumbu Nappe
"Solo" fm.
Gneiss de Puiyan
MCT zone
biotite gneiss
marble
quartzite/ mica qtzt
garnet-mica schist 2
calc silicate
graphite schist
psammite
marble
amphibolite
garnet-mica schist1
Phaplu a.g.
Alampu-Poyan Schist
Khare Phyllites
ChaguChilangka
les nappes inferieures
MCT zone
augen g.
Lower Cryst. sheet
"Khali Khola" Schist
Phaplu a.g.
Kathmandu Nappe
Jiri fm.
Melung fm.
Ecaille de Kharte
Ecaille de Kharikhola
Ecaille de Pangu
Ecaille de Kemje
Kathmandu Nappe
Okhandhunga fm.
Ramechap group
Okhandhunga fm.
Okhandhunga fm.
Nawakot Nappe
Okhandhunga fm.
Phyllade de Wapsa Kani
Nawakot Nappe

Figure 2.2

made an effort not to introduce new stratigraphic nomenclature; consequently I refer to rock units by lithology or existing formation names. The three major subdivisions that I use are the Lesser Himalaya, the MCT zone, and the Tibetan Slab.

TECTONIC STRATIGRAPHY

Lesser Himalaya

In eastern Nepal the Lesser Himalayan units, generally low-grade metasediments, occur between the Main Central Thrust zone in the north and the Main Boundary Thrust in the south. In the southern hills of the Lesser Himalaya the low-grade units are overlain by the Mahabharat Crystallines, which may be a klippen of the Higher Himalayan crystallines (Maruo and Kizaki, 1983). In this study only the uppermost unit of the Lesser Himalaya, the Okhaldhunga Unit of Maruo et al. (1979), was sampled.

The Okhaldhunga Unit consists primarily of muscovite and chlorite-bearing phyllite and psammite. These rock types occur in alternate layers with thicknesses that range from millimeters to tens of meters. The percentage of quartz present in different layers varies from ~5% to ~80%. The presence of chlorite, even in minor amounts, gives these rocks a slight green color. Weathering commonly affects the phyllite layers to the point of making them friable and difficult to sample.

The metamorphic assemblage of rocks within the Okhaldhunga Unit generally includes: muscovite, quartz, chlorite, ± plagioclase,± ilmenite. The plagioclase occurs as subrounded grains, which may be detrital in origin, and

Maruo et al. (1979) recognized graded bedding in this unit. The upper 100-200m has been metamorphosed to biotite grade, and garnets occur in the upper ~100m.

According to Maruo et al., (1979), the overall thickness of the Okhaldhunga Unit is about 6000m. They propose a correlation with the Dalings in Sikkim, which Gansser (1964) suggests is Precambrian or early Cambrian in age. Bordet refers to these rocks as the "phyllades de Wapsa Kani." The Okhaldhunga Unit is also correlative with the Ramechap Group of Schelling (1987).

Main Central Thrust Zone

The MCT was originally defined as a structural and metamorphic break in Garhwal (Gansser, 1964). In eastern Nepal there is no sharp structural or metamorphic break at the MCT. There is a gradual increase in metamorphism up section and a zone of highly strained rocks across ~5 km between the Lesser Himalaya and the Tibetan Slab, herein called the MCT zone. With regard to the intensity of deformation, the bounds of the zone are gradational but, in an effort to eliminate ambiguity, an upper and lower bound have been designated. The lower bound is easy to recognize in the field and is the contact of the Okhaldhunga Unit with the overlying augen gneiss. Maruo and Kizaki (1981) refered to this contact as the Phaplu Thrust. The upper boundary of the MCT zone is within a biotite gneiss at a level where strain decreases upwards and migmatites of the Tibetan Slab first appear. In the Dudh Kosi valley this contact is near the village of Poyan.

The MCT zone consists of a variety of lithologies including: augen gneiss, quartzite, amphibolite, calc-silicate rock, graphitic schist, mica schist,

and marble. Plate 2, A-A' is a cross section through the MCT zone along the ridge between the Dudh Kosi and Hinku valleys, where a relatively good exposure of this section occurs. Metamorphic grade increases across the MCT zone from chlorite grade in the upper Lesser Himalaya to sillimanite grade in the upper MCT zone and Tibetan Slab. The biotite and garnet isograds are actually in the uppermost Okhaldhunga Unit of the Lesser Himalaya, while the staurolite and kyanite isograds occur in the lower MCT zone (Plate 2, A-A'). The sillimanite isograd occurs in the upper MCT zone. Isograds are roughly parallel to lithologic contacts in this area, but in central Nepal isograds are slightly oblique to formation boundaries and to the MCT (Colchen et al., 1986). Lithologic thicknesses vary from several meters to several hundred meters, so only the thicker units of those discussed below are shown on the map (Plate 1).

The lowermost unit in the MCT zone is an augen gneiss, known in this area as the Phaplu augen gneiss (Maruo & Kizaki, 1981). This unit is characterized by mylonitization and the presence of K-feldspar porphyroclasts (Fig. 2.3). The degree of mylonitization and size of porphyroclasts varies within the unit. Typically, porphyroclasts range in size from 0.5-5.0 cm, though larger augen may be found. The matrix consists of alternating layers (1-3mm thick) of recrystallized quartz and biotite or muscovite (Fig. 2.4). The percentage of matrix in the rock is ~75-95%.

The mineralogy within the Phaplu augen gneiss consists of: quartz, biotite, muscovite, K-feldspar, with minor plagioclase and tourmaline. Small garnets occur locally. Some K-feldspar augen show a myrmekitic texture possibly related to an early high temperature history. MCT deformation, at this level, probably did not reach temperatures high enough for myrmekite formation (see Chapter 3).

Figure 2.3 Phaplu augen gneiss. A mylonitic hand sample shows the presence of K-feldspar porphyroclasts. Speciman is ~10 cm long.

Figure 2.4 Phaplu augen gneiss in thin section. Matrix of augen gneiss, under crossed nicols, shows recrystallized quartz. Length of image is 4mm.

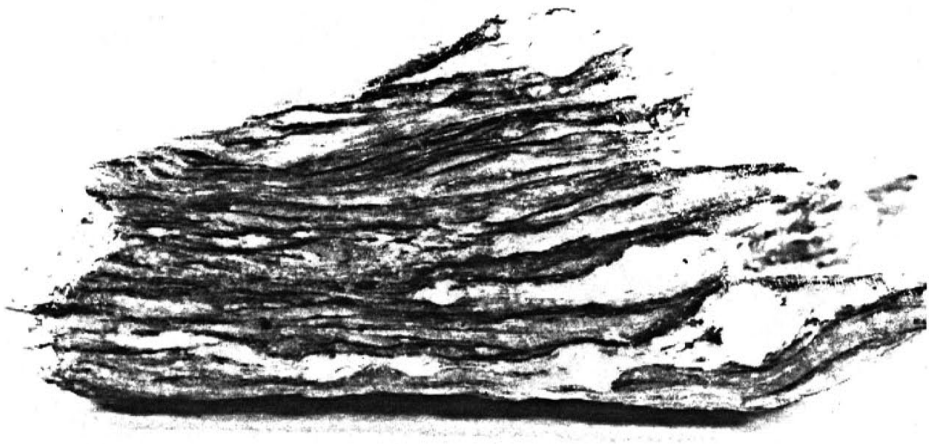

Figure 2.3

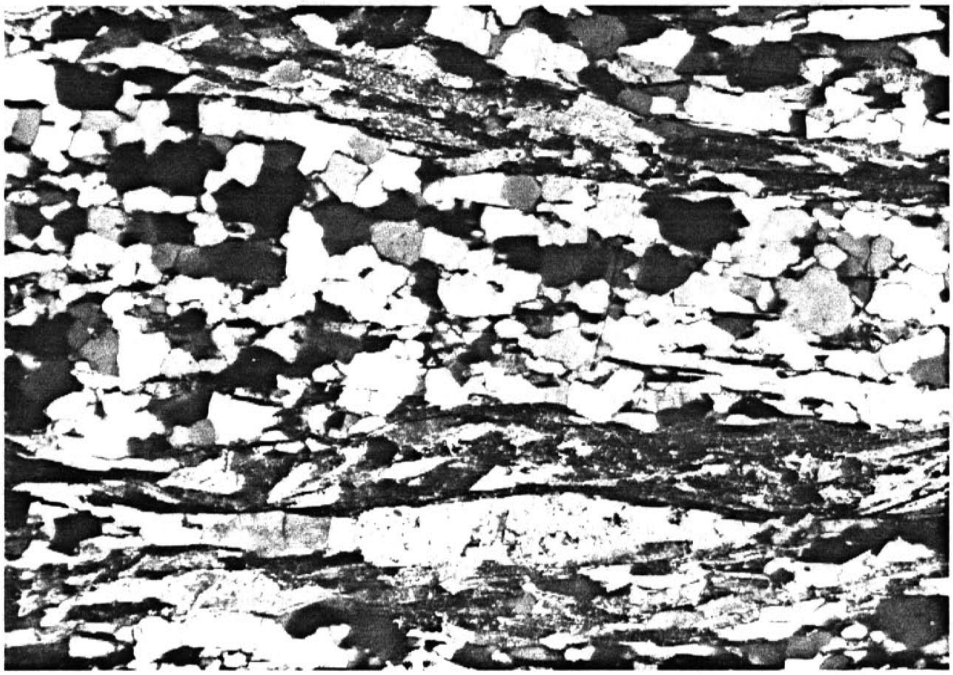

Figure 2.4

Pods of several different lithologies can be found within the Phaplu augen gneiss. A nearly bimineralic garnet-bearing chlorite schist can be found in some areas. Garnets in this schist are 3-6 cm in diameter and contain helicitic graphite inclusion trails. Inclusion trails are not continuous with the matrix foliation, thus suggesting some degree of deformation after garnet growth. An amphibolite horizon is exposed on the ridge between the Dudh Kosi and Hinku rivers within the augen gneiss. This layer or pod is just ~2 m thick and contains the assemblage: biotite, hornblende, epidote and quartz. Thin intervals of garnet and staurolite bearing psammite can also be found in the upper part of the augen gneiss. These slices of different lithologies may be slivers of underlying or overlying units which became incorporated along imbricate faults during MCT deformation. Alternatively they may represent lithologic variation in the pre-metamorphic stratigraphy.

Similar augen gneiss units have been documented at approximately the same structural horizon in other parts of the range (Das & Pande, 1973; Acharyya, 1978; LeFort, 1975). In central Nepal the augen gneiss is known as the Ulleri augen gneiss (LeFort, 1975). Different workers have suggested different protoliths for this unit. Gansser (1964) proposed that the protolith was an intrusive granite. LeFort (1975) suggests that the augen gneiss was of volcano-sedimentary origin.

The unit overlying the augen gneiss is a garnet-mica schist (garnet-mica schist 1, see fig. strat. column). This rock contains the assemblage: quartz, biotite, garnet, staurolite, muscovite, and minor chlorite. Anhedral garnets contain abundant quartz inclusions to the point of being poikiloblastic (Fig. 2.5).

Thin (<1m thick) quartzite layers occur within the lower part of this mica schist unit.

An amphibolite unit, comprised of two lithologies: a hornblende amphibolite and a tremolite-bearing schist, overlies the mica schist. These lithologies alternate within the unit. The massive, black hornblende amphibolite contains primarily hornblende and quartz. Irregular quartz segregations are common. The tremolite schist consists of tremolite, quartz, green biotite, and muscovite. Some tremolite grains have pleochroic cores of either actinolite or hornblende. The preferred orientation of biotite defines the foliation.

Overlying the amphibolite is a cream-colored marble. The mineralogy is predominantly calcite with some quartz and muscovite. Calcite grains are polygonal and probably recrystallized with almost no twinning.

The next unit up-section is a very fine-grained (<0.05-0.10 mm) psammite. The bimineralic assemblage consists of quartz and biotite. Quartz grains show undulatory extinction. Biotite defines the dominant schistosity present both in thin section and hand sample. In hand sample a second cleavage has developed slightly oblique to the schistosity, but is unrecognizable in thin section.

A fine-grained graphite schist overlies the quartz-biotite psammite. The mineralogy includes: graphite, quartz, muscovite and biotite. The graphite is concentrated in pods that are outlined by an S-C fabric (Berthé et al., 1979). This unit is thin but is continuous and it can be followed from the ridge between the Dudh Kosi and Hinku rivers to the next ridge to the east.

Above the graphite schist on the ridge east of the Hinku river there is float

Figure 2.5 Poikiloblastic garnet from the garnet-mica schist 1 unit of the MCT zone. This image, in plane-polarized light, is 4mm long.

Figure 2.6 Deformation zones within the quartzite unit from the upper MCT zone. Thin (1-3mm) shear zones are characterized by ribbon texture in quartz with fibrolitic sillimanite lining the grain boundaries. This image, in plane-polarized light is 13 mm long.

Figure 2.5

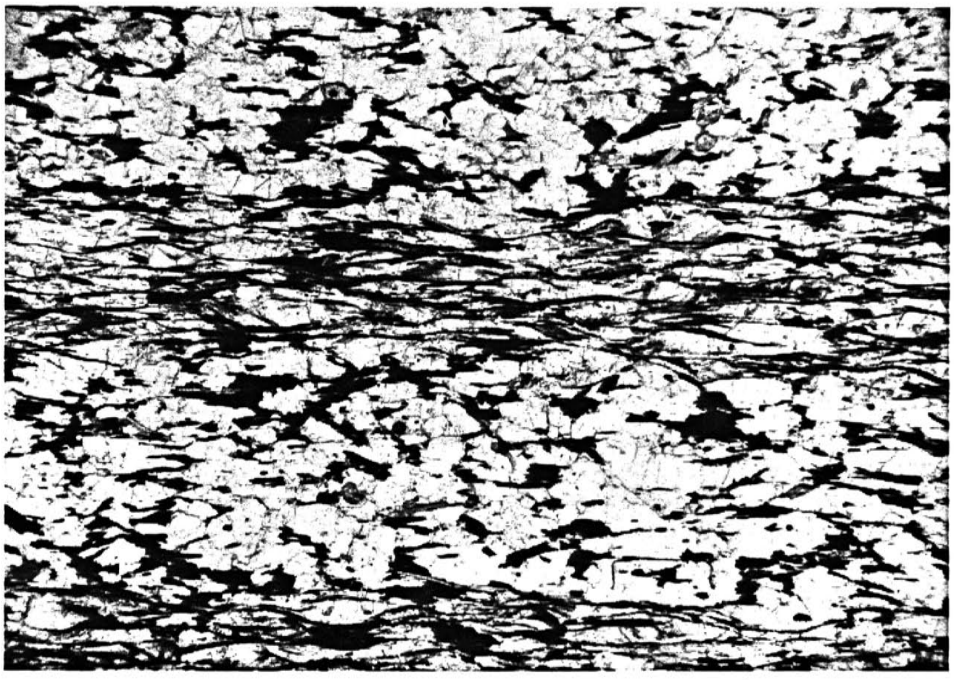

Figure 2.6

of a green and white banded calc-silicate. The stratigraphic position of this unit is unclear, but the abundance of the float suggests a relatively local source. The white layers consist primarily of sub-rounded quartz grains and the green layers consist of actinolite and calcite. Actinolite grains align parallel to the compositional layering. Amphiboles occur locally in radial aggregates. A talc-rich rock also occurs at about this structural level just west of the Hinku at a village called Shibuche.

The next unit up in the sequence is a thick section (1500 m) of garnet-mica schist (garnet-mica schist 2, see Fig. 2.2). This unit is refered to as part of the Khare Phyllites by Schelling (1987), the Khari Khola schists by Maruo and Kizaki (1981), and the Écaille de Kharte by Bordet (1961). The assemblage consists of quartz, muscovite, biotite, garnet, ± staurolite, ± kyanite, ± plagioclase, ± tourmaline, and ± graphite. Kyanite is present in the middle and upper part of this unit (Plate 2, section A-A'). Staurolite exists in the lower part of the mica schist up to, and slightly above, the kyanite isograd. Weathering occasionally makes this unit friable.

A thin amphibolite horizon occurs within the kyanite zone of the mica schist unit. The assemblage of this horizon consists of: hornblende, biotite, quartz, calcite, sphene, and plagioclase. Up-section, but still within the kyanite zone, there is a horizon of eastonite-schist, within which some previous workers have placed the MCT (A. Bassett, pers. comm.). In addition to eastonite this horizon contains muscovite, kyanite, cordierite, plagioclase, and quartz. Kyanite grains are always overgrown by plagioclase and quartz in this horizon.

A thin unit of gray marble overlies garnet-mica schist 2. This unit is nearly pure calcite with minor scapolite and muscovite.

Structurally above the marble is a ~500 m thick unit of alternating quartzite and micaceous quartzite. The alternation occurs both at a thin section scale and at outcrop scale. Micaceous layers dominate toward the top of this unit . The mineralogy of the quartz-rich layers consists of quartz, biotite, muscovite, and fibrolite. In the micaceous layers garnet, plagioclase, K-feldspar and minor kyanite are also present.

Deformation in quartz-rich layers is concentrated in thin (1-3 mm) zones. Quartz grains in these zones have a ribbon texture with fibrolitic sillimanite along grain boundaries (Fig. 2.6). Micaceous layers also appear to be the site of more intense shearing. Fibrolite occurs in these zones and occasionally ribbon quartz grains are bounded by micas.

An augen gneiss unit overlies the micaceous quartzite unit. This rock is similar in appearance to the Phaplu augen gneiss but is more quartzo-feldspathic and of higher metamorphic grade. The assemblage includes quartz, plagioclase, K-feldspar, biotite, muscovite, garnet and in some samples sillimanite. Myrmekites are present. Quartz grains are irregular and grain size varies due to subgrain formation. Larger quartz grains show undulatory extinction.

A thin (10-20 m) sliver of gray marble overlies the augen gneiss on the ridge between the Dudh Kosi and Hinku rivers southwest of the village of Poyan. This marble is not exposed along the main trail south of Poyan, nor is it exposed farther east between the Hinku and Hongu rivers.

The uppermost unit of the MCT zone, as defined here, is a biotite gneiss. The assemblage of this unit consists of: quartz, biotite, plagioclase, fibrolite, and garnet. Both anhedral and euhedral garnets are present. Most garnets have

inclusion-rich cores with slightly fewer inclusions in the rims. Closely spaced zones of sheared biotite and fibrolite define the schistosity. Ribbon quartz occurs in these high strain zones. Between the zones quartz grains have embayed grain boundaries and show sub-grain development. Most quartz grains have undulose extinction.

Tibetan Slab

The Tibetan Slab or Higher Himalaya is the upper plate to the north-dipping MCT zone. The placement of the lower boundary of the Tibetan Slab at the village of Poyan just east of the Dudh Kosi is based on the decrease in strain north of this point and the appearance of migmatites. Like the MCT zone, the Tibetan Slab consists of a variety of lithologies. In the lower part of the Slab it was possible to follow some lithologies for ~10 km along strike. Toward the upper section detailed mapping was limited by time and the terrain. Leucogranitic material, either in the form of leucosome from anatectite or injected material, increases in volume toward the north.

The lowermost rocks in the Tibetan Slab do not differ in mineralogy from the biotite gneiss at the top of the MCT zone, but they are less defomed. Quartz and feldspar grain boundaries tend to be straight rather than embayed and there are fewer sub-grains. Biotite grains show more random orientation toward the north. It is common, however, to see 1-2 mm wide shear zones in a thin section. In these shear zones sizes of quartz grains are reduced and fibrolite is concentrated and aligned with biotite parallel to foliation. If garnets are present, biotites wrap around the garnets. It is possible that these micro-shears developed after MCT movement, but because their appearence is so similar to the upper MCT zone it is more likely that they were synchronous.

At the Zatrwala pass east of Lukla a green calc-silicate rock overlies the biotite gneiss (Fig. 2.1, Plate 1). This unit is distinctive and can be traced from just east of Lukla, over the Zatrwala pass, down to the Hinku river and up to the ridge east of the Hinku. The mineralogy consists of: quartz, plagioclase, diopside, scapolite, sphene and traces of biotite. In thin section the rock generally appears undeformed, but there are small pockets where quartz grain size has been significantly reduced. At the lower contact of this unit there is a 10 m wide transition zone with alternating ~0.5 m thick layers of biotite gneiss and calc-silicate rock.

The majority of rock in the middle and upper levels of the Tibetan Slab is a biotite gneiss. The assemblage is generally quartz, plagioclase, K-feldspar, biotite, ± garnet, ± sericite, ± fibrolite, ±cordierite. Embayed grain boundaries are common, but rocks are not as deformed as within the MCT zone. Quartz grain size has been reduced within small zones in a thin section, and commonly these zones exhibit myrmekitic intergrowths of feldspar and quartz. Garnets are typically anhedral, and sometimes they are elongate parallel to foliation. K-feldspar grains are sericitized in many samples. The modal percentages of the constituent minerals vary, so that rock types range from biotite schist to leucocratic gneiss.

In the upper Tibetan Slab, both at Panch Pokhri in the upper Hongu valley and at Ngozumba in the upper Gokyo valley (Fig. 2.1), fibrolite occurs in ~5 mm thick mats, which are circular (20-30 mm in diameter) when viewed on the foliation plane. Within these mats individual fibrolite grains are sometimes parallel to foliation and sometimes the aggregates are internally folded. In the upper Gokyo valley the fibrolite mats are within a biotite schist that occurs as layers and lens shaped bodies within a leucogranitic matrix (Fig. 2.7).

Figure 2.7 Biotite schist layers within leucogranite in the upper Tibetan Slab, Ngozumba. Field of view is ~100m.

Figure 2.8 Folded amphibolite boudin within biotite gneiss in the Tibetan Slab, Mera La. In the upper center portion of the photo is a lense or boudin of actinolite-bearing amphibolite.

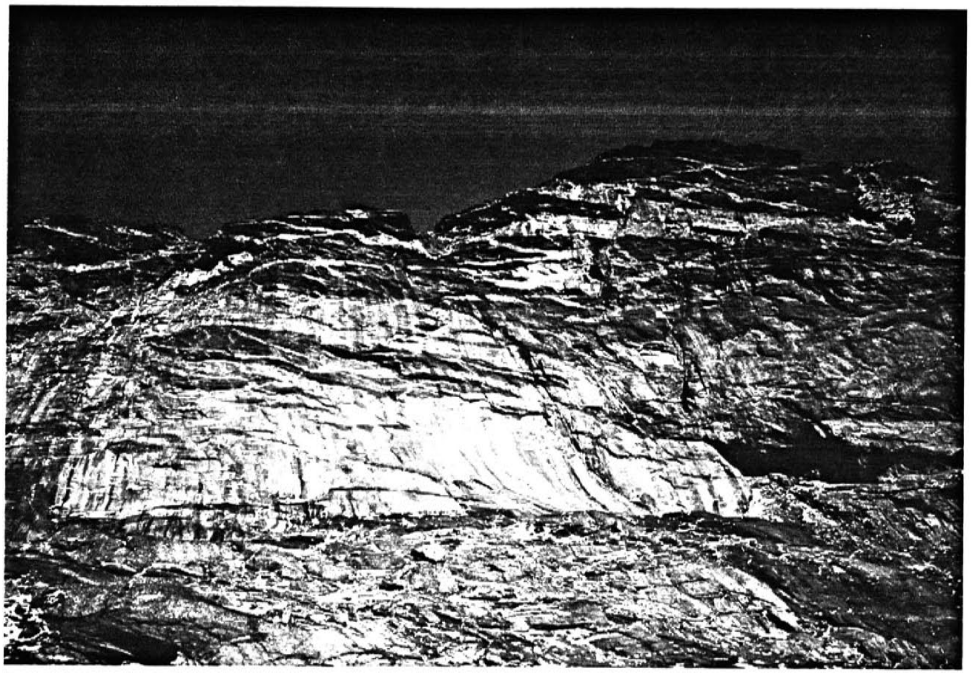

Figure 2.7

Figure 2.8

Augen gneiss units also occur within the Tibetan Slab. These rocks occur most frequently as river cobbles along the Dudh Kosi river south of Namche, though an augen gneiss does exist in outcrop on the route between Namche and Thame.

Calc-silicate rock occurs in outcrop by the trail south of Namche and at Mera La between the upper Hinku and the Hongu river valleys. Similar lithologies were found to the north in float in the upper Hongu valley and in the upper Gokyo valley. The mineralogy consists of quartz, plagioclase, diopside, sphene, ±calcite, ±epidote, and ±garnet. South of Namche the calc-silicate unit is tightly folded.

Amphibolites also occur in the middle and upper Tibetan Slab. On the east side of Mera La amphibolite occurs as lenses or boudins that have been folded in with the biotite gneiss (Fig. 2.8). The amphibole in this rock is coarse-grained actinolite. In the Gokyo valley a hornblende amphibolite was collected for $^{40}Ar/^{39}Ar$ age dating (see Chapter 4).

Rocks throughout the Tibetan Slab are migmatized and intruded by leucogranitic pegmatites. In some places cross-cutting relations suggest multiple intrusions. Toward the north leucogranitic intrusives increase in volume. The largest granitic body in the study area is exposed on the south face of Nuptse (Fig. 2.9). Mineralogy of the leucogranite varies somewhat, but generally includes: quartz, plagioclase, K-feldspar, biotite, muscovite, and tourmaline. Toumaline can be found in radial aggregates or it may be in small individual grains. Often muscovite only occurs as sericite within the K-feldspars. The leucogranite is generally not foliated in this area. A variety of workers have

Figure 2.9 Aerial view to the northeast of Nuptse, Everest, and Lhotse. Leucogranite contact with the overlying black biotite gneiss, which has been injected with a network leucogranitic dikes, exposed on the south face of Nuptse. The top of Everest is seen just left of center along the skyline of this photo and Lhotse is the peak seen just right of center. Photo courtesy of Brad Washburn.

Figure 2.9

courtesy of Brad Washhburn

Figure 2.10 Mt. Everest, view to the east. Approximate location of the "yellow band" and probable site of the normal fault contact between the Tibetan Slab and the overlying Tethyan Himalaya is shown.

Figure 2.11 Gyachung Kang, view to the northeast. Probable site of normal fault contact is shown and its identification is based on observed color difference and slight angular discordance. Float rock of carbonate and shale, which lithologies of the Tethyan Himalaya are found in the glacial moraine southwest of this peak.

Figure 2.10

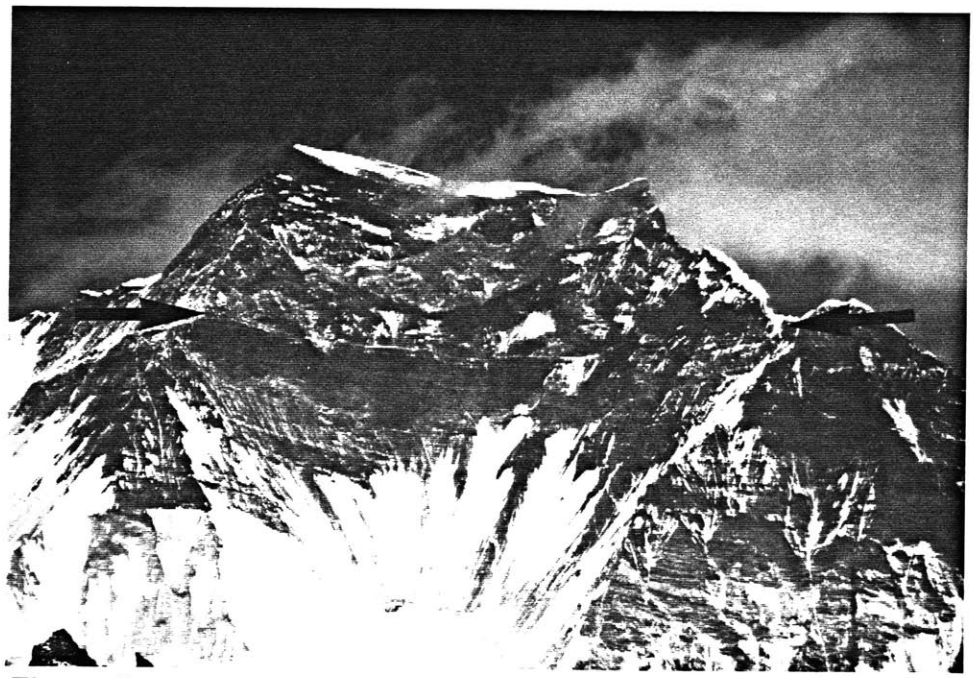

Figure 2.11

dated leucogranites from the Everest region with a variety of techniques and the age is generally considered to be late Oligocene- early Miocene. See chapter 4 for a summary of ages.

The upper contact of the Tibetan Slab is a normal fault first identified in this area by Burg et al. (1984). The normal fault is visible, but not readily accessible, at two places in the study area. The classic "yellow band" of Mt. Everest approximately marks the normal fault (Fig.2.10). Above this level lithologies of carbonate and shale are a lower metamorphic grade than gneisses of the uppermost Tibetan Slab. Float rock of the carbonate and shale are found in the lateral moraine of the Khumbu glacier. The normal fault contact can also be seen on the south face of Gyachung Kang at the head of the Gokyo valley (2.11).

STRUCTURE

A study of structures, from micro- to macro-scale, can yield useful clues regarding the deformational history of an area. Microstructures and metamorphic textures are also useful for determining the temporal relationship between deformation and metamorphism. In an effort to decipher the complex deformational and metamorphic history in eastern Nepal microstructural, textural, and macrostructural data were compiled and are discussed in the following sections. Interpretations of metamorphic textures are consistent with those described in Spry (1969).

Lesser Himalaya

Outcrop of the Okhaldunga Unit in the study area occurs as a small structural dome. Figure 2.12 shows the spread of schistosity orientations

Figure 2.12 Plot of poles to schistosity, Lesser Himalaya. Plot is a lower hemisphere, equal area projection.

Lesser Himalaya
poles to
schistosity

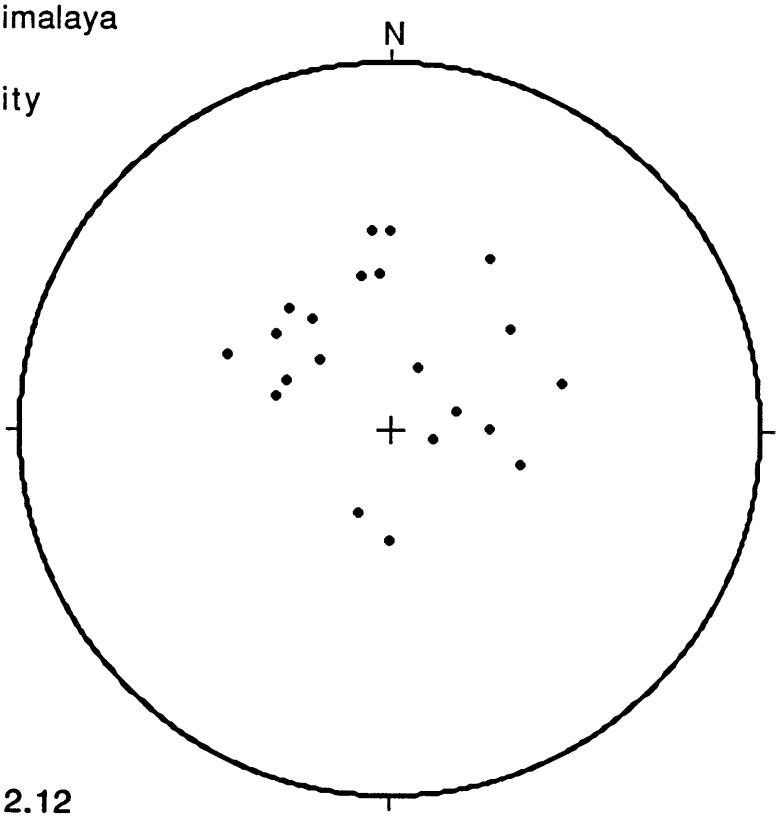

Figure 2.12

around this dome. The shortage of S-plunging points reflects sampling inconsistency rather than lack of N-dipping schistosity. This dome may be the result of the superimposition of a broad N-S trending fold, as seen to the east in the Arun valley (Hashimoto et al., 1973),and a broad E-W trending fold, as seen to the north in the upper Tibetan Slab (this study). These folds may have developed in separate events or they may be related to ramping on a lower structure (MBT). The combination of a ramp and a lateral ramp could simultaneously create N-S and E-W trending structures.

Micas define the dominant schistosity in the Okhaldunga Unit. This schistosity is commonly crenulated particularly in the most mica-rich rocks. The axes of the crenulation trend, predominantly, E-W, but in some cases there is a very short wavelength (<2mm) crenulation with N-S axes. If there is true graded bedding in this formation, as previously mentioned, then schistosity must be roughly parallel with original bedding. There is evidence, however, that an earlier foliation has been folded. Figure 2.13 is a photomicrograph which shows a folded and broken quartz layer. The layering of micas is not affected by this fold, suggesting that the dominant schistosity formed after an earlier folding event.

In addition to the large and small scale folding there has been internal shearing. Figure 2.14 shows a sharp angular discordance within the foliation possibly due to late brittle movement. Other samples from the Okhaldunga Unit show an S-C fabric that suggests ductile deformation. The sense of shear inferred from this fabric is "top-to-the-south" on both the north and south sides of the dome. I interprete this fabric to be the result of thrust movement that pre-dates formation of the dome.

Figure 2.13 Folded quartz layer in the Okhaldhunga Unit. The two limbs of the fold are intact, whereas the hinge has been attenuated. The dominant schistosity is oblique to the lower limb and is not folded by around the axis of the fold, suggesting that schistosity development postdates this folding event. Length of image is 13 mm.

Figure 2.14 Angular discordance within Okhaldhunga Unit. The discordance, which is indicated by the arrows, may be due to late brittle deformation. Length of image is 13 mm.

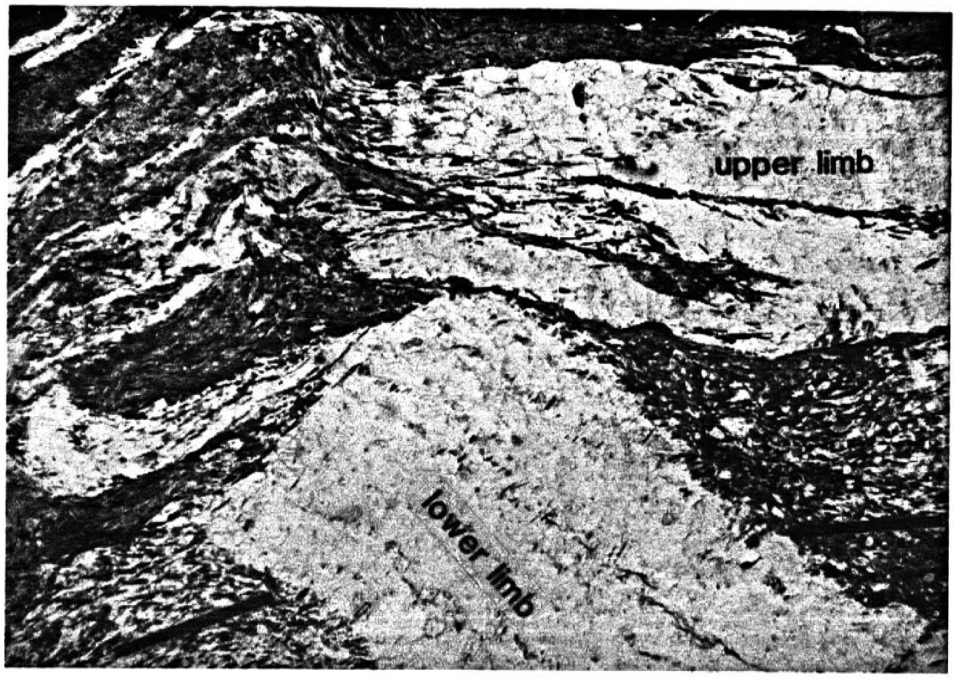

Figure 2.13

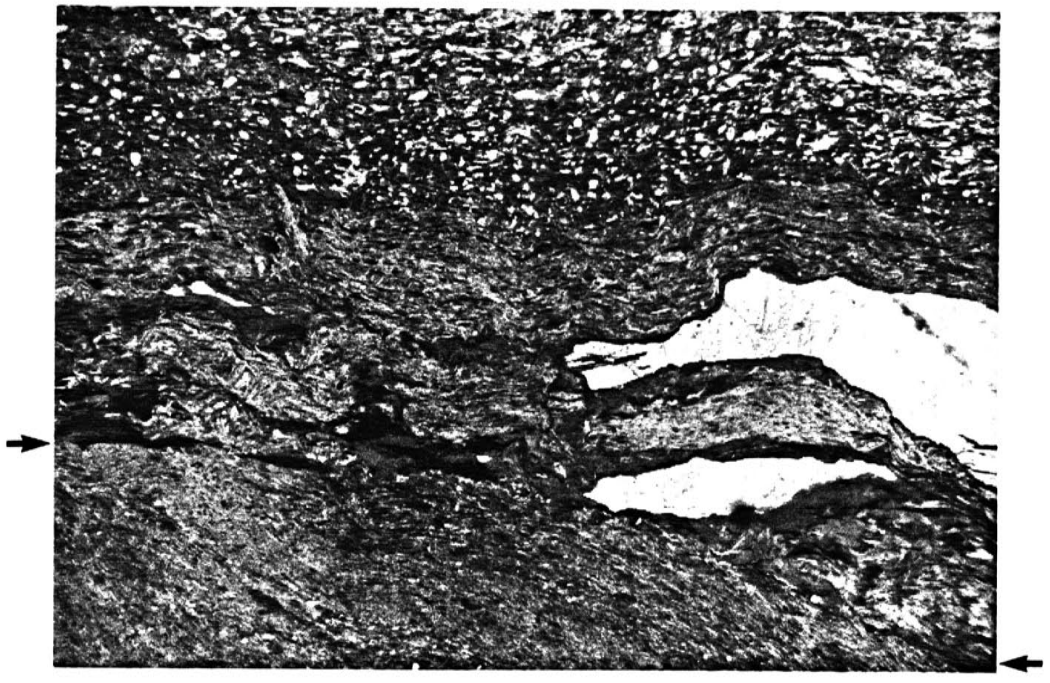

Figure 2.14

Garnets of the Okhaldhunga formation are small (≤1mm), but have sigmoidal inclusion trails that are continuous with foliation, suggesting syn-tectonic garnet growth. Occasional inclusion-free overgrowths may indicate minor post-tectonic garnet growth.

Main Central Thrust Zone

Within the MCT zone lithologic contacts are roughly parallel to schistosity. Between the Dudh Kosi and Hongu rivers schistosity dips northward ~30-60°. East of the Hongu schistosity dips east to southeast ~25-50°. This change in schistosity orientation is due to the same broad folds which caused doming of the Lesser Himalaya in this area. Figures 2.15a&b show plots of schistosity orientation for MCT zone outcrops west of the Hongu and east of the Hongu. Mineral lineations west of the Hongu plunge gently N-N30E (Fig 2.16a), and east of the Hongu they plunge gently S-S50E (Fig. 2.16b).

Textures from various lithologic units shed some light on the relative timing of mineral growth and deformation. Quartz grains in the Phaplu augen gneiss are generally recrystallized, but there are zones of very fine quartz grain size that may reflect size reduction during a deformation that post-dates foliation development. In garnet-mica schist 1 inclusion trails are helicitic, but are not continuous with the matrix foliation thus suggesting syn-tectonic garnet growth followed by some degree of continued shear deformation.

Garnets in garnet-mica schist 2 suggest a complex history of deformation and metamorphism. Below the kyanite isograd garnets occur in two sizes: 1-2mm and <1mm. The larger garnets have helicitic quartz inclusion trails in the

Figure 2.15 Plots of poles to schistosity , MCT zone. a) Data are from the region west of the Hongu river. b) Data are from the region east of the Hongu river. Plots are lower hemisphere, equal area projections.

MCT zone
west of Hongu
poles to schistosity

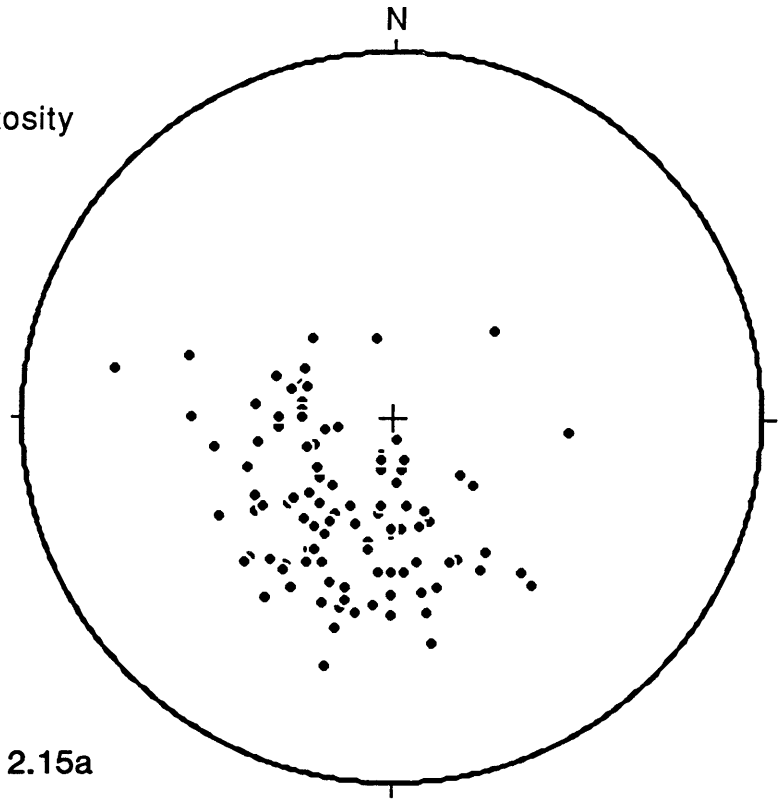

Figure 2.15a

MCT zone
east of Hongu
poles to schistosity

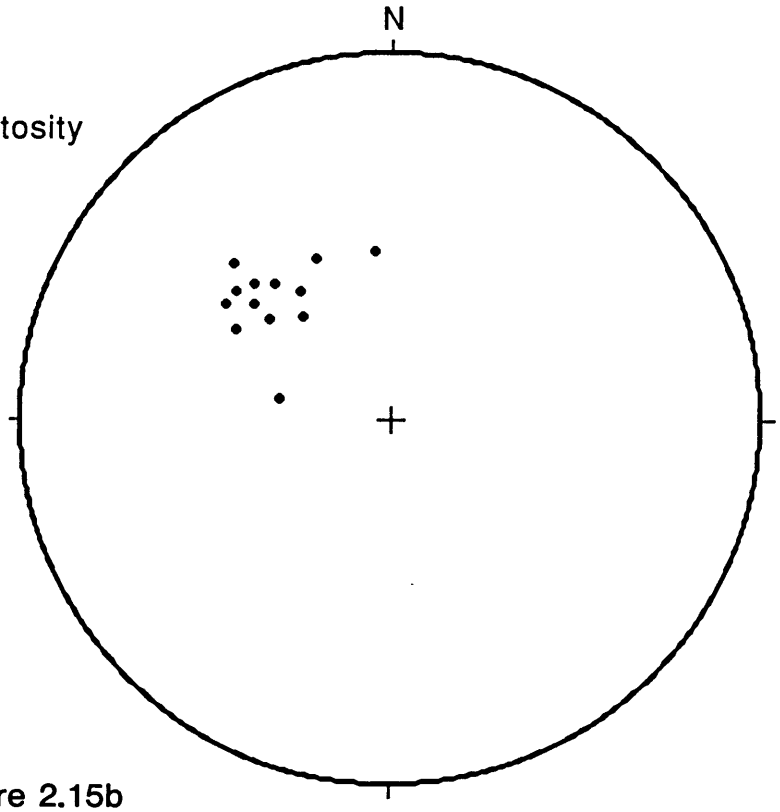

Figure 2.15b

Figure 2.16 Plots of lineation, MCT zone. a) Data are from the region west of the Hongu river. b) Data are from the region east of the Hongu river. Plots are lower hemisphere, equal area projections.

MCT zone lineation
west of the Hongu

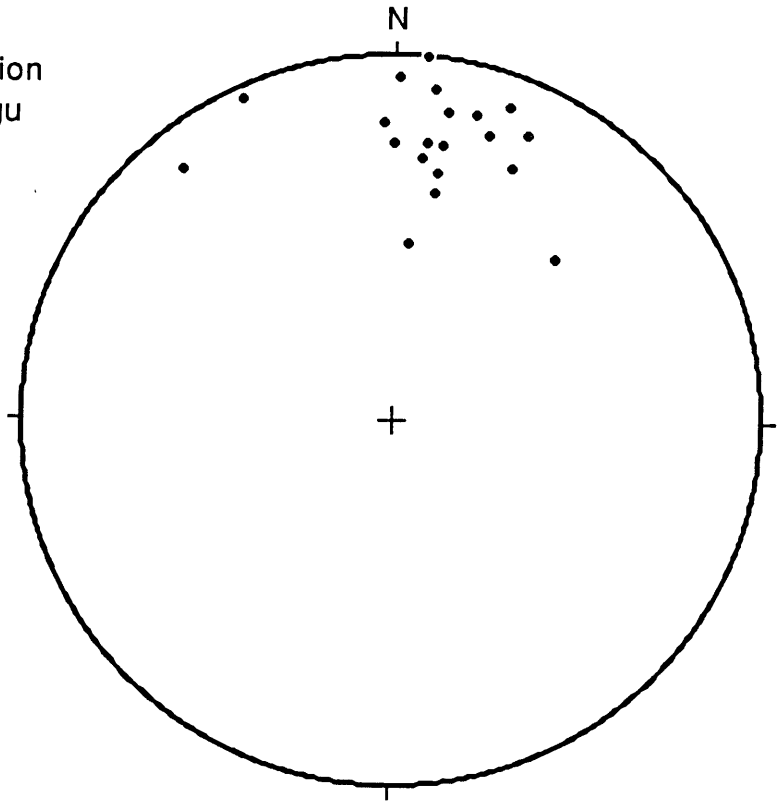

Figure 2.16a

MCT zone lineation
east of the Hongu

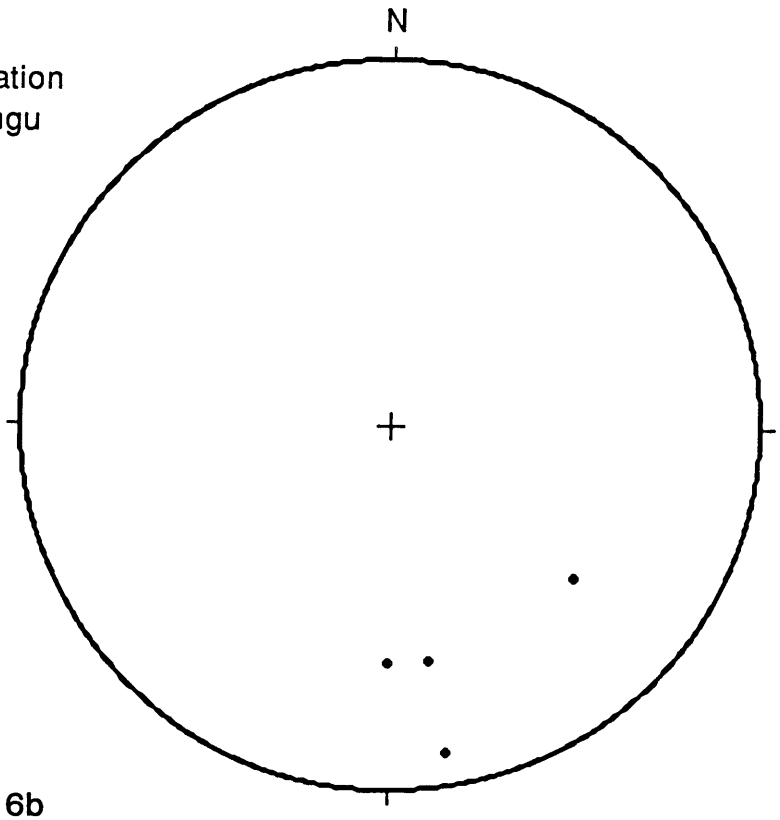

Figure 2.16b

core and an inclusion-free rim. Smaller garnets are inclusion-free. The inclusion trails in the large garnets are indicative of syn-tectonic garnet growth, but the inclusion-free rims suggest a second stage of garnet growth that could be syn- or post-tectonic. Within the kyanite zone one sample has helicitic trails in both the core and overgrowth of the garnets, thus suggesting two stages of syn-tectonic garnet growth.

Textural relations with phases other than garnet in garnet-mica schist 2 are also complex. In some cases the mica foliation wraps around staurolite grains suggesting pre- or syn-tectonic growth, but in other cases staurolites appear to cut across the foliation suggesting post-tectonic growth. Quartz grains are coarse and polygonal except where grain growth appears to have been limited by micas. This relation suggests quartz recrystallization following schistosity development. Undulatory extinction, however, suggests a degree of later strain. In one sample kyanite is actually bent around a garnet suggesting deformation after growth of kyanite. One possible explanation is that the kyanite grew during a pre-MCT metamorphic event and was deformed during MCT movement. Another possibility is that the kyanite grew during MCT movement and was bent during a later deformation.

Garnets of the quartzite/micaceous quartzite have helicitic cores with relatively inclusion-free rims, but the garnets are elongate and inclusion-free rims exist only at the long ends (Fig. 2.17). Helicitic cores suggest early syn-tectonic garnet growth, and the relation with matrix micas suggests that tectonism also followed garnet growth. Perhaps the two stages of garnet growth occured during a single tectonic progression. Alternatively the inclusion-free garnet rims may have grown between two tectonic events.

Figure 2.17 Elongate garnet from the quartzite/micaceous quartzite unit in the upper MCT zone. Garnets are characterized by a helicitic core with rims that contain many fewer inclusions and exist only at the long ends of the garnet. The image is seen in plane-polarized light and is 4mm long.

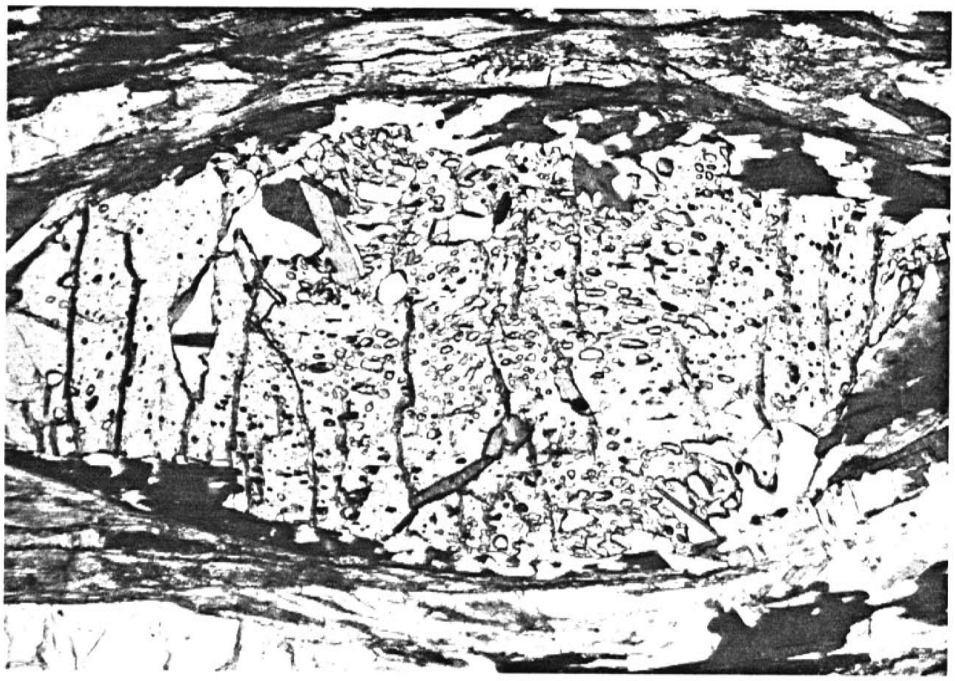

Figure 2.17

Structures within the upper augen gneiss of the MCT zone are complex. Figure 2.18 shows the lower contact of this unit which is tectonic and slightly oblique to the S_1 schistosity. This figure also shows shear zones within the augen gneiss which have a thrust sense and are oblique to both the S_1 schistosity and the lithologic contact. Figure 2.19 is a close up of one of these shear zones.

Pressure shadows around garnets in the biotite gneiss at the top of the MCT zone suggest pre- or syn-tectonic garnet growth.

Tibetan Slab

Schistosity in the Tibetan Slab in the Hinku and Hongu valleys and the Dudh Kosi valley south of Namche is generally north-northeast dipping (Fig. 2.20a). North of Namche a series of broad E-W trending folds affect the schistosity(Plate 1, Plate 2 section B-B'). Figure 2.20b is a stereo plot of poles to schistosity from the Gokyo valley where these folds are visible. The poles do not fall on a great circle suggesting that rocks are not folded around a single axis trend, but rather deformation is more complex. To the northeast of Namche in the village of Thame a large recumbent fold can be seen on the north face of the peak Kongde Ri (Fig. 2.21). The style of this fold is different than those mapped in the Gokyo valley, but it affects rocks of the same structural level. Thus perhaps deformation related to this folding phase together with the broad E-W folding is responsible for the scatter of foliation orientations in the upper Tibetan Slab.

Many of the rocks within the Tibetan Slab show evidence for a minor degree of shear. There are also, however, zones of much more intense

Figure 2.18 Lower contact of the augen gneiss unit in the upper MCT zone. Contact is outlined by the dashed line and is slightly oblique to the schistosity.

Figure 2.19 Shear zone near the lower contact of the augen gneiss unit, upper MCT zone. Shear zone cuts the dominant schistosity, suggesting that this shear deformation postdates schistosity development. Bending of the schistosity into the shear zone indicates probable thrust sense of shear (photo taken to the east, so south is to the right in this picture).

Figure 2.18

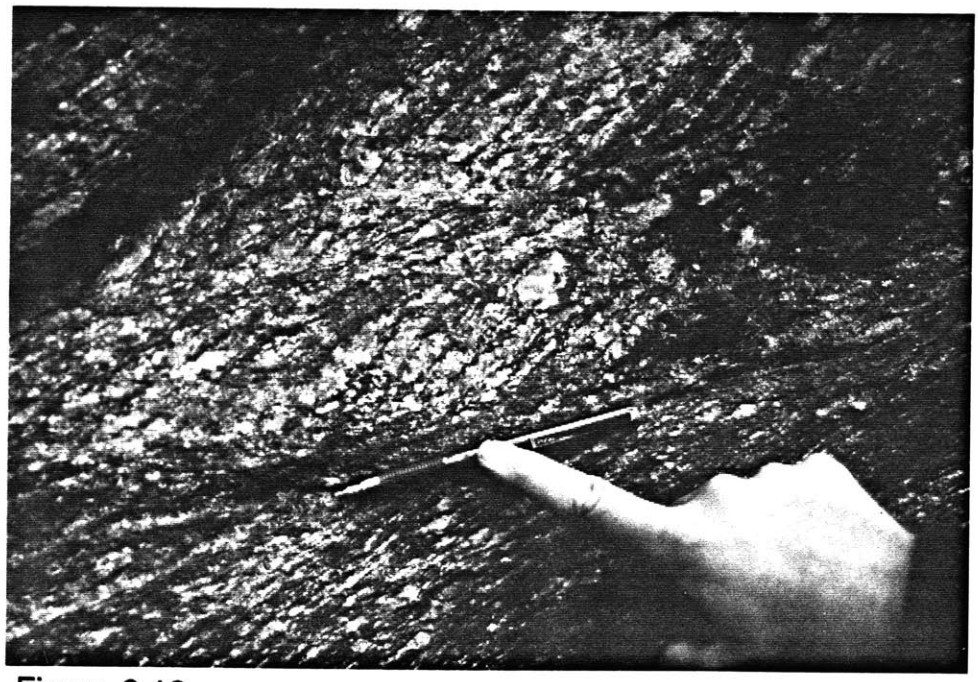

Figure 2.19

Figure 2.20 Plots of poles to schistosity, Tibetan Slab. a) Data are from the Hinku and Hongu valleys and the region south of Namche in the Dudh Kosi valley. b) Data are from the Gokyo valley, north of Namche. Plots are lower hemisphere, equal area projections.

TIBETAN SLAB
south of Namche

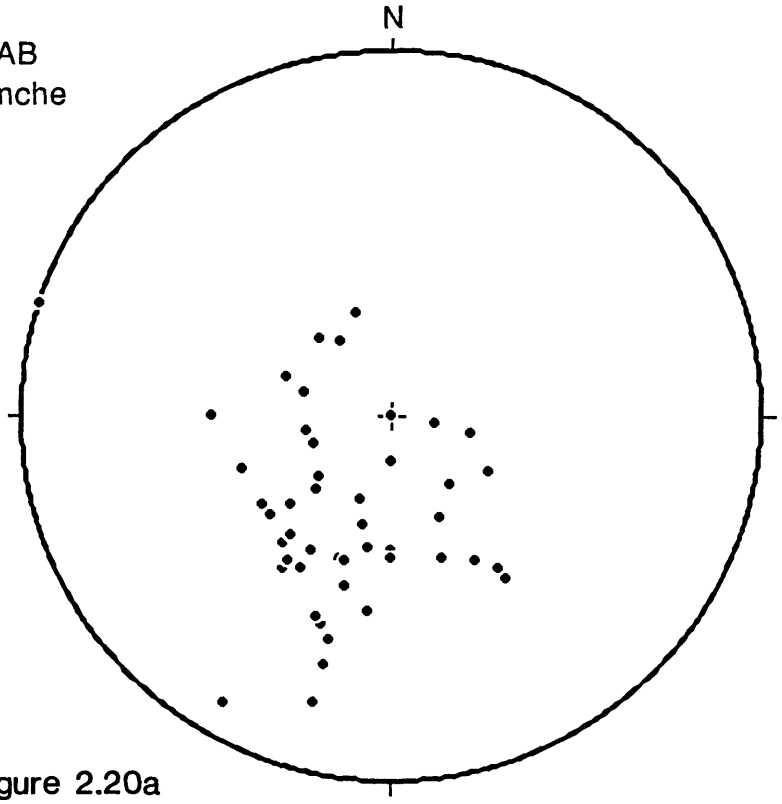

Figure 2.20a

TIBETAN SLAB
north of Namche

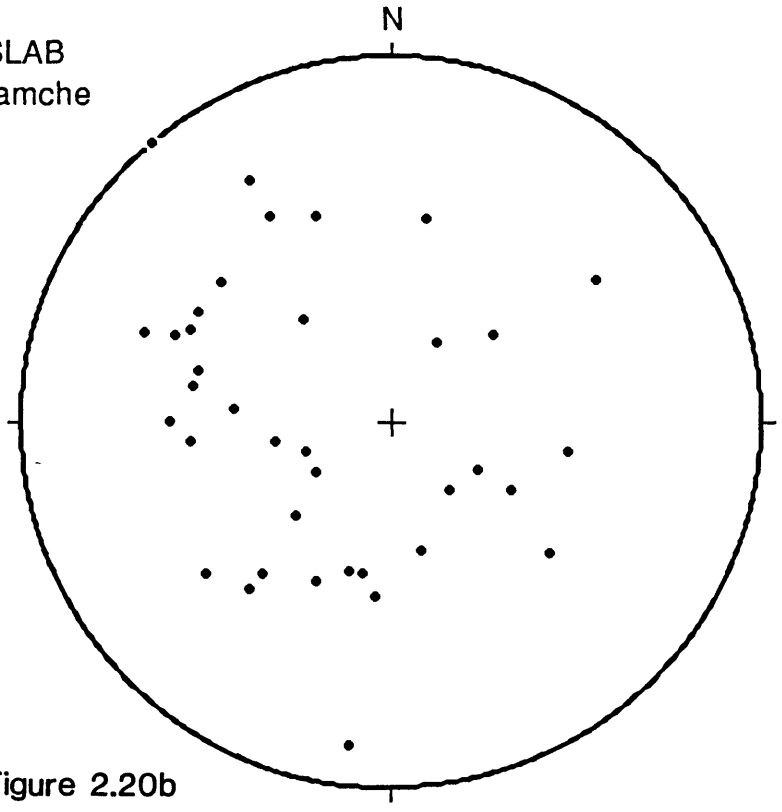

Figure 2.20b

Figure 2.21 Recumbant folds in the Tibetan Slab, north face of Kongde Ri. Traces of the axial planes are indicated by the dotted lines. Vertical relief on the face is ~1400m.

Figure 2.22 Protomylonitic texture from a shear zone within the Tibetan Slab. Shear zone is north of Namche near Kumjung. Orientation of broken K-feldspar porphyroclasts suggests top-to-the-north sense of shear. North is to the left in this photo (crossed nicols). Image is 13 mm long.

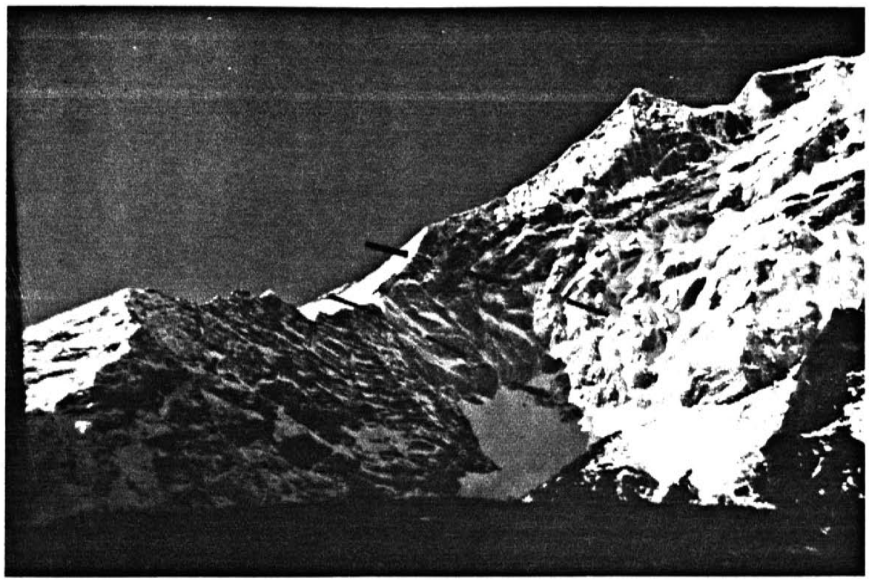

Figure 2.21

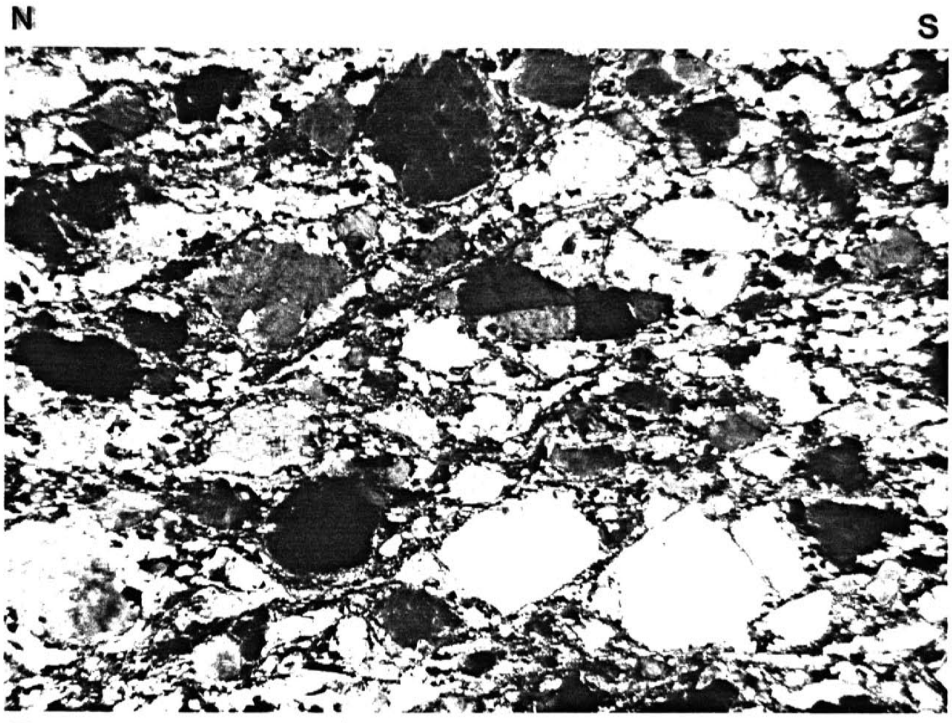

Figure 2.22

deformation. These zones are recognized by protomylonitic textures. Three of these zones were recognized along the Dudh Kosi river and its northern continuation, the Imja Khola. One zone occurs northeast of Lukla near Chaunrikharka, one farther north near Ghat (these two are at quite similar structural levels and may represent the same structural zone), and one north of Namche near Khumjung. Figure 2.22 shows the protomylonitic texture from the northernmost zone. The asymmetry of K-feldspars actually suggests normal (top displaced down to the north) sense of shear.

Structural Evolution

Structural data and observations at all scales have been compiled to outline a structural evolution of the study area. Indications of relative timing are not always evident and perhaps should be the subject of future study. With the available data the following evolution is proposed.

D_0 -- Evidence for the earliest deformation is seen in folds in the Lesser Himalaya which pre-date the dominant schistosity. This early deformation may also be responsible for some helicitic inclusion trails in garnets.

D_1 -- Major MCT shear deformation characterizes the D_1 deformation. The dominant schistosities across the lower Tibetan Slab, the MCT zone, and the upper part of the Okhaldhunga Unit are generally parallel and they are interpreted to be coeval and a result of D_1 deformation. The major metamorphism, accompanied by porphyroblast growth, across the lower Tibetan Slab, the MCT zone and the Okhaldunga Unit occured during the D_1 deformation. This deformation was also responsible for quartz sub-grain

development and recrystallization.

D_2 -- The D_2 deformation consists of late thrust-sense shearing as seen in the augen gneiss at the top of the MCT zone (Fig. 2.18 & 2.19) and possibly in several places in the Tibetan Slab. This event may also have caused quartz grain-size reduction in the MCT zone and crenulation development in the Lesser Himalaya, both of which post-date D_1.

D_3 -- Normal-sense shear deformation characterizes D_3. This deformation occurs within the Tibetan Slab and at its upper contact with the Tethyan sedimentary sequence. There is no solid evidence for the relative timing of this deformation which could be coeval with thrust deformation or it may post-date the thrust events.

D_4 -- The D_4 deformation consists of the development of broad folds which affect the Lesser Himalaya, the MCT zone, and the Tibetan Slab. As discussed above, the doming of the Lesser Himalaya and MCT zone in the study area could be the result of one event, or it could be the result of the superimposition of two events. Scattered schistosity orientations in the upper Tibetan Slab suggest multiple events at that structural level.

D_5 -- The D_5 deformation consists of minor brittle deformation which can be seen in the field in the MCT zone and petrographically in samples from one location in the Lesser Himalaya. There is no evidence for major displacement associated with brittle deformation.

SUMMARY

Field and petrographic study of the Main Central Thrust zone and adjacent units in eastern Nepal was aimed at understanding the

tectonostratigraphic position of the MCT zone, its deformational history (and that of the adjacent units) and its relation to metamorphism. The MCT is a zone (3-5 km thick) consisting of a variety of lithologies characterized by nearly penetrative shear deformation. Metamorphic isograds (Plate 2, section A-A') suggest a gradual increase in metamorphic grade across this zone from staurolite-grade in the structurally lower levels to sillimanite-grade in the upper MCT zone and overlying Tibetan Slab.

Underlying the MCT zone are the chlorite-bearing schistose and psammitic rocks of the Okhaldhunga Unit of the Lesser Himalaya. Metamorphic grade increases up-section as biotite and garnet are present in the upper 100-200 hundred meters.

The Tibetan Slab, consisting of schist, calc-silicate rock, amphibolite, and migmatitic gneiss, overlies the MCT zone. Leucogranitic material has intruded the Tibetan Slab in the form of dikes, sills and larger bodies. The volume of this leucogranitic material increases toward the north.

The structural evolution of this region of eastern Nepal is complex. Based on structural analysis and petrographic study of metamorphic textures a six-part deformational history has been proposed: D_0 - early folding, which is seen in the Okhaldhunga Unit; D_1 - MCT shear deformation accompanied by metamorphism and schistosity development in the MCT zone and adjacent units; D_2 - post-MCT thrust movement in the upper MCT zone and possibly the lower Tibetan Slab; D_3 - normal-sense shear deformation within the Tibetan Slab and at its upper contact with the Tethyan Himalaya; D_4 - broad folding of the Lesser Himalaya, the MCT zone, and the Tibetan Slab; and D_5 - minor brittle deformation in the MCT zone and the Lesser Himalaya. There is

evidence for the relative timing for most of these events, but the absolute timing is unclear, thus several of these events may be parts of one continuous deformation.

Chapter 3: THERMOBAROMETRIC CONSTRAINTS ON THE THERMAL HISTORY OF THE MAIN CENTRAL THRUST ZONE AND TIBETAN SLAB, EASTERN NEPAL HIMALAYA

Submitted to *Journal of Metamorphic Geology*
August, 1987
revised December, 1987

ABSTRACT

The Main Central Thrust (MCT) south of Mt. Everest in eastern Nepal is a 3 to 5 kilometer- thick shear zone separating chlorite-bearing schist in the lower plate from sillimanite-bearing migmatitic gneiss in the overlying Tibetan Slab. The metamorphic grade increases through the MCT zone toward structurally higher levels. Previous workers have suggested that either post- or syn-metamorphic thrust movement has caused this inversion of metamorphic isograds. In an effort to quantify the increase in grade and constrain proposed structural relations between metamorphism and slip on the fault, four well-calibrated thermobarometers were applied to pelitic samples collected along two cross-strike transects through the MCT zone and Tibetan Slab. Results show an increase in apparent temperature up-section in the MCT zone from 778K to 990K and a decrease in temperature to ~850K in the lower Tibetan Slab, which is consistent with syn-metamorphic thrust movement. A trend in calculated pressures across this section is less well-defined but, on average, decreases up-section with a gradient of ~28 MPa/km, resembling a lithostatic gradient. Pressure-temperature paths for zoned garnets from samples within the MCT zone, modeled using the Gibbs' Method, show a significant decrease in temperature and a slight decrease in pressure from core to rim, which might be expected for upper plate rocks during syn-metamorphic thrust movement. Samples from the uppermost Tibetan Slab yield higher temperatures and pressures than those from the lower Tibetan Slab which may be evidence for later "resetting" of thermobarometers by intrusion of the large amounts of leucogranite at that structural level.

INTRODUCTION

An inversion of metamorphic isograds in the Himalaya has been recognized in the vicinity of the Main Central Thrust (MCT), an intraplate subduction zone, for over 100 years (Oldham, 1883; Gansser 1964). During the past century the MCT and this metamorphic inversion have been identified and described all along the range. Nevertheless, only in the past 25 years has there been an appreciation for the significance of structural features such as the MCT, which may have over 100km of displacement (Gansser, 1966, Fuchs and Sinha, 1978; Brunel and Andrieux, 1977; Stöcklin, 1980). The more difficult task, and one that has received much recent attention, is to understand the relationships between movement on the MCT, metamorphic inversion, and leucogranitic magmatism in the upper plate of the MCT (Maruo and Kizaki, 1983; Brunel and Kienast, 1986; Hubbard, 1986; Le Fort et al., 1986; Schärer et al., 1986; Silverberg and Hodges, 1986). A thermobarometric study by Le Fort et al. (1986) in central Nepal suggests that the most recent metamorphism occurred during thrust movement along the MCT, and resulted from the emplacement of hot rocks at the base of the upper plate over cooler rocks of the lower plate. Maruo and Kizaki (1983) document an increase in temperature towards higher levels in the MCT zone and attribute this to frictional heat from discrete thrust planes. Brunel and Kienast (1986) suggest that the apparent metamorphic inversion is the result of post-metamorphic structural imbrication in the MCT zone. Each of these three models implies a different pattern of pressures and temperatures recorded by mineral equilibria (Figure 3.1). In an effort to distinguish among conflicting models, thermobarometry was combined with modeling of P-T paths for a suite of samples from the MCT zone and overlying Tibetan Slab in eastern Nepal.

Figure 3.1 Apparent temperature-depth and pressure-depth profiles resulting from: a) syn-metamorphic thrust movement, b) post-metamorphic thrust movement, c) frictional heating, dotted line represents addition of frictional heat to a syn-metamorphic thrust temperature profile. The addition of frictional heat moves the depth of maximum temperature closer to the level of the thrust plane.

Figure 3.1

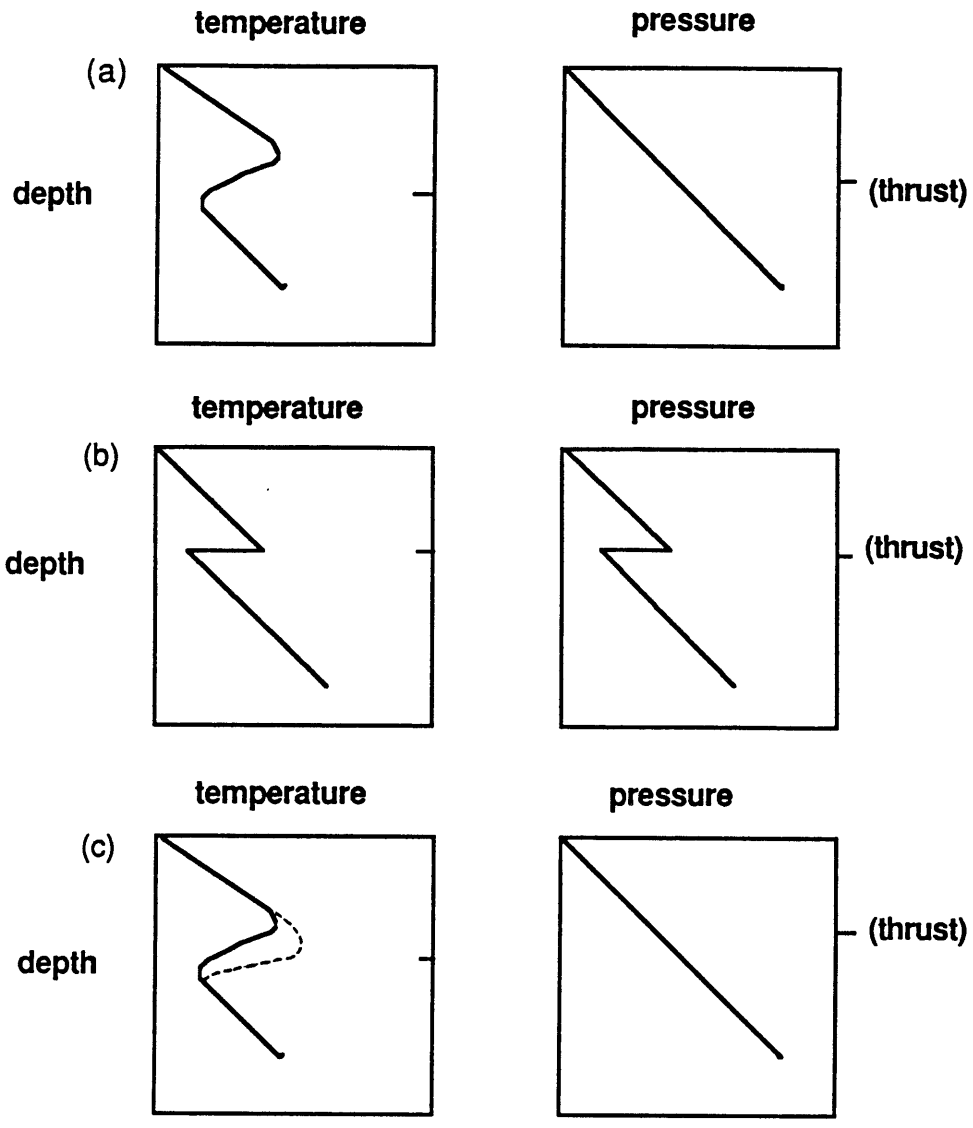
temperature
pressure
(a)
depth
(thrust)
temperature
pressure
(b)
depth
(thrust)
temperature
pressure
(c)
depth
(thrust)

GEOLOGIC SETTING

In the study area in eastern Nepal (Fig. 3.2) the Main Central Thrust (MCT) zone separates the chlorite-bearing sequence of the Lesser Himalaya from the overlying sillimanite grade gneisses of the Tibetan Slab. As in central Nepal (Pêcher, 1977), this thrust is recognized as a shear zone 3-5km in structural thickness. Within the zone a variety of lithologies are continuously mylonitic, though there are localized, foliation-parallel bands of higher strain. Rock types include augen gneiss, pelitic schist, calc-silicate rock, marble, slate, quartzite, amphibolite and a banded biotite gneiss. The majority of these lithologies are also represented in both the overlying Tibetan Slab and the underlying Lesser Himalaya, however in the MCT zone lithologic units are generally thinner and more highly strained than in the adjacent structural blocks. Contacts between these units in the MCT zone are roughly parallel to the foliation. The units are generally laterally continuous, though local discontinuities exist; these could be due to structural or stratigraphic truncation or poor exposure.

The apparent metamorphic grade across the MCT zone gradually increases toward structurally higher levels. Staurolite occurs in a mica schist unit within the lower MCT zone. Kyanite occurs together with staurolite in a few samples from the upper part of the staurolite-bearing section. Fibrolitic sillimanite and kyanite occur in the upper kyanite zone in the mid-upper MCT zone. Prismatic sillimanite and fibrolite occur together locally above the kyanite zone. Garnet can be found throughout both the MCT zone and overlying Tibetan Slab.

The upper and lower boundaries of the MCT zone are not distinct, so for the sake of discussion the author defines boundaries that include the majority of

Figure 3.2 Generalized tectonic map of the study area in eastern Nepal showing sample locations.

Figure 3.2

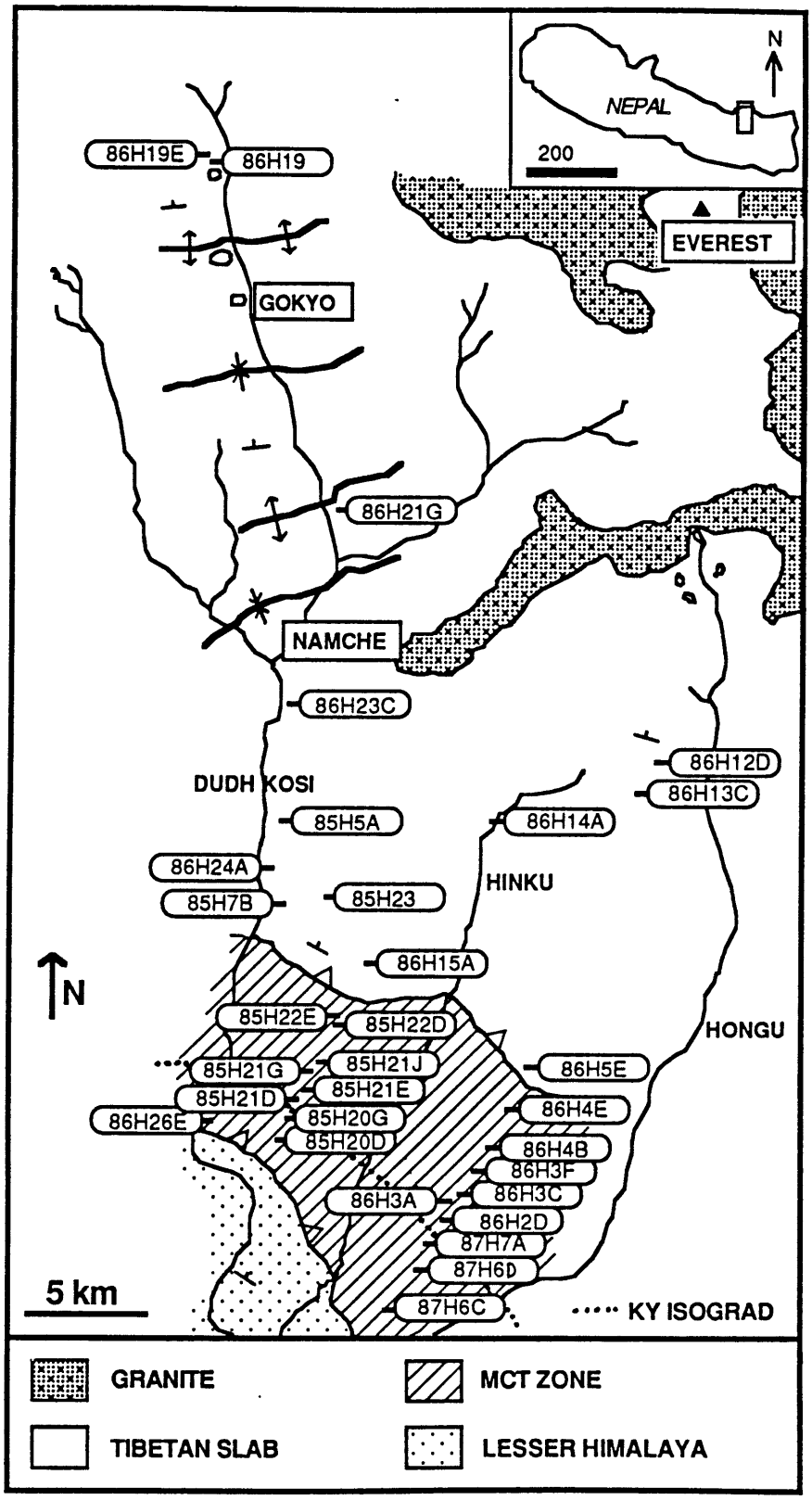
N
NEPAL
200
EVEREST
86H19E
86H19
GOKYO
86H21G
NAMCHE
86H23C
86H12D
86H13C
DUDH KOSI
85H5A
86H14A
86H24A
HINKU
85H7B
85H23
86H15A
N
85H22E
85H22D
HONGU
85H21G
85H21J
86H5E
85H21D
85H21E
86H4E
86H26E
85H20G
85H20D
86H4B
86H3F
86H3C
86H3A
86H2D
87H7A
87H6D
87H6C
5 km
KY ISOGRAD
GRANITE
MCT ZONE
TIBETAN SLAB
LESSER HIMALAYA

high strain zones. The lower boundary of the MCT zone is the contact of the lowermost augen gneiss within the zone (Phaplu augen gneiss) with the underlying fine-grained chlorite-muscovite schist of the Lesser Himalaya. The upper boundary of the MCT zone is within the upper gneiss unit but separates less-deformed, occasionally migmatitic gneisses to the north from the underlying more highly strained biotite gneisses of the upper MCT zone.

Below the MCT zone the Lesser Himalayan sequence consists of a thick section of fine-grained, intercollated pelites, psammites and quartzites. The pelites and psammites are generally light green and contain chlorite, muscovite, quartz, and occasionally plagioclase or K-feldspar. Garnet and minor biotite are found locally in the upper part of this unit.

The Tibetan Slab, which includes the majority of high peaks in this part of eastern Nepal, overlies the MCT zone. Lithologies of the Tibetan Slab consist of pelitic schist, gneiss, calc-silicate rock, minor amphibolite, and granite. The schist and gneiss units were not differentiated at the scale of mapping though their lithologies include: granitic gneiss, migmatite, course-grained augen gneiss, biotite-garnet gneiss and biotite-sillimanite schist, which occurs as pods within the granite in the upper section of the Tibetan Slab. North of the study area, in southern Tibet, the upper boundary of the Tibetan Slab is marked by a normal fault contact with low-grade calcareous rocks of the Tibetan Sedimentary sequence (Burg et al, 1984; Burchfiel and Royden, 1985). The normal fault may crop out in two places in this part of Nepal: once across the top of Mt. Everest and once across the top of a neighboring peak, Gyachen Kang.

Gneisses of the Tibetan Slab are foliated, though foliation is somewhat less penetrative than probable coeval mylonitic fabrics within the MCT zone.

This foliation is consistently oriented N70-80°W; 30-40°NE in both the Tibetan Slab and the MCT zone south of Namche. North of Namche (Fig. 3.2) the foliation is folded by E-W trending broad folds. Mylonite zones also occur within the Tibetan Slab, but the magnitude of displacement across them is unclear. Textural evidence is consistent with post-metamorphic movement and asymmetric augen suggest both normal and thrust sense of shear in various high-strain zones.

Granitic segregations containing the assemblage: quartz +K-feldspar +plagioclase +biotite ±tourmaline ±muscovite ±garnet ±sillimanite occur throughout the Slab. The quantity of leucogranitic bodies, and their size, increases toward the north. Intrusions appear as both dikes and sills and non-systematic cross-cutting relationships imply multiple generations. Some of the small granitic pods are interpreted as in-situ melts. Several of the largest granitic bodies are exposed on the peak Baruntse in the uppermost Hongu valley and on the south face of Nuptse, south of Mt. Everest (Fig. 3.2).

SAMPLE SELECTION AND PETROGRAPHY

Samples were collected along two cross-strike transects, one following the Dudh Kosi drainage and one generally following the ridge between the Hinku and Hongu drainages. For thermobarometry, samples were chosen that include the assemblage garnet +biotite +quartz +plagioclase ±aluminosilicate (kyanite and/or sillimanite) ±muscovite ±rutile ±ilmenite. Eighteen samples were collected along the Dudh Kosi transect, which is 44km long and includes samples from the lowest unit in the MCT zone, the Phaplu Augen gneiss, to the invaded schists and gneisses of the upper Tibetan Slab high in the Gokyo valley. The Hinku-Hongu transect follows a ridge in the vicinity of the MCT

zone, but to the north it drops into the Hinku valley, and then crosses over into the upper Hongu valley. Thirteen samples were chosen from this route. Sample locations are shown in Fig.3.2.

Metamorphic textures vary with lithology and structural level but generally correlate between the two transects. Within the MCT zone, garnets are predominantly euhedral with an average diameter of 1-2mm. Helicitic inclusion trails are common in cores of the larger garnets. The foliation defined by the inclusions is discontinuous with matrix foliation. Inclusion-free overgrowths surround most helicitic garnets. Some samples have a bimodal size distribution with small inclusion-free garnets possibly coeval with overgrowths on the larger garnets. Though there is evidence for multi-stage garnet growth, the latest episode was either syn- or pre-kinematic relative to the existing foliation.

Garnets within the Tibetan Slab are generally subhedral to anhedral with a diameter of ~2-3mm. These samples are less deformed than those within the MCT zone so the relative timing of mineral growth and foliation development is difficult to ascertain.

Fibrolitic sillimanite occurs as mats and along the foliation plane both in the upper MCT zone and in the Tibetan Slab. Kyanite, which occurs only within the MCT zone, is pre- or syn-kinematic as it is aligned along the foliation plane and locally is bent around garnet porphyroblasts.

THERMOBAROMETRY

Techniques

In order to determine pressures and temperatures the garnet-biotite (GB)

geothermometer (Ferry and Spear, 1978) was applied together with 3 well-calibrated geobarometers (GAQP - Newton and Haselton, 1981; GMPB - Hodges and Crowley, 1985; and GRAIL - Bohlen et al., 1983; see Table 3.1). Mineral analyses were performed on the JEOL 733 Superprobe at MIT. In each sample the analyzed phases were in mutual contact or close proximity. All rim analyses were made as close to the grain boundary as possible (~3-5μm) in an effort to determine compositions of latest equilibration. Garnets were analyzed adjacent to quartz, plagioclase and biotite. Two or three analyses were carried out for each spot and, generally, two or three garnets were analyzed for each sample. The reported compositions (Table 3.2 and 3.3) are averages of all analyses of a particular phase in each sample. A Monte Carlo technique (Hodges and McKenna, 1987) was used to propagate standard deviations of measured compositions through a simultaneous solution of the thermobarometers in order to determine the precision of the calculated pressures and temperatures.

Some samples had assemblages suitable for either GAQP or GMPB. In these instances, GB-GAQP and GB-GMPB temperatures and pressures were nearly indistinguishable. For those samples the reported temperatures and pressures are from GB-GAQP. One sample, 85H21D, did not contain plagioclase, so for that case only the GRAIL equilibrium was used together with GB.

In samples 86H4B, 86H14A, and 86H12D, garnet compositions adjacent to biotite were different from those measured adjacent to plagioclase or quartz, implying localized Fe-Mg re-equilibration between garnet and biotite. In an attempt to correct for this effect, biotite analyses 10-15μm away from garnet, and garnet rim analyses away from biotite were used to calculate pressure and

Table 3.1 Thermobarometers

GB	$Mg_3Al_2Si_3O_{12} + KFe_3AlSi_3O_{10}(OH)_2 = Fe_3Al_2Si_3O_{12} + KMg_3AlSi_3O_{10}(OH)_2$ garnet biotite garnet biotite	Ferry and Spear (1978)
GAQP	$Ca_3Al_2Si_3O_{12} + 2Al_2SiO_5 + SiO_2 = 3CaAl_2SiO_8$ garnet ky/sil quartz plagioclase	Newton and Haselton (1981)
GMPB	$Fe_3Al_2Si_3O_{12} + Ca_3Al_2Si_3O_{12} + KAl_3Si_3O_{10}(OH)_2 = 3CaAl_2Si_2O_8 + KFe_3AlSi_3O_{10}(OH)_2$ garnet garnet muscovite plagioclase biotite	Hodges and Crowley (1985)
GRAIL	$3FeTiO_3 + Al_2SiO_5 + 2SiO_2 = 3Fe_3Al_2Si_3O_{12} + 3TiO_2$ ilmenite ky/sil quartz garnet rutile	Bohlen et al. (1983)

(solution models for impure phases as described in Hodges and Royden (1984))

Table 3.2 Composition Data - Dudh Kosi transect

sample number: component	86H26E	85H20D	85H20G	85H21D	85H21E	85H21G	85H21J	85H22D	85H22E
Xalm	0.526	0.802	0.822	0.735	0.724	0.813	0.805	0.835	0.812
	(0.025)	(0.004)	(0.004)	(0.011)	(0.012)	(0.010)	(0.005)	(0.005)	(0.009)
Xpyr	0.026	0.108	0.123	0.153	0.139	0.125	0.128	0.082	0.100
	(0.003)	(0.003)	(0.003)	(0.011)	(0.012)	(0.010)	(0.003)	(0.003)	(0.008)
Xgrs	0.279	0.072	0.046	0.094	0.117	0.032	0.042	0.049	0.044
	(0.030)	(0.002)	(0.002)	(0.006)	(0.007)	(0.002)	(0.005)	(0.002)	(0.002)
Xsps	0.170	0.018	0.009	0.018	0.020	0.030	0.024	0.034	0.044
	(0.017)	(0.002)	(0.001)	(0.002)	(0.001)	(0.003)	(0.002)	(0.004)	(0.003)
Xann	0.549	0.383	0.394	0.368	0.412	0.438	0.443	0.499	0.523
	(0.047)	(0.003)	(0.009)	(0.003)	(0.010)	(0.009)	(0.010)	(0.002)	(0.047)
Xphl	0.249	0.428	0.427	0.441	0.415	0.373	0.352	0.282	0.270
	(0.023)	(0.003)	(0.011)	(0.010)	(0.010)	(0.008)	(0.009)	(0.002)	(0.030)
Xab	0.778	....	....	....	....	0.888	0.800	0.713	0.722
	(0.003)	....	....	....	....	(0.003)	(0.002)	(0.035)	(0.009)
Xan	0.212	....	....	....	....	0.104	0.195	0.277	0.271
	(0.003)	....	....	....	....	(0.003)	(0.001)	(0.034)	(0.009)
Xmu	0.657	.*	.*	.*	.*	0.692	0.718	0.757	0.800
	(0.010)	.*	.*	.*	.*	(0.014)	(0.007)	(0.011)	(0.030)
AlSi	....	....	....	.ky	.ky	.ky	.ky	.sil	.sil

sample number: component	86H15A	85H7B	85H23	86H24A	85H5A	86H23C	86H21G	86H19C	86H19E
Xalm	0.682	0.732	0.764	0.686	0.763	0.730	0.711	0 680	0.728
	(0.013)	(0.005)	(0.012)	(0.006)	(0.011)	(0.002)	(0.005)	(0.007)	(0.002)
Xpyr	0.125	0.201	0.106	0.149	0.118	0.225	0.129	0.122	0.139
	(0.012)	(0.005)	(0.006)	(0.004)	(0.008)	(0.003)	(0.004)	(0.006)	(0.001)
Xgrs	0.147	0.031	0.049	0.113	0.042	0.029	0.029	0.069	0.041
	(0.010)	(0.002)	(0.011)	(0.002)	(0.002)	(0.001)	(0.001)	(0.002)	(0.001)
Xsps	0.046	0.037	0.081	0.052	0.076	0.020	0.131	0.129	0.092
	(0.005)	(0.002)	(0.007)	(0.003)	(0.011)	(0.001)	(0.005)	(0.006)	(0.002)
Xann	0.453	0.346	0.403	0.465	0.480	0.280	0.455	0.441	0.462
	(0.010)	(0.014)	(0.009)	(0.008)	(0.050)	(0.005)	(0.002)	(0.005)	(0.004)
Xphl	0.386	0.462	0.380	0.376	0.337	0.582	0.342	0.373	0.343
	(0.009)	(0.014)	(0.012)	(0.008)	(0.033)	(0.006)	(0.002)	(0.004)	(0.003)
Xab	0.537	0.746	0.752	0.441	0.680	....	0.742	0.568	0.628
	(0.005)	(0.021)	(0.005)	(0.018)	(0.022)	....	(0.002)	(0.007)	(0.003)
Xan	0.454	0.238	0.239	0.552	0.311	....	0.241	0.418	0.354
	(0.005)	(0.021)	(0.005)	(0.018)	(0.022)	....	(0.002)	(0.007)	(0.003)
Xmu	0.804	....	....	....	....	....	....	....	....
	(0.010)	....	....	....	....	....	....	....	....
AlSi	....	.sil	.sil	....	.sil	.sil	.sil	....	.sil

Numbers in parantheses are 2s sample standard deviations. *mineral present; analysis not used for thermobarometry

Table 3.3 Composition Data - Hinku-Hongu transect

component	sample number: 87H6C	87H6D	87H7A	86H2D	86H3A	86H3C	86H3F
Xalm	0.832	0.504	0.826	0.803	0.649	0.781	0.833
	(0.007)	(0.010)	(0.007)	(0.007)	(0.010)	(0.008)	(0.010)
Xpyr	0.069	0.027	0.121	0.140	0.091	0.134	0.104
	(0.003)	(0.002)	(0.006)	(0.005)	(0.007)	(0.007)	(0.010)
Xgrs	0.082	0.238	0.043	0.032	0.074	0.031	0.031
	(0.006)	(0.013)	(0.005)	(0.006)	(0.007)	(0.003)	(0.001)
Xsps	0.017	0.232	0.010	0.026	0.186	0.054	0.032
	(0.005)	(0.008)	(0.001)	(0.003)	(0.008)	(0.003)	(0.003)
Xann	0.498	0.565	0.442	0.407	0.432	0.462	0.492
	(0.012)	(0.010)	(0.013)	(0.012)	(0.007)	(0.008)	(0.011)
Xphl	0.312	0.265	0.369	0.400	0.385	0.360	0.316
	(0.012)	(0.008)	(0.014)	(0.015)	(0.006)	(0.007)	(0.010)
Xab	0.815	0.768	0.870	0.892	0.701	0.872	0.855
	(0.037)	(0.042)	(0.001)	(0.004)	(0.009)	(0.003)	(0.003)
Xan	0.183	0.225	0.125	0.106	0.295	0.121	0.142
	(0.037)	(0.042)	(0.001)	(0.004)	(0.009)	(0.003)	(0.002)
Xmu	0.702	0.670	0.648	0.647	0.712	0.717	0.707
	(0.037)	(0.012)	(0.091)	(0.034)	(0.012)	(0.020)	(0.032)
AlSi	....	....	....	.ky	....	.ky	ky.sil

component	sample number: 86H4B	86H4E	86H5E	86H14A	86H13C	86H12D
Xalm	0.727	0.704	0.779	0.736	0.770	0.742
	(0.005)	(0.030)	(0.007)	(0.010)	(0.022)	(0.014)
Xpyr	0.152	0.092	0.104	0.193	0.087	0.081
	(0.004)	(0.017)	(0.007)	(0.010)	(0.010)	(0.005)
Xgrs	0.075	0.049	0.065	0.020	0.034	0.022
	(0.002)	(0.007)	(0.002)	(0.002)	(0.004)	(0.001)
Xsps	0.046	0.156	0.053	0.051	0.129	0.156
	(0.001)	(0.032)	(0.002)	(0.005)	(0.022)	(0.015)
Xann	0.416	0.539	0.422	0.405	0.576	0.486
	(0.006)	(0.022)	(0.018)	(0.017)	(0.021)	(0.002)
Xphl	0.382	0.293	0.384	0.424	0.239	0.292
	(0.004)	(0.015)	(0.015)	(0.015)	(0.013)	(0.002)
Xab	0.557	....	0.608	0.814	....	0.802
	(0.011)	....	(0.007)	(0.011)	....	(0.023)
Xan	0.432	....	0.388	0.182	....	0.191
	(0.011)	....	(0.007)	(0.011)	....	(0.023)
Xmu	....	.*	....	....	.*	0.781
	....	.*	....	....	.*	(0.006)
AlSi	.sil	....	.sil	.sil	.sil	.sil

Numbers in parantheses are 2s sample standard deviations. *mineral present; analysis not used for thermobarometry

temperature. Euhedral garnets seem to provide the most stable rim composition data whereas anhedral garnets may have experienced significant retrogression as rim compositions are often quite variable.

Results

Figures 3.3a and b are plots of temperature and pressure vs. structural distance from the kyanite isograd for the Dudh Kosi transect. The position of the MCT zone in these plots is indicated by the bar at the top of the figures. Temperatures within the MCT zone show a distinct increase whereas pressures exhibit a less clear trend. Above the MCT zone the temperature trend takes two dips to relatively low (~800K) temperatures before climbing to an average temperature of about 1000K for the northernmost samples. The pressure profile above the MCT zone shows a peak at 976±206MPa and then levels out at ~500MPa.

Figures 3.4a and b are temperature-distance and pressure-distance plots for the Hinku-Hongu transect. Like the Dudh Kosi transect, temperatures from the Hinku-Hongu transect within the MCT zone show an increase from ~790K to 990K. Pressures within the MCT zone do not exhibit a consistent trend but vary between 500 and 800MPa. Above the MCT zone temperatures drop to 866K, climb to 997K and drop again to 861K. Pressures above the MCT zone are generally lower than those within the zone. Temperatures and pressures from both transects are tabulated with their uncertainties in Table 3.4.

Discussion of Thermobarometric Results

For purposes of discussion, data sets from both the Dudh Kosi and Hinku-Hongu transects were combined (Figs. 3.5a and b). In the most general

Figure 3.3 Thermobarometric results from the Dudh Kosi transect plotted versus structural distance above the kyanite isograd. Error bars indicate 2 estimated standard deviation precision. a) Temperature. b) Pressure.

Figure 3.3(a)

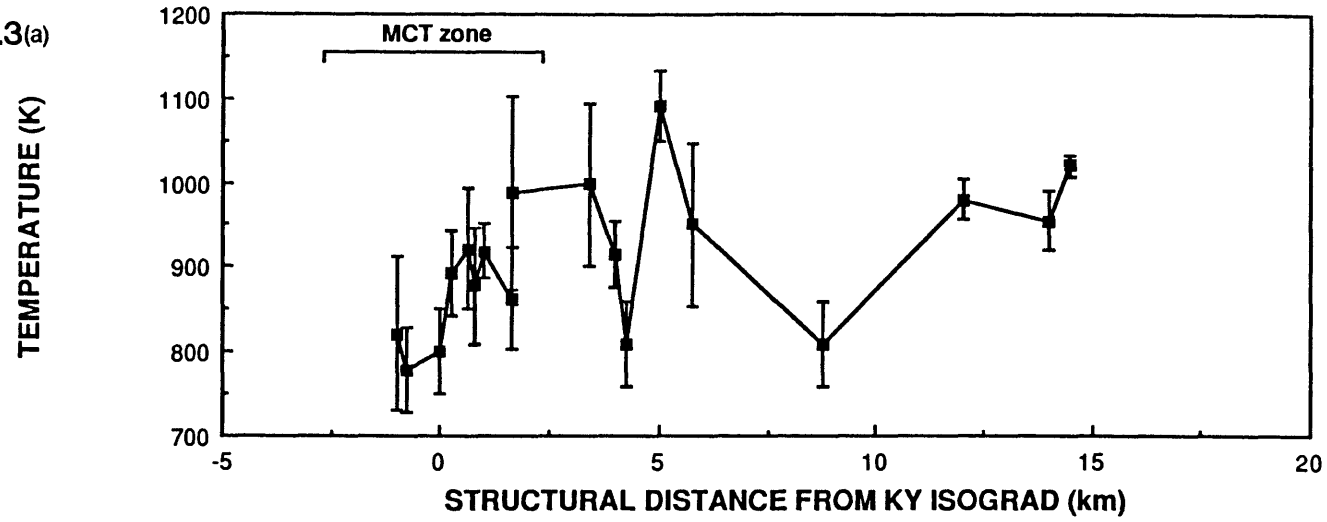

Figure 3.3(b)

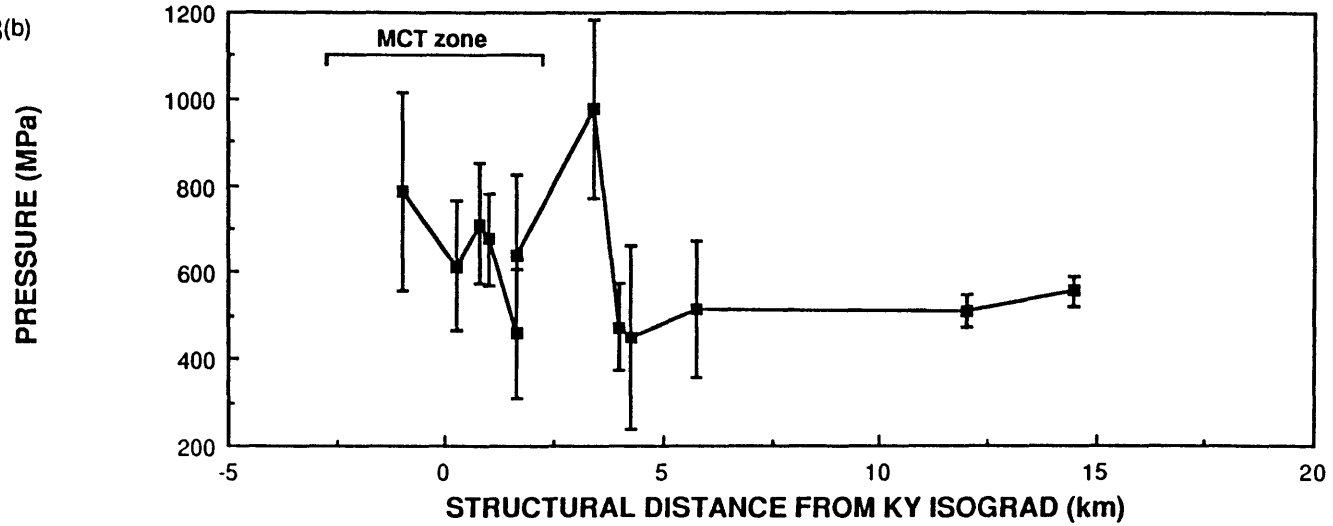

Figure 3.4 Thermobarometric results from the Hinku-Hongu transect plotted versus structural distance above the kyanite isograd. Error bars indicate 2 estimated standard deviation precision. a) Temperature. b) Pressure.

Figure 3.4(a)

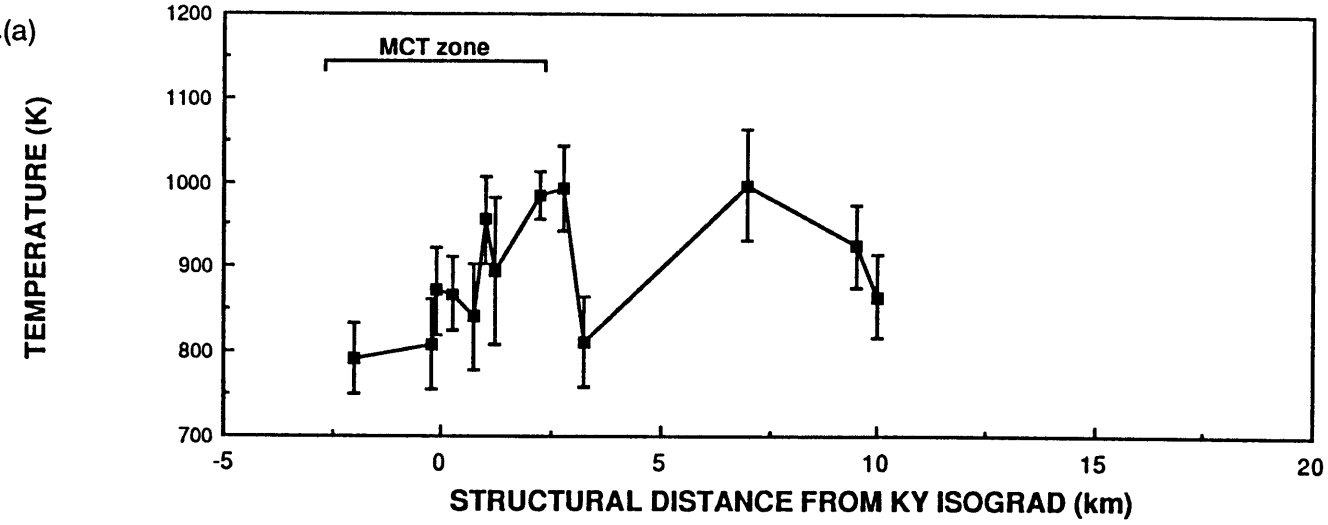

Figure 3.4 (b)

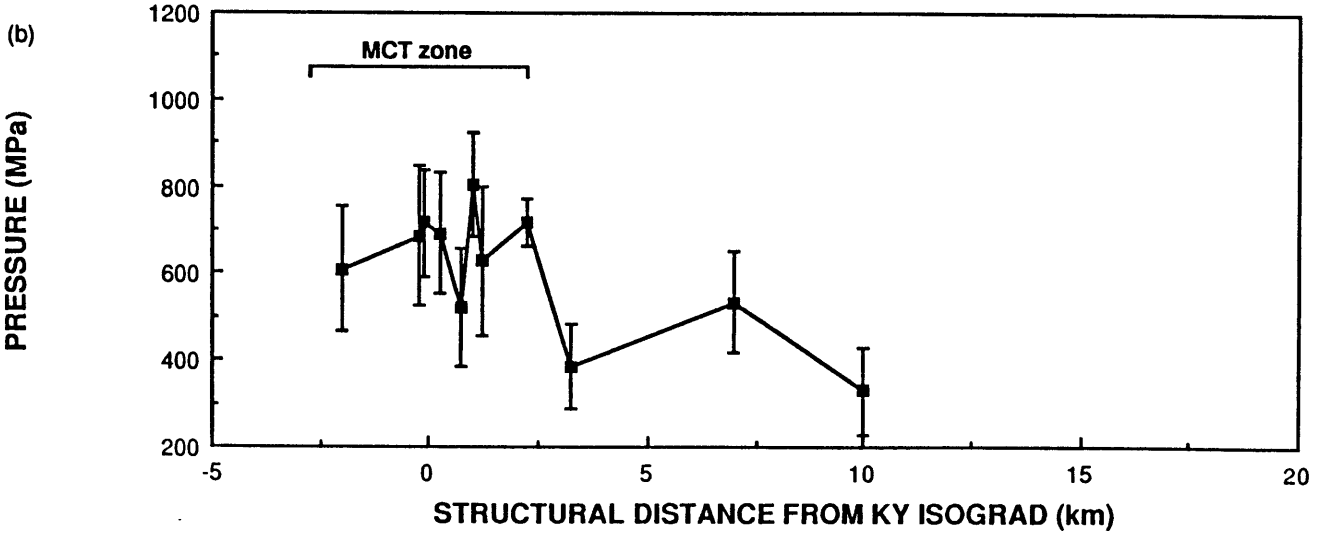

Table 3.4 Calculated Temperatures and Pressures

sample number	structural distance (km)	temperature (K)		pressure (MPa)	
Dudh Kosi Transect:					
86H26E	-1.00	821	±91	787	±228
85H20D	-0.75	778	±50	....	....
85H20G	-0.02	800	±50	....	....
85H21D	0.25	893	±50	615	±150
85H21E	0.62	922	±70	....	....
85H21G	0.80	878	±68	712	±139
85H21J	1.00	918	±32	678	±106
85H22D	1.63	863	±60	460	±150
85H22E	1.65	988	±114	641	±184
86H15A	3.43	998	±96	976	±206
85H7B	4.00	915	±38	473	±101
85H23	4.25	809	±50	451	±212
86H24A	5.00	1090	±42	....	....
85H5A	5.75	950	±95	516	±156
86H23C	8.75	810	±50	....	....
86H21G	~12.00	980	±24	509	±37
86H19C	~14.00	955	±35	....	....
86H19E	~14.50	1020	±12	557	±34
Hinku-Hongu Transect:					
87H6C	-2.00	793	±42	609	±144
87H6D	-0.25	808	±53	685	±160
87H7A	-0.13	872	±51	715	±123
86H2D	0.25	868	±43	691	±139
86H3A	0.75	842	±63	521	±137
86H3C	1.00	956	±52	803	±121
86H3F	1.20	895	±87	627	±170
86H4B	2.25	984	±28	714	±54
86H4E	2.75	993	±50	....	....
86H5E	3.25	812	±53	385	±96
86H14A	7.00	997	±65	533	±118
86H13C	9.50	925	±50	....	....
86H12D	10.00	866	±50	328	±102

sense there are three possibilities for the relationship of thrusting to latest metamorphic equilibration (or closure of thermobarometers) : 1) pre-metamorphic, 2)syn-metamorphic, or 3) post-metamorphic. The first case can be eliminated on textural evidence from samples within the MCT zone as metamorphic minerals have not grown across the foliation plane. The second case would result in a temperature profile that reflects the juxtaposed or overturned isotherms resulting from a "hot over cold" thrust scenario, as proposed be Le Fort (1975). The pressure gradient for this case should reflect a normal lithostatic gradient (Fig. 3.1a). The third case would result in saw-toothed shaped temperature and pressure profiles (Fig. 3.1b).

The curve shown in figure 5a is the lowest order polynomial (5 th order) which reasonably fits the data, excluding the northernmost three samples. Although the curve yields a correlation coefficient of only 0.65, it displays a trend consistent with Le Fort's (1975) model where isotherms have been overturned as the result of thrust emplacement. A higher order curve that provides a better fit to the data points on this part of the temperature-distance plot would contain many local maximums and minimums. The variations in data along this curve could be due to minor post-metamorphic thrust imbrication.

Above the MCT zone (Fig. 3.5a) the temperature curve shows a degree of irregularity that may be due to structural breaks within the Tibetan Slab, for which there is some field evidence. There may also have been thermal effects due to relatively young (~14-24Ma, Schärer et al., 1986) granitic intrusion. Brunel and Kienast (1986) suggest that the intrusion of leucocratic material may have caused general heating of the upper Tibetan Slab, which would explain the higher temperatures recorded in the uppermost units. This hypothesis implies that, whereas calculated pressures and temperatures within the MCT

Figure 3.5 Thermobarometric results from the Dudh Kosi and Hinku-Hongu transects plotted versus structural distance above the kyanite isograd. Error bars indicate 2 estimated standard deviation precision. a) Temperature data with 5^{th} order polynomial fit to data from the MCT zone and lower Tibetan Slab. b) Pressure data with straight line fit to data from the MCT zone and lower Tibetan Slab (slope ~28 MPa/km)..

Figure 3.5 (a)

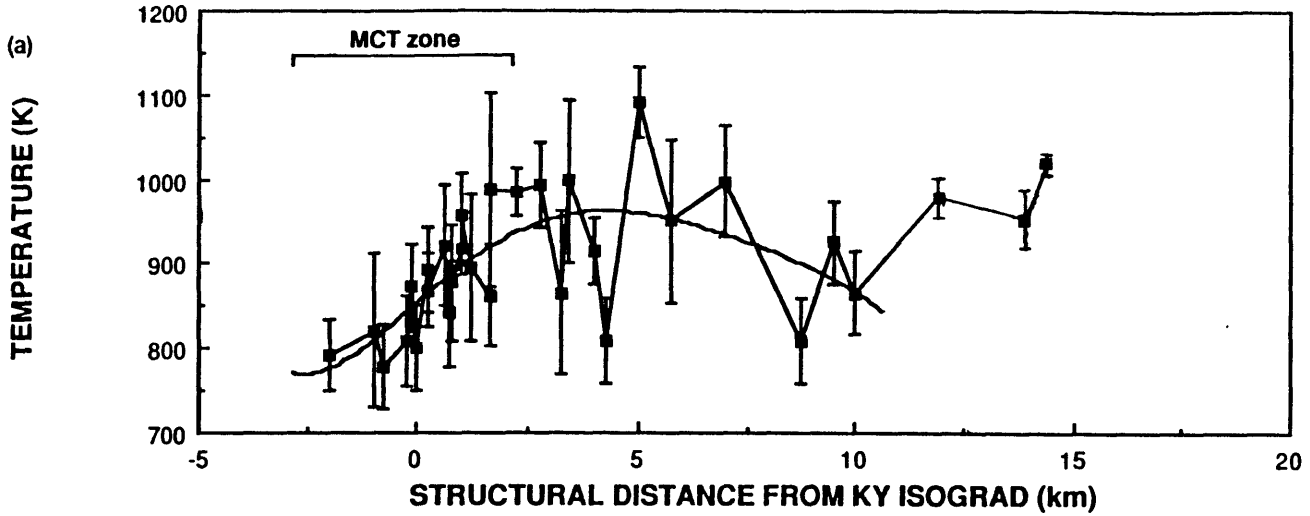

Figure 3.5(b)

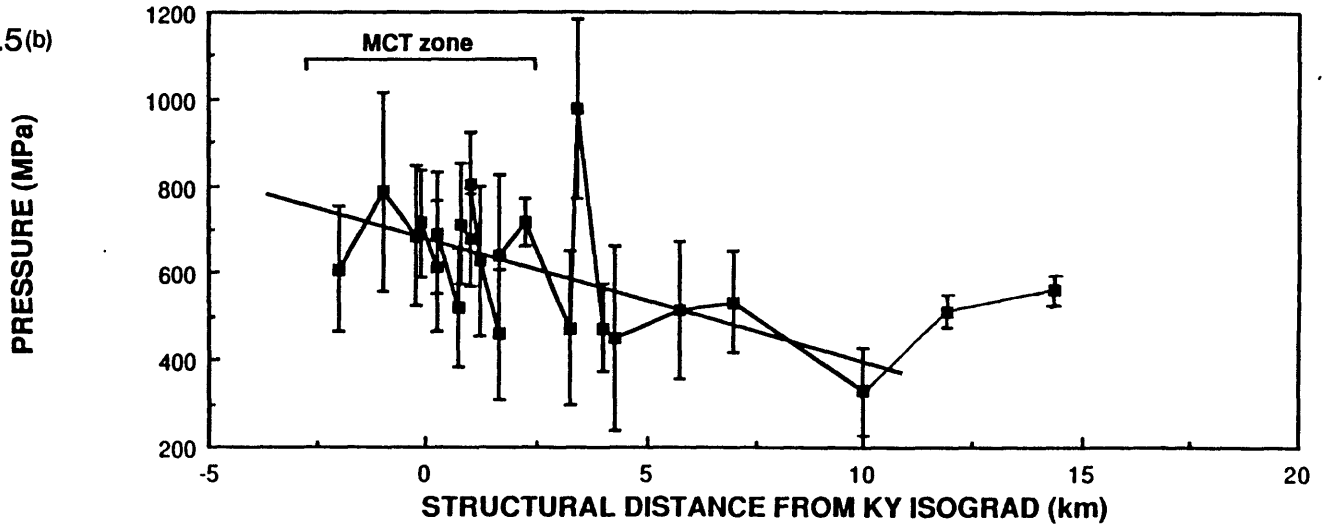

zone may represent thrust-related conditions, the pressure-temperature conditions of the upper units may be related to granitic intrusion, and possibly were recorded at a different time. There may also be a more localized effect that granitic intrusion has had on the re-equilibration of the thermobarometers. Chilled margins indicate that at least some of the granites intruded into cooler country rock. Some of the samples north of the MCT were collected close to small intrusive bodies and the thermobarometers may have been "reset" at these locally higher temperatures. Other samples may have been far enough from intrusives that they were, in effect, insulated from localized heating and resetting. The northernmost three samples, 86H19E, 86H19C, and 86H21G, are from the region characterized by low-amplitude, long-wavelength, E-W trending folds, and therefore their structural level is approximate. These three samples have recorded approximately the same temperatures, but whether this is an artifact of structural level or regional heating by the granites is unclear.

The apparent pressure profile within 10km of the kyanite isograd places additional constraints on the relationship between metamorphism and thrusting. Post-metamorphic thrusting predicts an increase in pressures across the thrust zone into the hanging wall. Syn-metamorphic thrusting predicts pressures that reflect a normal lithostatic gradient, decreasing up section. In figure 3.5b a straight line was fit to pressure data from the MCT zone and lower Tibetan Slab. The slope of this line is 28 MPa/km, which approximates a realistic lithostatic gradient. This trend strongly supports syn-metamorphic thrusting. Frictional heating along the thrust plane would yield similar trends; however, it is not likely to be the only cause of elevated temperatures across a twelve kilometer zone(structural width of elevated temperatures Fig. 3.5a). Also, the peak temperatures due to frictional heating should correspond to the zone of

maximum thrust displacement (Brewer, 1981), but the peak apparent temperatures in Fig. 3.5a are not even within the MCT zone. Though frictional heating could have locally contributed to increased temperatures, the data strongly suggest that the observed temperature profile is a result of syn-metamorphic thrusting. There are local minimums and maximums within the data trend that could be due to slight post-metamorphic fault movement, or a degree of later retrograde re-equilibration (Hodges and Royden, 1984), and/or local affects of granitic intrusion (only for samples from ~3km and north).

MODELING OF PRESSURE-TEMPERATURE PATHS

Mineral rim thermobarometry provides pressure-temperature information about a sample's latest equilibration but does not shed light on the earlier burial, uplift or thermal history of that sample. In hopes of reconstructing portions of the pressure-temperature paths of rocks within the MCT zone, five samples with garnets having plagioclase and/or biotite inclusions were examined utilizing the Gibbs' Method of Spear and Selverstone (1983). For samples 85H21G and 85H21J, which have adjacent plagioclase and biotite inclusions, it is also possible to calculate pressures and temperatures for the cores through simultaneous solution of GB and GAQP (St. Onge, 1987). The use of GAQP for garnet cores assumes the presence of aluminosilicate during garnet growth. This assumption is probably not unreasonable as other samples actually have sillimanite inclusions in garnet.

As discussed by Spear and Selverstone (1983), the Gibbs' Method requires the input of n independent compositional monitoring parameters for samples with a variance of n. The five analyzed samples have a variance of 3-5. Three monitoring parameters can always be accomodated by zoning of

garnet compositional components, but samples with a variance of 4 require either a plagioclase or biotite inclusion within the garnet, while samples with a variance of 5 require both inclusion types. Due to the potential for late Fe-Mg exchange use of biotite inclusions has been avoided where possible.

Table 3.5 summarizes the compositional monitors used for each sample and Fig. 3.6 is a plot of the resultant path segments. Samples 85H21G, 85H21J and 86H2D have a variance of 4. Plagioclase inclusions were used as monitors for samples 85H21G and 85H21J. 86H2D lacked plagioclase inclusions, so a biotite inclusion monitor was used. Sample 85H5A has a variance of 5 hence biotite and plagioclase inclusion monitors were used. Sample 86H3F contains both kyanite and sillimanite and has a variance of three. This sample has plagioclase inclusions so plagioclase was used as a monitor in addition to two garnet components. For this sample the technique required the assumption that the assemblage, including kyanite and sillimanite, existed at the start of garnet growth, which requires the path to follow the kyanite - sillimanite reaction curve. In an effort to get around this problem an additional two paths were modeled for this sample assuming no sillimanite in the assemblage and then no kyanite in the assemblage. The resulting paths were virtually identical to the path for which the presence of both early kyanite and sillimanite was assumed.

The dotted paths in Fig. 3.6 were calculated using thermobarometry (GB and GAQP) with garnet core composition and biotite and plagioclase inclusion compositions. For sample 85H21G the thermobarometric path and the Gibbs' Method paths are nearly coincident. The thermobarometric path for sample 85H21J is, however, prograde while the Gibbs' method path drops in temperature. This discrepency may be either due to a problem in the

Figure 3.6 Pressure-temperature paths. Cross symbol represents rim pressure and temperature. Solid lines are Gibbs' Method paths from garnet core to rim (cross). Dotted lines are paths derived using thermobarometry.

Figure 3.6

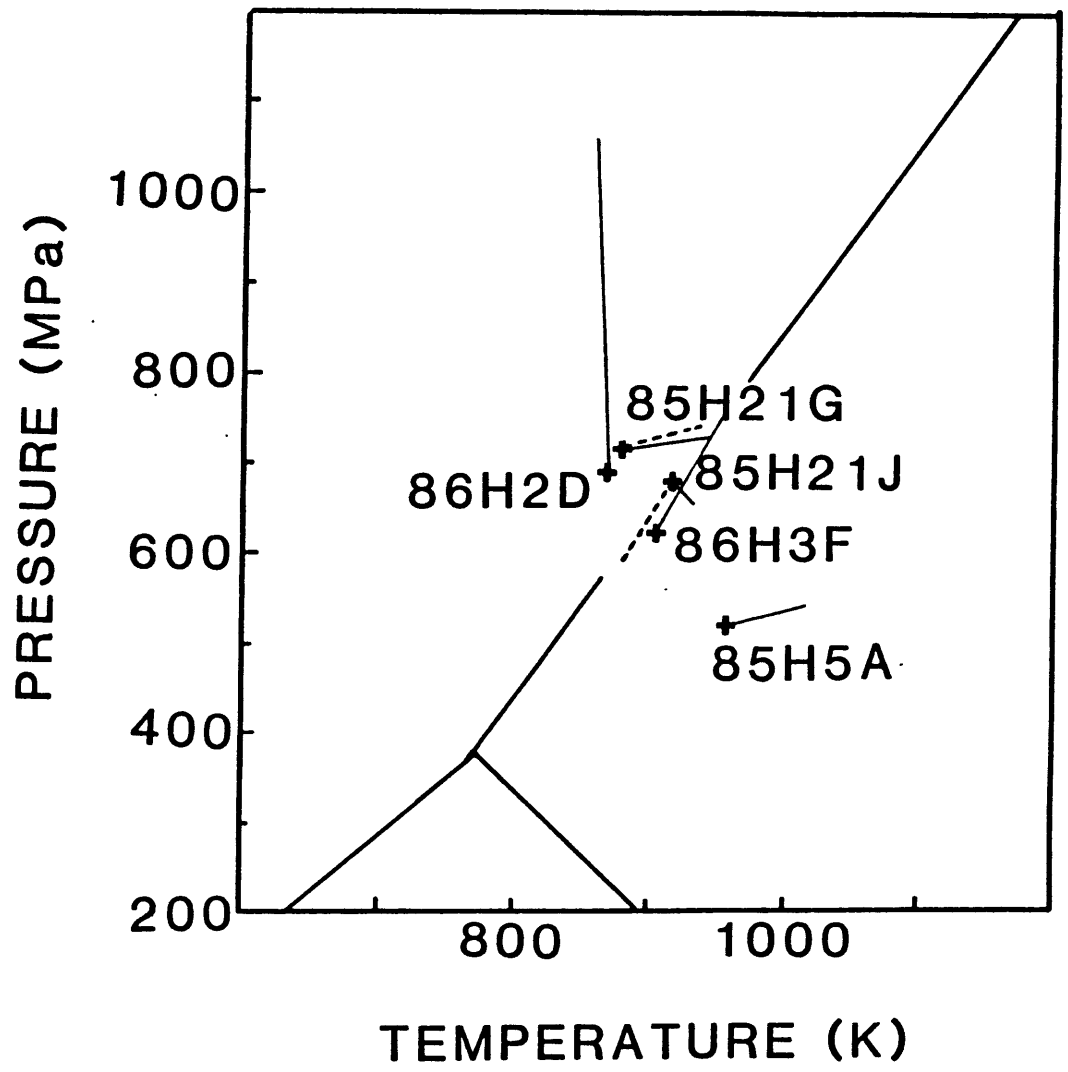
PRESSURE (MPa)
1000
800
600
400
200
800
1000
TEMPERATURE (K)
85H21G
86H2D
85H21J
86H3F
85H5A

Table 3.5 Gibb's Method Monitors and Results

	.....garnet core.....			bi incl.	pg incl.	core	core
sample	ΔXalm	ΔXgrs	ΔXsps	ΔXann	ΔXan	temperature (K)	pressure (MPa)
85H21G	-0.041	0.004	0.016	....	0.054	949	729
85H21J	-0.021	0.012	0.006	....	0.081	927	657
85H5A	-0.069	0.001	-0.038	-0.136	0.059	1018	542
86H2D	-0.026	0.002	-0.009	-0.076	....	859	1065
86H3F	-0.053	0.009	0.135	....	0.039	950	754

assumption of early aluminosilicate, or there may have been Fe-Mg exchange between garnet and the biotite inclusion. This latter possibility better explains the lack of consistency between the thermobarometric path and the paths of other samples.

For samples 85H21G, 85H5A, and 86H3F the Gibb's method paths all drop in pressure and temperature. Thermobarometry suggests that rim temperatures and pressures reflect conditions of syn-metamorphic thrust movement. The samples for which paths were modeled all come from within the MCT zone or the lowermost Tibetan Slab. Their path segments are consistent with the suggested relative timing of thrusting versus metamorphic equilibration if the location of major thrust displacement is at or below the lowermost sample, 85H21G. If the major thrust break were structurally higher than this sample locality, one would expect to see a significant increase in pressure as well as an increase in temperature for any paths below the thrust.

The short path segment for sample 85H21J also shows a decrease in temperature, but the pressure increases slightly. This path, though short, is anomalous. Sample 86H2D also has an anomalous path segment which decreases dramatically (~400MPa) in pressure with a very slight increase in temperature. This nearly isothermal path, calculated with a biotite inclusion monitor, may result from Fe-Mg re-equilibration between the garnet and biotite inclusion.

CONCLUSION

The Main Central Thrust, in the studied region of eastern Nepal, is a 3-5km thick zone. Results of thermobarometry from samples collected across the zone and into the overlying Tibetan Slab show an increase in temperature

upsection through the zone and into the lower portion of the Slab, thence a decrease in the mid-level of the Slab. Pressures across this same section exhibit a trend that resembles a lithostatic gradient. These results, together with the modeled pressure-temperature paths, are consistent with the juxtaposition of a "hot" upper plate over a "cold" lower plate, proposed by Le Fort (1975). Local variation in temperature and pressure may result from post-metamorphic thrust movement as suggested by Brunel and Kienast (1986), but the lack of major discontinuities in the average pressure trend suggests that post-metamorphic fault movement was minor. Metamorphic textures suggest that garnets from the MCT zone began growing before MCT movement, but overgrowths and/or final equilibration may have occured synchronous with thrust movement. Temperatures and pressures from the northernmost samples are nearly constant at ~1000K and 530MPa. These elevated temperatures may be a product of heat introduced with the intrusion of granitic material.

Clearly the Himalaya is a complex orogen and many factors have influenced the thermal history of the area. The data presented here are a first attempt to quantify the metamorphic temperatures and pressures in eastern Nepal. Further thermobarometric and geochronologic data will better constrain metamorphic conditions and the cooling history of this region. Lateral variations are important in the Himalaya (Hodges et al., submitted), so individual areas may have to be considered somewhat independently.

ACKNOWLEDGMENTS

The author thanks Kip Hodges, Liz Schermer, Peter Tilke, Peter Molnar, Leigh Royden and Jim Lowell for helpful reviews of the manuscript and valuable discussions on Himalayan tectonics. Two anonymous reviewers also

provided helpful comments. The much-appreciated logistical and "good will" support in the field was provided by Mountain Travel Nepal and Sange Dorje Sherpa. This research was financially supported by The American Alpine Club, The Explorer's Club, The Geological Society of America and U.S. National Science Foundation grant EAR-8414417.

Chapter 4: $^{40}AR/^{39}AR$ AGE CONSTRAINTS IN THE MCT ZONE AND TIBETAN SLAB, EASTERN NEPAL

INTRODUCTION

Collision between the Indian continent and the Eurasian continent occured between ~40 and 50 Ma (Molnar, 1984). Convergence between these two continents has continued to the present, thus creating the spectacular Himalayan range and the elevated Tibetan Plateau. The original zone of collision, the Indus-Tsangpo suture, is marked by ophiolitic rocks in southern Tibet. The high peaks and rugged topography of the Himalaya coincide with metamorphic and intrusive rocks within the Indian Plate. These crystalline rocks are part of the upper plate to a major, north-dipping thrust known as the Main Central Thrust (MCT).

The MCT is a major intracontinental fault zone which accomodated portions of the post-collisional convergence between India and Eurasia. This structure may have accomodated more than 100 km of displacement (Gansser, 1981). It has been proposed that movement on the MCT may have influenced metamorphism and the development of leucogranites in the Himalaya (LeFort, 1975, 1981). Unfortunately there are few data available to test these hypotheses because the necessary information includes the relative and absolute ages of metamorphism, thrusting and leucogranitic emplacement. The leucogranites have been dated (see LeFort et al., 1987 for summary), but the timing of metamorphism and deformation along the MCT has not been studied in detail.

In the Everest area of eastern, Nepal the MCT is a thrust zone in which temperatures reached 500-700°C during thrusting (Hubbard, in press). Amphibolite occurs in the lower part of the zone where calculated temperatures include the closure tempurature for the K-Ar system in hornblende (~500°C).

This coincidence provides an opportunity to date thrust movement and to compare this age with the ages of metamorphism within the hanging wall and with the ages of leucogranites. In this paper we report the results of an $^{40}Ar/^{39}Ar$ study of hornblendes, biotites, muscovites and potassium feldspars from the MCT zone and its upper plate from this region.

GEOLOGIC SETTING

Three laterally continuous, north-dipping thrusts have been identified in the Himalaya (see Fig. 1.1) : 1) the southernmost, and possibly seismically active, Main Frontal Thrust; 2) the Main Boundary Thrust; and to the north 3) the Main Central Thrust. The Main Frontal thrust (MFT) separates terraced alluvial deposits from the overiding Early Miocene - Late Pleistocene age molassic rocks of the Siwaliks (Gansser, 1981). To the north the Siwaliks are overridden along the Main Boundary Thrust (MBT) by the Lesser Himalayan sequence which consists of a predominantly clastic sedimentary sequence of Precambrian to late Paleozoic age, although fossil control is scarce (Stöcklin, 1980). This sequence generally has been metamorphosed to a low grade; but local areas remain unmetamorphosed . The Main Central Thrust (MCT) forms the northern boundary of the Lesser Himalaya. The upper plate to this structure is the Tibetan Slab with high-grade sillimanite-bearing gneissic rocks which have been subjected to widespread anatexis and intuded by leucogranitic material. Rocks adjacent to the MCT are characterized by an inverted metamorphism such that metamorphic grade increases toward structurally higher levels(Gansser, 1964: Pêcher, 1977; Hodges et al., in press). Because these rocks are generally homoclinally dipping to the north, the metamorphic grade increases northward. A variety of ideas have been proposed that link the

inverted metamorphism with deformation along the MCT (LeFort, 1975; Maruo and Kizaki,1983; Brunel and Kienast, 1986). In central Nepal, LeFort (1981) proposed that the formation and emplacement of the leucocratic Manaslu pluton in the Tibetan Slab is also related to movement on the MCT. Radiometric ages, from a variety of techniques, vary from 14.3±0.6 to 25.0±0.5 Ma (two sigma age uncertainties are reported, herein, for all dating techniques) for intrusives within the Tibetan Slab (Schärer et al., 1986; Deniel et al., 1987). Although movement on the MCT is generally thought to predate movement on the MBT, there are no unambiguous age constraints for the development of either structure.

Study Area

The structural setting and tectonic stratigraphy of the Everest region have been described in detail in Chapter 2. In general the MCT in this area is a 3-5km-thick, north-dipping shear zone consisting of a variety of lithologies including: augen gneiss, slate, phyllite, quartzite, talc-schist, amphibolite, pelitic schist, calc-silicate rock, and banded biotite gneiss Metamorphic grade increases up-section from chlorite-bearing schist in the Lesser Himalaya, which contains garnets in the upper ~100 m, through the staurolite and kyanite isograds in the lower MCT zone, to sillimanite-bearing gneiss in the upper MCT zone and across the Tibetan Slab. Metamorphic isograds and lithologic contacts are roughly parallel to the dominant schistosity.

The lower boundary of the MCT zone is a lithologic contact between an augen gneiss in the MCT zone and a chlorite-muscovite schist in the uppermost Lesser Himalaya. The Lesser Himalayan section is a thick sequence of fine-grained psammite, schist, and quartzite. Locally biotite and garnet occur in the uppermost unit of chlorite-muscovite schist.

The upper boundary of the MCT zone is within a biotite gneiss unit at a level that separates highly sheared rocks of the thrust zone from overlying, less-deformed but migmatized gneissic rocks of the Tibetan Slab. Shear zones do exist north of the MCT zone, but deformation does not appear to be as wide-spread. Lithologies within the Tibetan Slab include biotite gneiss, calc-silicate rock, quartzite, augen gneiss, granitic gneiss and pelitic schist. Garnet and sillimanite are common in pelitic and gneissic rocks throughout this section. Anatexis and small-scale granitic intrusions occur in the lower Tibetan Slab, but the frequency and volume of granitic material increases toward the north. There are several large leucogranitic bodies in this region such as the south face of Nuptse or the Makalu massif, but the majority of the granitic material occurs in networks of dikes and sills. Some of the larger intrusives have retained xenoliths of the country rock. Schistosity within these xenoliths has often remained parallel to the country rock schistosity in the area. Cross-cutting relationships in the dikes and sills suggest multiple generations of intrusion.

Metamorphism

Metamorphic assemblages across the MCT zone and into the Tibetan Slab suggest an increase in metamorphic grade towards higher structural levels. Mineral rim thermobarometric data (Hubbard, in press) from samples across the MCT zone and lower Tibetan Slab in eastern Nepal show an increase up section in temperatures of metamorphic equilibration from 505±50°C (2 sigma uncertainty) in the lower MCT zone to 725±96°C at about 1.5 kilometers structurally above the upper boundary of the MCT zone (Fig. 4.1). Above that level temperatures decrease to 593±50°C at ~8 km above the MCT zone. Pressures across the same section decrease from 685±160 MPa in the

Figure 4.1 Summary of thermobarometric data plotted against structural distance from the kyanite isograd (from Hubbard, in press). a)temperature; b)pressure.

Figure 4.1(a)

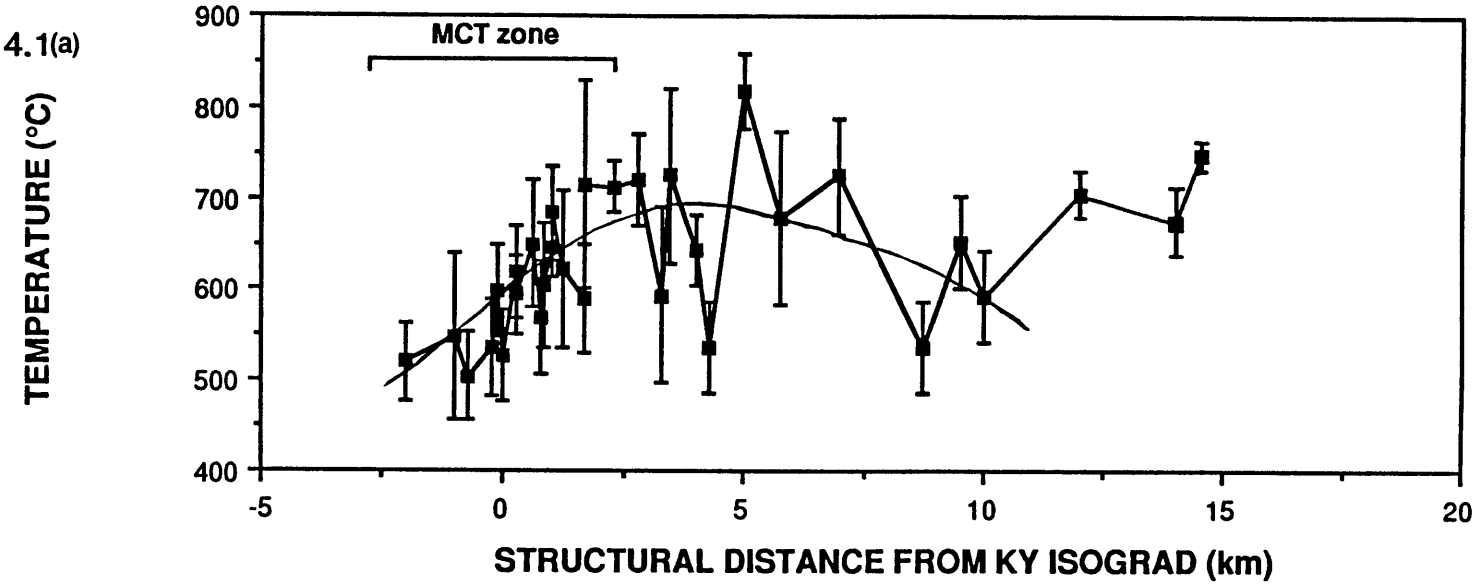

Figure 4.1(b)

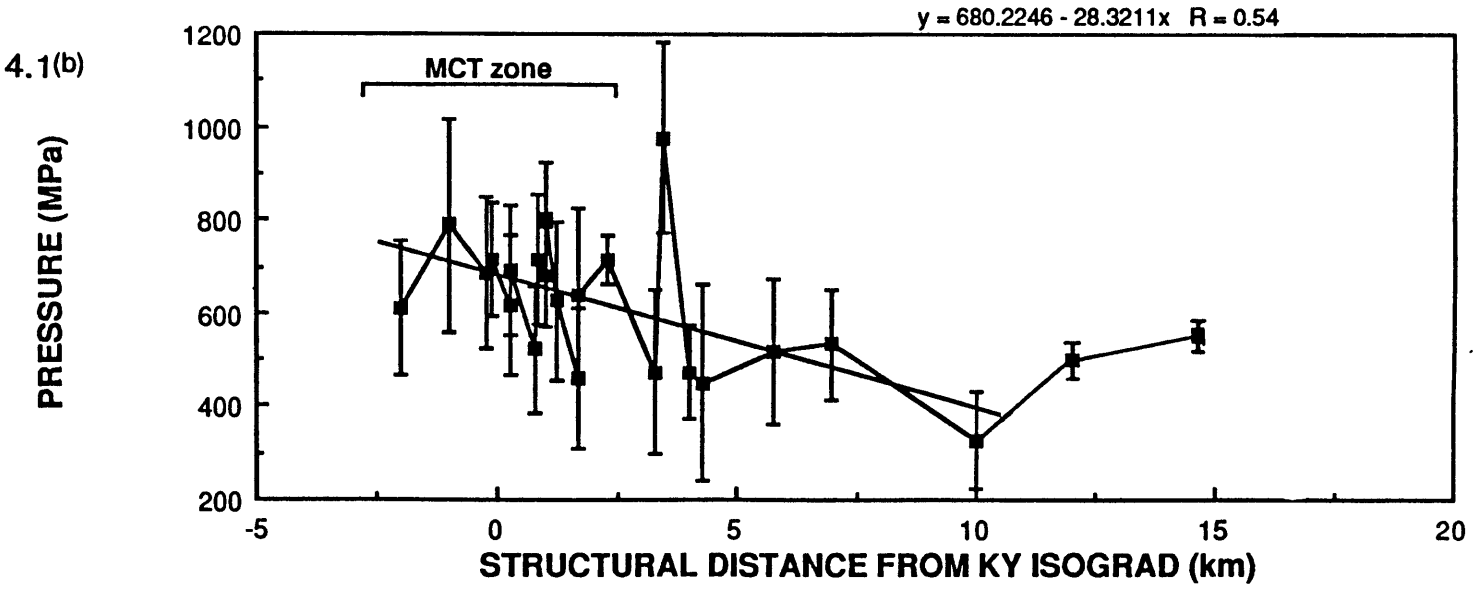

lower MCT zone to 328±102 MPa at ~8 km above the MCT zone (Fig. 4.1). These data support the model of LeFort (1975) that metamorphism was synchronous with movement on the MCT.

In the upper Tibetan Slab, metamorphic temperatures and pressures from samples across a folded section are nearly uniform with average values of 712°C and 533 MPa. It has been proposed (Hubbard, in press) that these samples either came from one structural horizon thus experiencing identical uplift histories or they may have been heated during the period of leucogranitic intrusion in this area. In the latter case regional metamorphism in the upper Tibetan Slab would be the result of advection of heat during intrusion.

PREVIOUS GEOCHRONOLOGY

Tertiary Granites of the Everest Area

A small number of workers have attempted to obtain ages of the Tertiary leucogranites in eastern Nepal using a variety of techniques. Due to limitations of the individual techniques there has been a mixed degree of success. Table 4.1 summarizes the majority of existing age data for this region.

Ferrara et al. (1983) used the Rb/Sr method to obtain both whole rock isochrons and mineral isochrons for samples from the south side of the peaks Nuptse and Lhotse. Two whole-rock isochrons gave ages of 52±1 Ma and 13.7±7 Ma. One of the samples from the 52 Ma isochron yielded a 17.3±0.3 Ma internal isochron from K-feldspar, biotite, muscovite and whole rock. Another sample, not included in either whole rock isochron, had an internal four mineral isochron of 16.5±0.5 Ma. Ferrara et al. suggest that these Middle Miocene ages

Table 4.1. Previous Geochronologic Results, Eastern Nepal

SYSTEM	LOCATION	ROCK TYPE	MINERAL	AGE*	SOURCE
Rb/Sr	Lhotse glacier	leucogranite	(whole rock)	52±1 Ma	1
Rb/Sr	Lhotse glacier	leucogranite	w.r-Kf-mu-bi	17.3±0.3 Ma	1
Rb/Sr	Nuptse glacier	leucogranite	(whole rock)	13.7±7.0 Ma	1
Rb/Sr	Lhotse glacier	leucogranite	w.r.-to-Kf-mu-bi	16.5±0.5 Ma	1
Rb/Sr	near Na	orthogneiss	w.r-bi	15.6±0.6 Ma	1
Rb/Sr	near Na	orthogneiss	w.r.-bi	15.3±0.6 Ma	1
Rb/Sr	Lhotse glacier	paragneiss	w.r.-bi	16.4±0.3 Ma	1
U/Pb	Mt. Everest	leucogranite	monazite	14.3±0.6 Ma	2
U/Pb	Makalu	leucogranite	monazite	21.9±0.2 Ma	3
U/Pb	Makalu	leucogranite	monazite	24.0±0.4 Ma	3
U/Pb	N. side Everest	leucogranite	monazite	22-25 Ma	4
$^{40}Ar/^{39}Ar$	N. side Everest	leucogranite	biotite	17.1±0.2 Ma	4
$^{40}Ar/^{39}Ar$	N. side Everest	leucogranite	muscovite	16.7±0.4 Ma	4
$^{40}Ar/^{39}Ar$	N. side Everest	leucogranite	K-feldspar	16.2±0.2 Ma	4
K-Ar	Lho La Pass	leucogranite	biotite	19.0±2.0 Ma	5
K-Ar	Pumori	leucogranite	biotite	47.3±5.0 Ma	5
K-Ar	Everest basecamp	leucogranite	biotite	18.7±2.0 Ma	5
K-Ar	N. side Nuptse	mica schist	biotite	17.0±1.6 Ma	5
K-Ar	N. side Nuptse	amphibolite	hornblende	24.0±2.2 Ma	5
K-Ar	N. side Nuptse	biotite gneiss	biotite	18.0±1.6 Ma	5
K-Ar	N. side Nuptse	amphibolite	amphibole	56.2±4.4 Ma	5
K-Ar	Pangboche	amphibolite	biotite	39.5±4.0 Ma	5
K-Ar	Pangboche	amphibolite	hornblende	348±40 Ma	5
K-Ar	Tyangpoche	biotite gneiss	biotite	16.0±1.8 Ma	5
K-Ar	S. of Namche	augen gneiss	biotite	13.4±1.2 Ma	5
K-Ar	S. of Namche	migmatite	biotite	10.5±2.0 Ma	5
K-Ar	S. of Namche	migmatitic diorite	biotite	9.8±2.0 Ma	5
K-Ar	S. of Ghat	biotite gneiss	biotite	14.0±1.0 Ma	5
K-Ar	Puiyan (MCTZ)	augen gneiss	biotite	9.0±1.0 Ma	5
K-Ar	Puiyan (MCTZ)	biotite gneiss	biotite	5.5±0.6 Ma	5
K-Ar	N. of Khari-La(MCTZ)	biotite gneiss	biotite	3.4±0.2 Ma	5
K-Ar	S. of Khari-La(MCTZ)	mica schist	biotite	8.5±0.8 Ma	5

* with two sigma uncertainty

could represent a period of regional uplift, but they also recognize that Sr heterogeneity may be a problem in Himalayan leucogranites.

Schärer et al. (1986) determined a U-Pb age on monazite fractions of 14.4±0.6 Ma for a granite sample from the north side of Mt. Everest. This age is considerably younger than monazite ages determined by Copeland et al. (in press) from neighboring Everest granites at 20±1 Ma. This older age, however, is more consistent with the 21.9±0.2 Ma and 24.0±0.4 Ma ages determined by Schärer (1984) on monazites from granites of the Makalu massif, roughly 20 km to the southeast.

Copeland et al. (1987) also used the $^{40}Ar/^{39}Ar$ technique on biotite, muscovite, and K-feldspar from a granite just north of Everest and obtained cooling ages of 17.1±0.2, 16.7±0.4 and 16.2±0.2 Ma, respectively. Similar K-Ar ages were determined by Krummenacher et al. (1978) on biotites from granites near the Everest base camp in Nepal at 19.1±2 and 18.7±2 Ma. Krummenacher et al. (1978) also measured a 47.3±5.0 Ma biotite from the Everest region. This older age could either represent an older intrusion or excess Ar.

Metamorphic Rocks of the Tibetan Slab

Ferrara et al. (1983) attempted a Rb/Sr whole rock isochron from gneissic samples from the south face of Lhotse. Significant scatter in the data did not yield a meaningful age, but rather it led the authors to conclude that isotopic heterogeneity in the sedimentary protolith may be a signficant problem. They did obtain a 16.4±0.3 Ma biotite-whole rock isochron which is consistent with

ages of the leucogranites from the same area.

Krummenacher et al. (1978) obtained K-Ar biotite ages on schistose and gneissic rocks from across the Tibetan Slab. In general their ages range from 10.5±2.0 to 18.0±1.6 Ma. With a few exceptions the ages tend to decrease down section. One anomalously old age of 39.5±4 Ma may be due to excess Ar.

Metamorphic Rocks of the MCT Zone

Krummenacher et al. (1978) have also determined four K-Ar biotite ages from samples within the region that has been defined in this paper as the MCT zone. These ages range from 3.4±0.2 to 9.0±1.0 Ma suggesting more recent cooling at this level than within the upper Tibetan Slab.

SAMPLING

In order to see how cooling ages vary across this region samples were collected from four areas (Fig. 4.2): 1) the MCT zone; 2) the lower Tibetan Slab (a locality referred to as Ghat); 3) the upper Tibetan Slab away from intrusive rocks (a locality referred to as Na); and 4) the upper Tibetan Slab adjacent to and including leucogranitic intrusions (a locality referred to as Ngozumba). Multiple rock types from each location were chosen in an effort to maximize the number of datable minerals, thus maximizing the cooling history data for that area.

Figure 4.2 Simplified geologic map of the study area in eastern Nepal. Sample locations for $^{40}Ar/^{39}Ar$ study are indicated by the circled place names.

Figure 4.2

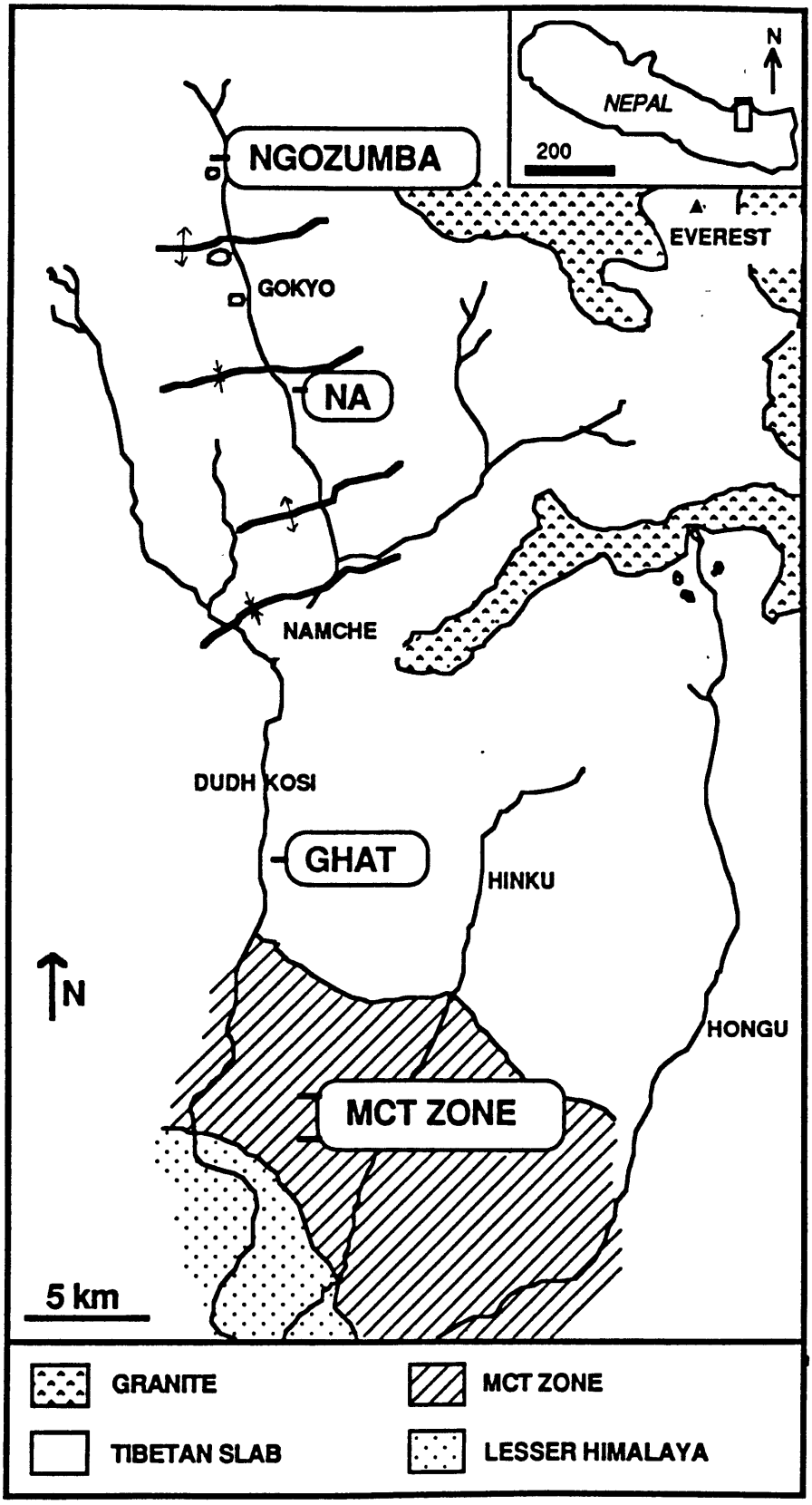
N
NEPAL
200
NGOZUMBA
EVEREST
GOKYO
NA
NAMCHE
DUDH KOSI
GHAT
HINKU
N
HONGU
MCT ZONE
5 km
GRANITE
MCT ZONE
TIBETAN SLAB
LESSER HIMALAYA

MCT zone

Four samples were collected in the MCT zone. Sample 87H13F is an augen gneiss from the lowest unit in the MCT zone. In this sample K-feldspar porphyroclasts (<1cm) are set in a foliated matrix of biotite, muscovite and recrystallized quartz. Sample 87H13E was collected ~5 m from 87H13F in a psammite horizon within this lower augen gneiss. The psammite contains the assemblage garnet-staurolite-biotite-quartz. Garnets are anhedral and poikiloblastic. Samples 87H12B and 87H12C came from a small amphibolite layer within a mica schist in the mid-section of the MCT zone. The assemblage of this amphibolite includes: hornblende, biotite, quartz, calcite, sphene and plagioclase. In sample 87H12C the biotite grains are oriented and concentrated in thin layers which define the foliation.

Lower Tibetan Slab -- Ghat

Two adjacent samples were chosen in the lower Tibetan Slab just south of the village of Ghat. Sample 87H21C is a biotite gneiss with an assemblage of quartz, plagioclase, biotite and K-feldspar. This sample has domains of fine grained recrystallized quartz and occasional myrmekitic textures, which may be associated with deformation (LaTour, 1987). Sample 87H21D is a pegmatite which appeared undeformed in the field, but when observed in thin section it shows a protomylonitic texture (fig. 4.3). Relict K-feldspar grains are surrounded by a fine grained matrix of recrystallized quartz, biotite and muscovite. Tourmaline is also present in 87H21D.

Upper Tibetan Slab -- Na

Two samples were collected south of Na in the Gokyo valley at a site > 200

m from visible leucogranitic intrusives. The intent was to analyze samples from this structural level whose thermal history reflects uplift and not intrusion. Sample 87H19A is an amphibolite and 87H19B is a tourmaline-bearing biotite gneiss. Both samples are foliated but neither show evidence of intense deformation.

Upper Tibetan Slab -- Ngozumba

The outcrop at Ngozumba (Fig. 4.4), in the upper Gokyo valley, consists of an augen gneiss (87H18A) that is intruded by pegmatite sills (87H18B) and cut by a tourmaline-bearing leucogranite (87H18C). Myrmekites are present in the augen gneiss and the pegmatite. The pegmatite and the leucogranite contain chlorite, and muscovite is sericitized in the augen gneiss, the pegmatite and the leucogranite.

ANALYTICAL TECHNIQUES

Mineral separates were obtained using standard magnetic and heavy liquid separation techniques. Sample preparation, irradiation, and analytical procedures are the same as those described in Harrison and FitzGerald (1986). Correction factors to account for interfering nuclear reaction products are given, together with the results for each sample, in Appendix 4.1.

Closure temperatures for hornblende, biotite and muscovite were estimated from hydrothermal diffusion studies (see McDougall and Harrison (1988) for a review). Closure temperatures for K-feldspars were calculated using the diffusion parameters estimated from measured ^{39}Ar release during laboratory heating. Three of the K-feldspars yielded reasonable values for closure temperature. Unfortunately the K-feldspars from gneissic and granitic

Figure 4.3 Protomylonitic texture in pegmatite from Ghat. Field of view is 13 mm.

Figure 4.4 Outcrop that was sampled at Ngozumba. The augen gneiss (ag), pegmatite (p), and leucogranite (lg) are labeled.

Figure 4.3

Figure 4.4

rocks of the upper Tibetan Slab were partly sericitized and gave calculated closure temperatures of <50°C. These low temperatures are probably an effect of the sericite and do not reflect the true closure temperature. For these samples a closure temperature of 200°C was assumed as this temperature is within the uncertainty of closure temperatures calculated for other K-feldspars of similar composition from the study area.

RESULTS

MCT zone

Muscovite, biotite and K-feldspar were analyzed from sample 87H13F, and biotite was analyzed from the adjacent sample 87H13E. Release spectra from both samples are shown in Figure 4.5. Biotite and muscovite from 87H13F yield plateaux at ~40 Ma and ~12 Ma, respectively. As biotite has a lower closure temperature than muscovite this reversal suggests the presence of excess argon. Excess argon is a common problem in biotites and can, in certain cases, yield erroneously old ages that are not identifiable with the isochron approach due to the high Ar solubility in biotite and high $^{40}Ar/^{36}Ar$ ratio of the trapped gas. Muscovite, however, is less susceptible to the problems of excess argon, so we interpret the muscovite isochron age of 12.0±0.2 Ma to be a meaningful cooling age. The K-feldspar release spectrum is "saddle-shaped" which is also a sign of excess argon (Harrison and McDougall, 1982). The minimum age on this spectrum at ~8 Ma appears sensible as it is consistent with the muscovite age. The closure temperature for this K-feldspar is calculated to be T_c=220±15°C.

Biotite was the only mineral analyzed in sample 87H13E. The release spectrum (Fig. 4.5) reveals an apparent ~100 Ma plateau and does not define an isochron array. A 90-100 Ma age pre-dates continental collision and is,

therefore, unlikely. This age is also inconsistent with the younger ages from sample 87H13F, which was collected just 5 meters away. Excess argon must, again, be the cause of this unrealisticly old age.

Age spectra from biotite and hornblende from sample 87H12C reveal an unexpected age reversal (Fig. 4.6). Again, the biotite was probably affected by excess argon as the plateau age of ~60 Ma is considerably older than hornblende, which has a much higher closure temperature. The hornblende data are complicated by the presence of two distinct trapped argon components (Heizler and Harrison, in press) but the sample yields a meaningful isochron age of 20.9±0.2 Ma (Fig. 4.6). This age is consistent with the muscovite and K-feldspar ages from sample 87H13F collected at a slightly lower structural level within the MCT zone. The biotite does not yield a sensible isochron array.

A hornblende separate from sample 87H12B gave a complex release spectrum which may reveal argon uptake superimposed on a diffusion loss profile from a Paleozoic age sample (Fig. 4.7).

Lower Tibetan Slab -- Ghat

Sample 87H21C gives a minimum age from the release spectra (Fig. 4.8) for K-feldspar of 3.6±0.2 Ma (T_c = 210±50) and a biotite isochron age of 9.1±0.2 Ma. Sample 87H21D is from the adjacent sheared pegmatite and yields a K-feldspar minimum age of 6.4±0.8 Ma (Fig. 4.9). Biotite and muscovite isochrons from 87H21D give ages of 7.5±0.6 Ma and 7.7±0.4 Ma respectively. The behavior of the spectra for the K-feldspars from these two samples are markedly different. Almost 50% of the ^{39}Ar released is younger than 5 Ma for sample 87H21C with the remaining gas fraction younger than 15 Ma. For sample 87H21D less than 50% of the ^{39}Ar released from the K-feldspar is younger than

Figure 4.5 Release spectra for mineral separates from samples 87H13E and 87H13F from the lower MCT zone.

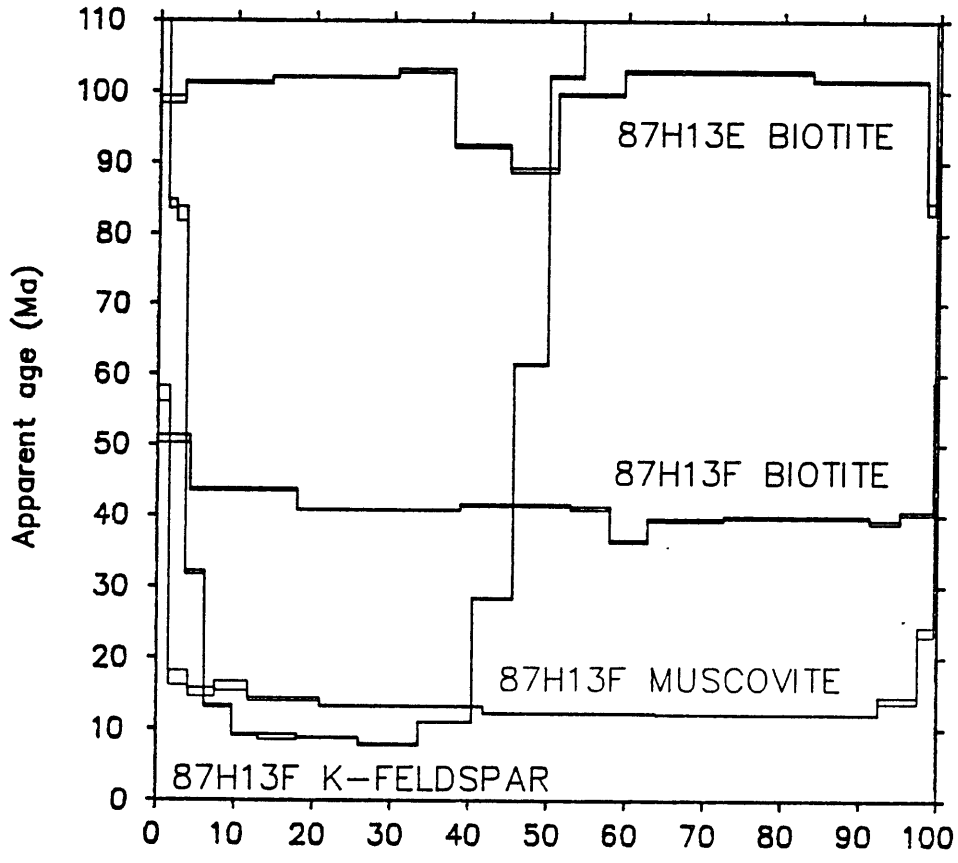
110
100
90
80
70
60
50
40
30
20
10
0
Apparent age (Ma)
87H13E BIOTITE
87H13F BIOTITE
87H13F MUSCOVITE
87H13F K-FELDSPAR
0
10
20
30
40
50
60
70
80
90
100
Cumulative % 39 Ar released

Figure 4.5

Figure 4.6 Release spectra for biotite and hornblende from sample 87H12C (MCT zone), shown together with the K/Ca plot and isochron plot for the hornblende. Two trapped components yield isochrons that indicate roughly the same age.

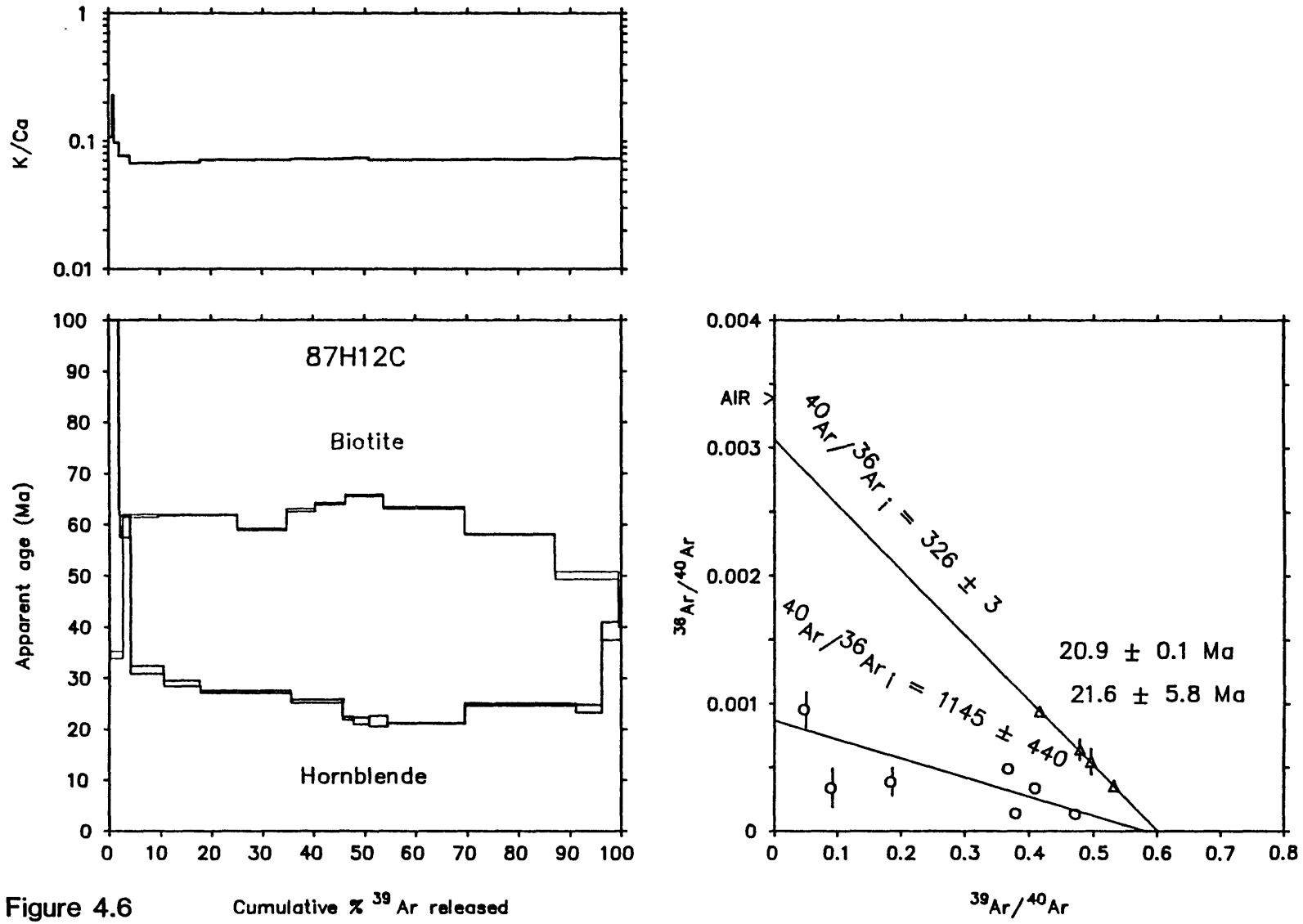
K/Ca
1
0.1
0.01
87H12C
Biotite
Hornblende
Apparent age (Ma)
100
90
80
70
60
50
40
30
20
10
0
0 10 20 30 40 50 60 70 80 90 100
Cumulative % 39 Ar released
AIR
0.004
0.003
0.002
0.001
0
38Ar/40Ar
40Ar/36Ar i = 326 ± 3
40Ar/36Ar i = 1145 ± 440
20.9 ± 0.1 Ma
21.6 ± 5.8 Ma
0 0.1 0.2 0.3 0.4 0.5 0.6 0.7 0.8
39Ar/40Ar

Figure 4.6

Figure 4.7 Release spectra and K/Ca plot for hornblende from sample 87H12B (MCT zone).

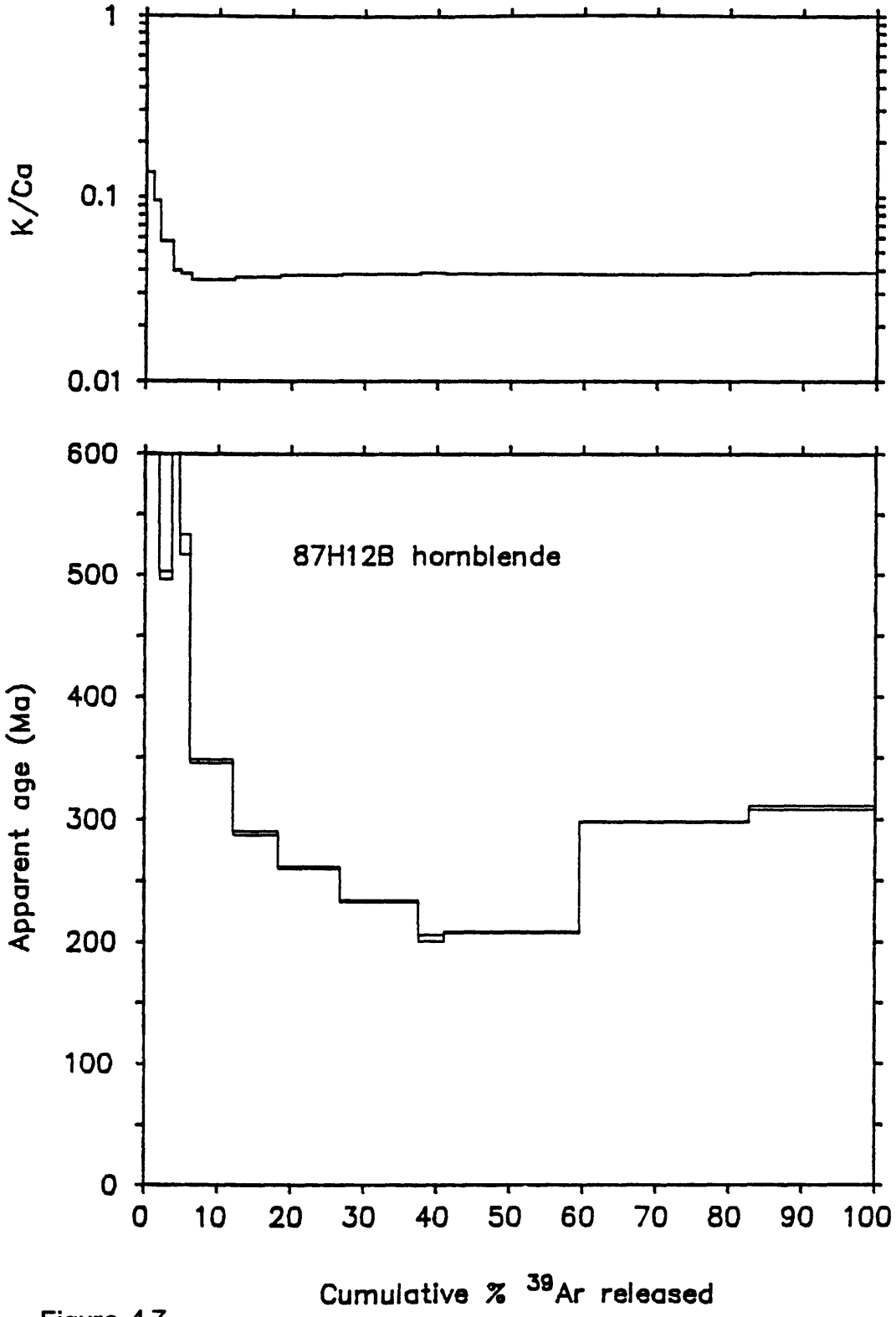
1
0.1
0.01
K/Ca
600
500
400
300
200
100
0
Apparent age (Ma)
87H12B hornblende
0
10
20
30
40
50
60
70
80
90
100
Cumulative % 39Ar released

Figure 4.7

Figure 4.8 Release spectra for biotite and K-feldspar from sample 87H21C (Ghat).

Figure 4.9 Release spectra for muscovite, biotite, and K-feldspar from sample 87H21D (Ghat).

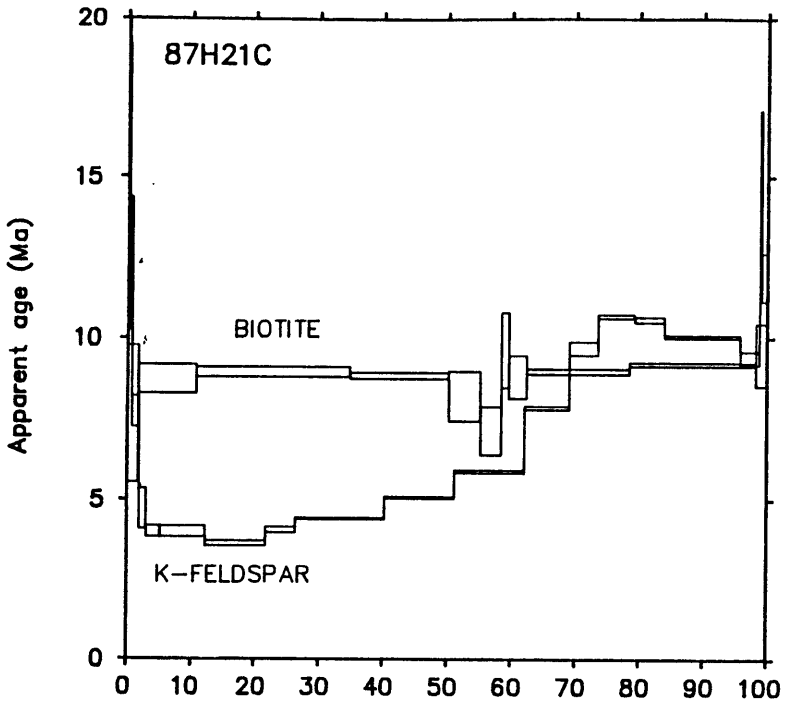

Figure 4.8

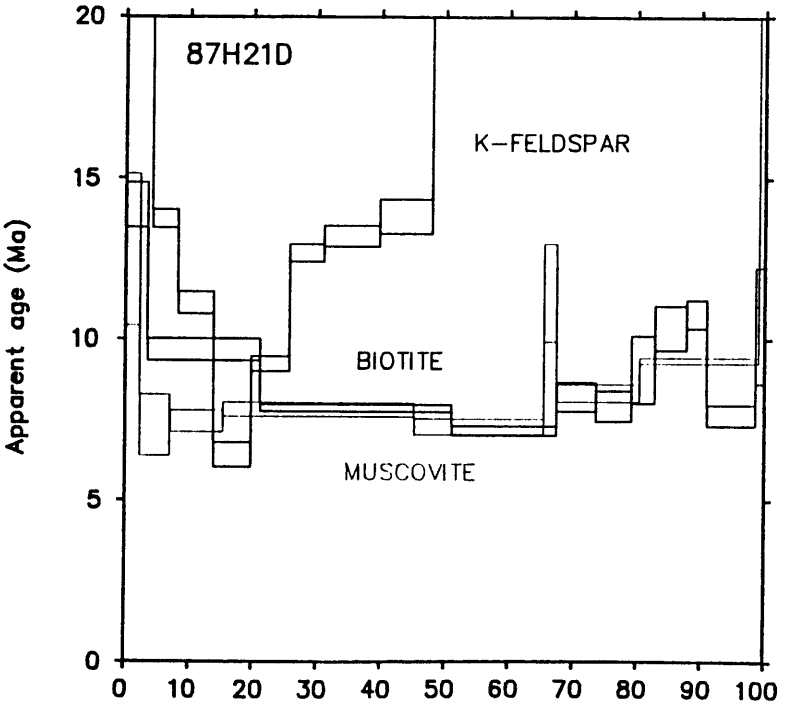

Figure 4.9

15 Ma with the remaining gas fractions older than 20 Ma. Though neither of these spectra yield plateaux, sample 87H21D appears to have been more affected by excess argon. Assuming that these two samples had the same low-temperature thermal history, biotites from both samples should yield the same ages. Either there has somehow been a difference in the thermal histories of these adjacent units or, more likely, the biotite from sample 87H21C has been affected by excess argon.

Upper Tibetan Slab -- Na

Release spectra for hornblende from sample 87H19A and biotite from sample 87H19B are shown together in Figure 4.10. The age spectum for the hornblende suggests marginal excess argon uptake with a minimum age on the spectrum of 22.7±4.4 Ma. A biotite isochron age for the 2nd through 9th increments gives an age of 20.2±0.2 Ma (MSWD=16.5, trapped $^{40}Ar/^{36}Ar$=299±10).

Upper Tibetan Slab - Ngozumba

Biotite and K-feldspar were analyzed from sample 87H18A, an augen gneiss in the upper Tibetan Slab (Fig. 4.11). The release spectrum for K-feldspar is irregular and, again, suggestive of excess argon. The minimum age on this spectrum is 18.7±0.8 Ma, which is older than the biotite isochron age of 17.2±0.8 Ma (steps 2-10, MSWD=4.9, trapped $^{40}Ar/^{36}Ar$=301±11).

Cooling ages were.obtained for muscovite, biotite and feldspar from the pegmatite sample 87H18B from Ngozumba (Fig. 4.12). As in sample 87H18A the feldspar age spectrum is irregular and yields a minimum age (21.7±0.8 Ma) which is older than the micas from this sample. The biotite and muscovite

Figure 4.10 Release spectra for biotite from sample 87H19B and hornblende from sample 87H19A (Na).

Figure 4.11 Release spectra for biotite and K-feldspar from sample 87H18A (Ngozumba).

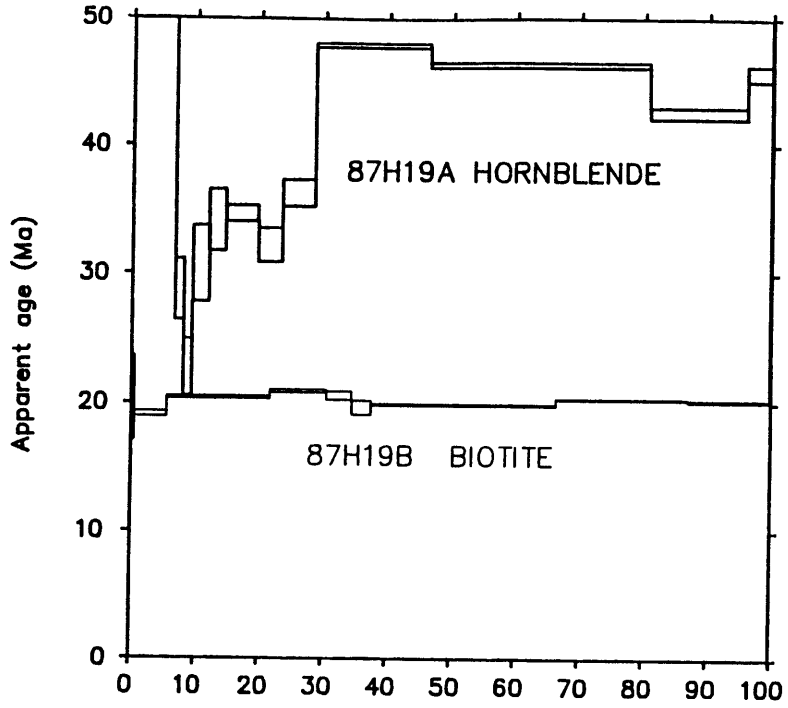

Figure 4.10

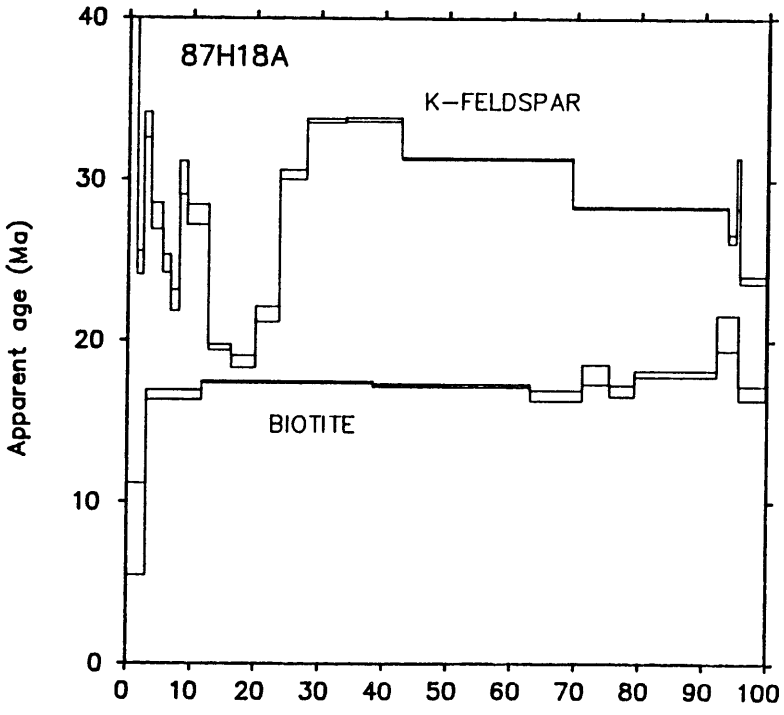

Figure 4.11

isochron ages are nearly indistinguishable at 16.8±1.4 Ma (steps 1-11, MSWD=33.7, trapped $^{40}Ar/^{36}Ar$=308±3) and 17.0±0.4 Ma (steps 2-10, MSWD=4.2, trapped $^{40}Ar/^{36}Ar$=285±18) respectively. The biotite release spectrum is somewhat irregular and there is scatter about the isochron as indicated by the high MSWD. K-feldspar and muscovite release spectra for the leucogranitic sample 87H18C are shown in Figure 4.13. Again the K-feldspar spectrum is irregular, but in this sample the minimum age of 15.5±1.8 Ma is younger than the muscovite isochron age of 16.6±0.4 (steps 1-11, MSWD=2.1,$^{40}Ar/^{36}Ar$=304±4).

TECTONIC IMPLICATIONS

A summary of the mineral ages from this study are given in Table 4.2. As discussed in the previous section some of these ages may reflect excess argon and are therefore less likely to be actual cooling ages. From the subset of data which were considered meaningful, a representative age from each site, for each mineral, was plotted versus mineral closure temperature (Fig. 4.14). Taken together, these ages should reveal a consistent pattern from which tectonic rates and timing can be inferred.

In the lower MCT zone, metamorphic temperatures ranged from ~500-550°C (Hubbard, in press) and have been interpreted as synchronous with movement on the MCT. The hornblende closure temperature (T_c=~500°C) falls within this range of metamorphic temperatures, and thus allows us to interpret the age of metamorphism and at least some of the movement on the MCT to be 20.9±0.2 Ma.

In the upper Tibetan Slab similar ages (15-20 Ma) to that of the MCT were recorded at Na and Ngozumba in the upper Tibetan Slab by biotite,

Table 4.2. Summary of $^{40}Ar/^{39}Ar$ ages

	SAMPLE #	ROCK TYPE	MINERAL	AGE	CLOSURE TEMP.
MCT zone:					
*	87H13F	augen gneiss	K-feldspar	8.0±0.2 Ma (M)	220±15°C
	87H13F	augen gneiss	biotite	36.3±0.4 Ma (M)	300±50°C
*	87H13F	augen gneiss	muscovite	12.0±0.2 Ma (I)	350±50°C
	87H13E	biotite gneiss	biotite	88.8±0.6 Ma (M)	300±50°C
	87H12C	amphibolite	biotite	58.3±3.4 Ma (I)	300±50°C
*	87H12C	amphibolite	hornblende	20.9±0.2 Ma (I)	500±50°C
	87H12B	amphibolite	hornblende	204.0±5.2 Ma (M)	500±50°C
Ghat:					
*	87H21C	biotite gneiss	K-feldspar	3.6±0.2 Ma (M)	210±50°C
	87H21C	biotite gneiss	biotite	9.1±0.2 Ma (I)	300±50°C
	87H21D	pegmatite	K-feldspar	6.4±0.8 Ma (M)	225±20°C
*	87H21D	pegmatite	biotite	7.5±0.6 Ma (I)	300±50°C
*	87H21D	pegmatite	muscovite	7.7±0.4 Ma (I)	350±50°C
Na:					
*	87H19B	biotite gneiss	biotite	20.2±0.2 Ma (I)	300±50°C
*	87H19A	amphibolite	hornblende	22.7±4.4 Ma (M)	510±50°C
Ngozumba					
	87H18A	augen gneiss	K-feldspar	18.7±0.8 Ma (M)	250(?)
	87H18A	augen gneiss	biotite	17.2±0.8 Ma (I)	300±50°C
	87H18B	pegmatite	K-feldspar	21.7±0.8 Ma (M)	250(?)
*	87H18B	pegmatite	biotite	16.8±1.4 Ma (I)	300±50°C
	87H18B	pegmatite	muscovite	17.0±0.4 Ma (I)	350±50°C
*	87H18C	leucogranite	K-feldspar	15.5±1.8 Ma (M)	250(?)
*	87H18C	leucogranite	muscovite	16.6±0.4 Ma (I)	350±50°C

(I) - age determined from isochron (M) - age is minimum on release spectra

Figure 4.12 Release spectra for muscovite, biotite, and K-feldspar for sample 87H18B (Ngozumba).

Figure 4.13 Release spectra for muscovite and K-feldspar for sample 87H18C (Ngozumba).

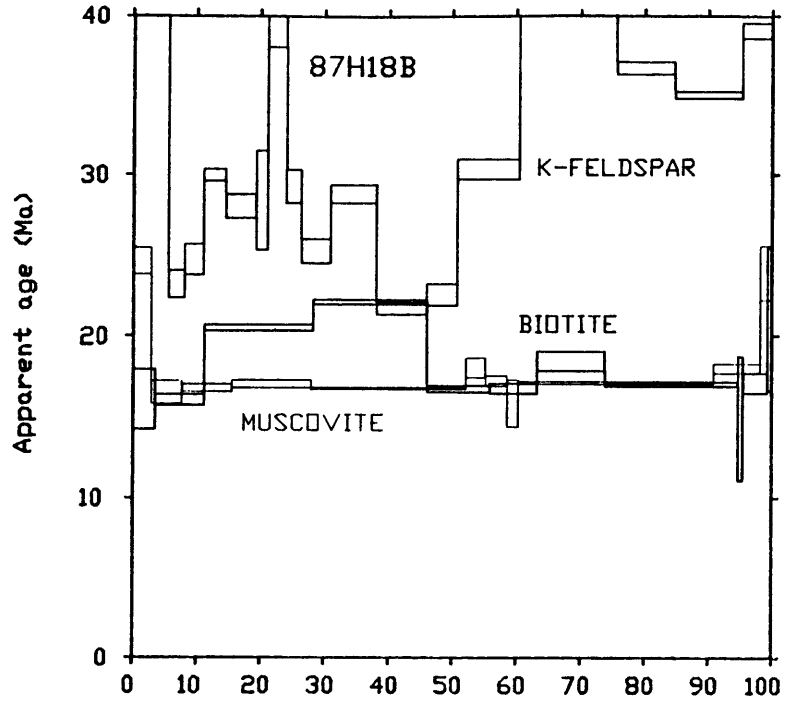

Figure 4.12 Cumulative $\%^{39}$ Ar released

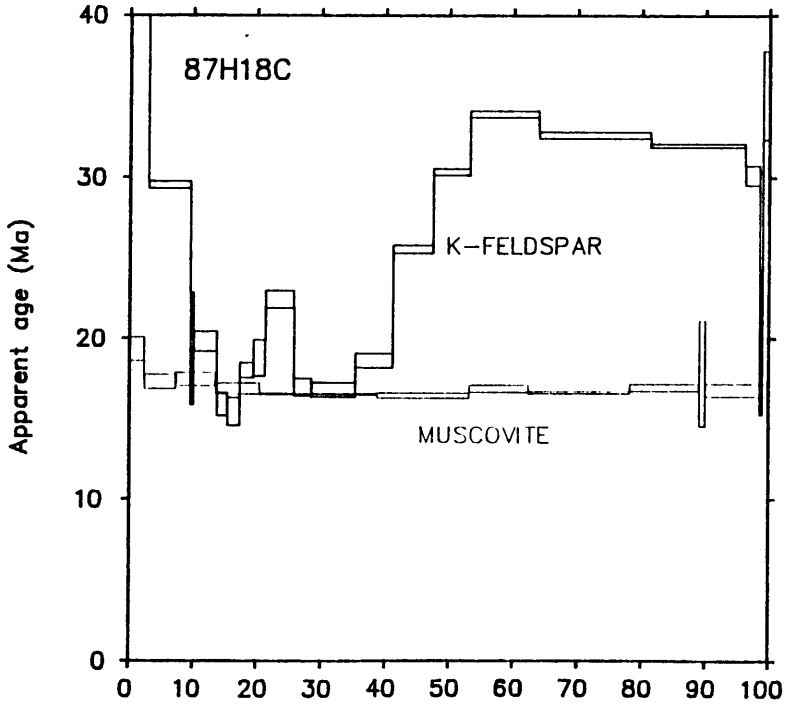

Figure 4.13 Cumulative $\%^{39}$ Ar released

Figure 4.14 Plot of age versus closure temperature for mineral separates from the MCT zone, Ghat, Na, and Ngozumba. Sample number and source of age (isochron or minimum from release spectra) are given in Table4.2.

FIGURE 4.14

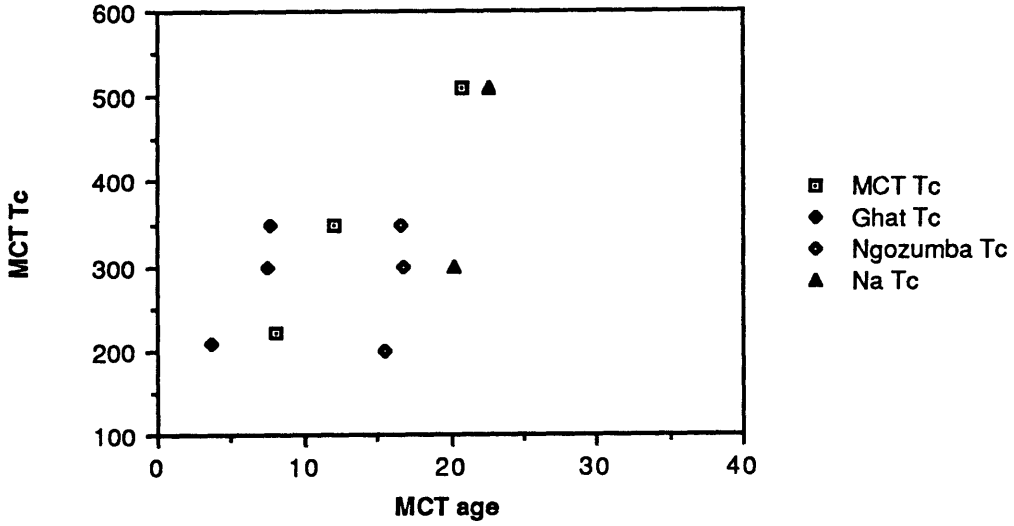
600
500
400
300
200
100
MCT Tc
0
10
20
30
40
MCT age
MCT Tc
Ghat Tc
Ngozumba Tc
Na Tc

muscovite and K-feldspar separates. Because the ages from Ngozumba include the leucogranite ages and show rapid cooling (Fig. 4.14) they have been interpreted to represent cooling immediately following leucogranitic intrusion. These ages are consistent with 17-19 Ma K-Ar biotite ages (Krummenacher et al., 1978) and 16-17 Ma Rb/Sr whole rock-mineral isochrons (Ferrara et al., 1983) for granite samples from the Everest area in Nepal, but are somewhat younger than the U-Pb monazite and zircon ages obtained by Copeland et al. (1988) for a granite sample from just north of Mt. Everest. Although field evidence suggests that the leucogranites in the Everest region represent multiple generations, the collective geochronologic data suggest that MCT metamorphism and deformation was generally coeval with leucogranitic intrusion in the upper Tibetan Slab.

The samples from Na were collected some distance (>200 m) from any observable intrusive rocks and permit us to examine the thermal history of the upper Tibetan Slab away from the direct influence of the leucogranites. Unfortunately, the hornblende age spectrum (Fig. 4.10) is complex. Its saddle shape is probably due to excess argon. Heating step #5 gives the minimum age of the saddle at 22.7±4.4 Ma. This age approaches the time of granitic intrusion suggested by the Ngozumba dates. One possible interpretation for this spectra is that steps 11-14 are the remains of a plateau at ~45 Ma that has been partially degassed at ~20 Ma and then overprinted by excess argon which is released in the first three steps. The 45 Ma age may correspond to tectonic events at the time of continental collision and the 20 Ma age could represent regional re-heating at the time of granitic intrusion. The 20.2±0.2 Ma biotite from Na (Fig. 4.10) is slightly older than the ~17 Ma micas from Ngozumba, and may confirm the significance of a ~20 Ma re-heating event.

Biotite and muscovite from a mylonitized pegmatite at Ghat recorded ~8 Ma ages. The significance of these young ages is either that they record the time of intrusion of this pegmatite or, more likely, that they record the age of the deformation. In either case the deformation is not younger than ~8 Ma. This deformation, which post-dates major MCT movement, indicates that there has been localized shear deformation within the Tibetan Slab and that this deformation is relatively young.

CONCLUSIONS

In the Everest region of eastern Nepal a $^{40}Ar/^{39}Ar$ hornblende age from the MCT zone suggests thrust movement and metamorphism at ~21 Ma. Mica ages from a leucogranite and adjacent gneiss within the Tibetan Slab support intrusion at about the same time. These data are consistent with the LeFort (1981) model of granite generation associated with movement on the MCT.

A middle Eocene hornblende age from the upper Tibetan Slab away from intrusives may be a remnant of early Barrovian metamorphism. The biotite age from this location is ~20 Ma, only slightly older than biotite ages from the leucogranites and adjacent gneisses and may result from regional heating due to leucogranitic intrusion.

The ~4-9 Ma ages from K-feldspars and micas from a shear zone in the lower Tibetan Slab indicate that relatively recent deformation has also been important in shaping the geochronologic history of this area.

ACKNOWLEDGMENTS

M.S.H. wishes to thank Sange Dorje Sherpa and Mountain Travel Nepal for logistical support during sample collection and Matt, Lynn and Ashley

Heizler for their endless hospitality during data collection. This research was financially supported by the American Alpine Club, The Explorer's Club, The Geological Society of America and U.S. National Science Foundation grant EAR-8414417 to K.V. Hodges.

APPENDIX 4.1

MCT ZONE

TEMP C	$^{40}Ar/^{39}Ar$	$^{37}Ar/^{39}Ar$	$^{36}Ar/^{39}Ar$ (E-3)	^{39}Ar (E-13 mol)	$\%^{39}Ar$ released	$^{40}Ar^*$ %	$^{40}Ar^*/^{39}Ar_K$	AGE ± 1 s.d. Ma
87H12B HORNBLENDE (J=0.007150;wt.=0.34809)								
700	962.7	3.614	439.2	0.216	0.884	86.5	835.5	3504 ± 26.1
800	138.1	5.160	114.1	0.193	1.67	75.5	105.1	1011 ± 18.7
900	48.26	8.615	14.57	0.358	3.14	91.6	44.80	501.3 ± 3.2
950	69.22	12.45	20.43	0.218	4.03	91.8	64.62	685.2 ± 7.2
990	49.75	12.98	12.33	0.297	5.24	93.7	47.42	526.8 ± 8.4
1020	30.17	14.00	5.467	1.21	10.2	97.3	29.78	348.2 ± 1.5
1040	24.30	13.53	3.594	1.27	15.4	98.8	24.36	289.7 ± 1.6
1050	22.21	13.21	4.929	1.75	22.5	97.0	21.82	261.5 ± 0.9
1070	19.51	13.03	3.935	2.21	31.6	98.0	19.38	234.1 ± 0.7
1090	17.38	12.78	5.475	0.719	34.5	94.6	16.74	204.0 ± 2.6
1130	17.38	12.95	4.040	3.80	50.0	97.7	17.18	209.0 ± 0.7
1170	25.25	13.04	3.603	4.76	69.5	99.0	25.28	299.7 ± 0.5
1200	26.32	12.74	3.577	3.53	84.0	98.9	26.33	311.2 ± 1.7
1450	15.01	9.460	4.691	3.91	100	94.5	14.32	175.8 ± 0.7

TEMP C	$^{40}Ar/^{39}Ar$	$^{37}Ar/^{39}Ar$	$^{36}Ar/^{39}Ar$ (E-3)	^{39}Ar (E-13 mol)	$\%^{39}Ar$ released	$^{40}Ar^*$ %	$^{40}Ar^*/^{39}Ar_K$	AGE ± 1 s.d. Ma
87H12C BIOTITE (J=.007164; wt.=.09817g)								
600	8.635	0.0528	19.91	4.09	2.68	31.3	2.709	34.7 ± 0.7
670	6.409	0.0403	5.052	10.6	9.59	75.9	4.872	61.9 ± 0.3
740	5.422	0.0125	1.658	23.8	25.2	90.0	4.886	62.1 ± 0.1
800	5.117	0.0092	1.409	14.7	34.8	90.8	4.654	59.2 ± 0.2
850	5.748	0.0124	2.513	8.70	40.5	86.1	4.960	63.0 ± 0.3
900	5.473	0.0157	1.242	8.90	46.3	92.3	5.060	64.2 ± 0.3
950	5.851	0.0126	2.090	11.4	53.7	88.5	5.188	65.8 ± 0.3
1030	5.285	0.0210	0.8432	24.2	69.6	94.3	4.991	63.4 ± 0.2
1100	4.726	0.0307	0.3446	26.8	87.1	96.8	4.579	58.2 ± 0.1
1200	4.041	0.0408	0.1965	18.8	99.4	97.3	3.939	50.2 ± 0.7
87	4.986	0.0501	5.450	0.850	100	65.3	3.332	42.6 ± 2.6

TEMP C	$^{40}Ar/^{39}Ar$	$^{37}Ar/^{39}Ar$	$^{36}Ar/^{39}Ar$ (E-3)	^{39}Ar (E-13 mol)	$\%^{39}Ar$ released	$^{40}Ar^*$ %	$^{40}Ar^*/^{39}Ar_K$	AGE ± 1 s.d. Ma
87H12C HORNBLENDE (J=.007019;wt.=0.35826g)								
700	267.5	4.632	603.1	0.274	0.624	33.4	89.85	882.2 ± 26.9
800	20.30	2.163	19.87	0.144	0.953	69.2	14.55	175.4 ± 7.7
900	10.88	5.093	4.706	0.431	1.93	88.0	9.822	120.3 ± 7.1
950	5.401	6.452	3.406	0.918	4.03	86.7	4.803	59.8 ± 2.1
990	2.650	7.415	1.958	2.87	10.6	93.9	2.535	31.8 ± 0.8
1020	2.730	7.299	2.918	3.13	17.7	83.6	2.322	29.2 ± 0.6
1040	2.462	6.973	2.375	7.81	35.5	88.0	2.191	27.5 ± 0.3
1050	2.145	6.809	1.772	4.49	45.7	93.6	2.041	25.7 ± 0.4
1060	2.434	6.742	3.638	0.918	47.8	69.3	1.772	22.3 ± 0.3
1080	2.124	6.676	2.719	1.36	50.9	78.2	1.729	21.8 ± 0.7
1100	2.049	6.991	2.555	1.61	54.5	81.2	1.724	21.7 ± 1.1
1130	1.915	6.912	2.195	6.61	69.6	87.1	1.691	21.3 ± 0.1
1170	2.125	6.865	1.924	9.44	91.1	92.2	1.979	24.9 ± 0.2
1200	2.167	6.695	2.258	2.27	96.2	85.9	1.910	24.0 ± 0.8
1450	3.747	6.812	3.513	1.65	100	81.9	3.134	39.3 ± 1.8
87H13E BIOTITE (J=.007179; WT.=.09723g								
600	12.69	0.0081	16.26	4.64	3.27	61.7	7.836	98.7 ± 0.5
670	8.639	0.0027	1.888	15.7	14.4	92.9	8.035	101.2 ± 0.2
740	8.333	0.0021	0.6293	23.0	30.6	97.2	8.100	102.0 ± 0.1
800	8.731	0.0020	1.729	10.3	37.8	93.5	8.173	102.9 ± 0.3
850	7.596	0.0023	0.8232	10.2	45.0	96.1	7.306	92.2 ± 0.2
900	8.001	0.0052	3.132	8.66	51.1	87.7	7.029	88.8 ± 0.3
950	9.795	0.0047	6.250	12.0	59.5	80.6	7.901	99.5 ± 0.2
1030	8.989	0.0029	2.622	34.2	83.6	90.8	8.168	102.8 ± 0.3
1100	8.295	0.0037	0.6204	21.1	98.5	97.2	8.065	101.5 ± 0.1
1200	7.068	0.0917	1.425	1.54	99.5	92.6	6.606	83.6 ± 0.8
1350	11.84	0.0604	5.611	0.647	100	84.5	10.14	126.7 ± 1.6
87H13F KSPAR (J=0.006927;wt.=0.146g)								
450	467.9	0.1630	218.1	0.460	0.152	86.2	403.5	2406 ± 9.9
500	132.3	0.0303	22.78	0.905	0.451	94.8	125.5	1129 ± 3.8
550	34.90	0.0108	2.405	2.42	1.25	97.7	34.15	383.0 ± 1.2
580	7.132	0.0048	0.6776	3.23	2.32	96.1	6.886	84.1 ± 0.6
610	6.923	0.0026	0.3661	4.27	3.73	97.4	6.768	82.7 ± 1.0
640	2.735	0.0041	0.3857	7.53	6.22	93.7	2.574	31.9 ± 0.3
670	1.131	0.0030	0.0894	10.8	9.79	92.8	1.058	13.2 ± 0.2
700	0.807	0.0026	0.0742	10.0	13.1	90.4	0.7384	9.2 ± 0.1
750	0.878	0.0030	0.3895	15.1	18.1	80.9	0.7157	8.9 ± 0.4
820	0.785	0.0034	0.0730	23.8	26.0	90.8	0.7163	8.9 ± 0.1
880	0.714	0.0038	0.0895	23.3	33.7	89.2	0.6407	8.0 ± 0.1
940	0.946	0.0031	0.0201	20.8	40.6	93.9	0.8929	11.1 ± 0.0
1000	2.391	0.0029	0.1764	15.5	45.7	95.6	2.292	28.4 ± 0.1
1050	5.098	0.0039	0.1557	13.0	50.0	98.0	5.005	61.5 ± 0.1
1100	8.513	0.0051	0.2013	13.1	54.3	98.7	8.407	102.1 ± 0.2
1200	19.37	0.0073	0.0993	41.3	68.0	99.6	19.29	226.3 ± 0.4
1250	23.31	0.0076	0.3207	61.0	88.1	99.4	23.17	268.5 ± 0.5
1300	19.97	0.0069	0.4293	26.7	97.0	99.1	19.80	231.8 ± 0.4
1350	21.56	0.0048	0.4480	6.11	99.0	99.1	21.38	249.2 ± 0.5
1550	23.62	0.0070	2.592	3.11	100	96.4	22.80	264.6 ± 0.9

TEMP C	$^{40}Ar/^{39}Ar$	$^{37}Ar/^{39}Ar$	$^{36}Ar/^{39}Ar$ (E-3)	^{39}Ar (E-13 mol)	$\%^{39}Ar$ released	$^{40}Ar^{*}$ %	$^{40}Ar^{*}/^{39}Ar_{K}$	AGE ± 1 s.d. Ma
87H13F BIOTITE (J=.007194;wt.=.10041g)								
600	10.50	0.0082	21.95	6.90	4.21	37.7	3.965	50.7 ± 0.5
670	7.335	0.0036	13.15	22.4	17.9	46.3	3.401	43.6 ± 0.2
740	3.377	0.0023	0.5370	34.4	38.8	93.8	3.171	40.7 ± 0.1
800	5.186	0.0032	6.457	23.1	53.0	62.3	3.232	41.5 ± 0.2
850	8.049	0.0085	16.28	8.26	58.0	39.6	3.192	41.0 ± 0.3
900	5.110	0.0094	7.578	7.93	62.8	55.1	2.824	36.3 ± 0.2
950	3.269	0.0061	0.5281	16.0	72.6	93.6	3.067	39.4 ± 0.2
1030	3.374	0.0036	0.7752	30.6	91.2	91.7	3.099	39.8 ± 0.2
1100	3.509	0.0070	1.423	6.46	95.2	86.3	3.041	39.0 ± 0.3
1200	3.345	0.0169	0.5262	7.02	99.5	93.6	3.144	40.3 ± 0.3
1350	5.494	0.4839	3.474	0.861	100	79.4	4.454	56.9 ± 1.9
87H13F MUSCOVITE (J=0.007163;wt.=0.09994g)								
650	19.36	0.0231	50.13	2.84	1.57	23.2	4.498	57.2 ± 1.1
720	2.567	0.0124	4.033	4.56	4.10	51.3	1.329	17.1 ± 1.0
780	3.116	0.0096	6.415	6.25	7.55	37.5	1.174	15.1 ± 0.6
820	3.110	0.0060	6.148	7.60	11.8	39.9	1.247	16.0 ± 0.7
860	2.794	0.0063	5.579	16.6	20.9	39.2	1.098	14.1 ± 0.2
900	2.036	0.0033	3.260	38.0	42.0	50.3	1.026	13.2 ± 0.1
970	1.260	0.0057	0.8884	39.8	64.0	75.3	0.9508	12.2 ± 0.1
1050	1.078	0.0072	0.3089	51.5	92.5	87.1	0.9400	12.1 ± 0.0
1120	1.246	0.0223	0.3526	9.25	97.6	87.2	1.096	14.1 ± 0.4
1200	1.867	0.2409	-.0585	3.72	99.7	97.9	1.854	23.8 ± 0.7
1350	8.501	2.765	5.704	0.577	100	80.2	6.969	87.9 ± 4.8

GHAT

TEMP C	$^{40}Ar/^{39}Ar$	$^{37}Ar/^{39}Ar$	$^{36}Ar/^{39}Ar$ (E-3)	^{39}Ar (E-13 mol)	$\%^{39}Ar$ released	$^{40}Ar^{*}$ %	$^{40}Ar^{*}/^{39}Ar_{K}$	AGE ± 1 s.d. Ma
87H21C K-SPAR (J=0.007028;wt.=0.15704g)								
450	173.6	0.0748	286.5	0.028	0.007	50.2	88.90	875.7 ± 67.1
500	17.46	0.0876	37.18	0.073	0.026	34.1	6.428	79.7 ± 51.0
550	2.136	0.0254	2.751	0.789	0.230	56.5	1.278	16.1 ± 3.1
600	1.083	0.0182	0.2150	1.93	0.728	85.8	0.9740	12.3 ± 2.0
650	0.771	0.0174	0.3844	4.48	1.89	77.1	0.6112	7.7 ± 0.5
680	0.494	0.0172	0.2540	4.36	3.01	72.2	0.3733	4.7 ± 0.6
710	0.409	0.0184	0.1592	8.38	5.17	75.1	0.3167	4.0 ± 0.2
750	0.396	0.0176	0.1120	27.5	12.3	79.3	0.3168	4.0 ± 0.2
800	0.375	0.0144	0.1405	36.8	21.8	76.1	0.2872	3.6 ± 0.1
850	0.407	0.0121	0.1352	18.1	26.4	77.8	0.3213	4.1 ± 0.1
900	0.424	0.0094	0.0958	53.9	40.3	82.0	0.3493	4.4 ± 0.0
950	0.480	0.0068	0.1082	42.0	51.2	83.2	0.4013	5.1 ± 0.0
1000	0.547	0.0061	0.1170	42.4	62.1	84.8	0.4655	5.9 ± 0.1
1050	0.694	0.0077	0.0899	27.0	69.1	89.0	0.6212	7.9 ± 0.1
1100	0.864	0.0112	0.1726	17.4	73.6	88.2	0.7666	9.7 ± 0.2
1150	0.945	0.0114	0.1813	22.0	79.2	89.0	0.8448	10.7 ± 0.1
1200	0.947	0.0066	0.2153	18.2	83.9	87.9	0.8367	10.6 ± 0.1
1250	0.923	0.0038	0.2743	45.8	95.8	85.9	0.7949	10.1 ± 0.0
1300	0.969	0.0072	0.6069	11.8	98.8	76.0	0.7430	9.4 ± 0.2
1350	1.697	0.0323	1.340	0.948	99.0	69.7	1.257	15.9 ± 1.2
1550	2.100	0.0264	3.770	3.75	100	44.2	0.9408	11.9 ± 0.7

TEMP C	$^{40}Ar/^{39}Ar$	$^{37}Ar/^{39}Ar$	$^{36}Ar/^{39}Ar$ (E-3)	^{39}Ar (E-13 mol)	$\%^{39}Ar$ released	$^{40}Ar^*$ %	$^{40}Ar^*/^{39}Ar_K$	AGE ± 1 s.d. Ma
87H21C BIOTITE (J=0.007196;wt.=0.09946g)								
600	7.927	0.0268	24.67	2.31	1.80	7.42	0.5910	7.7 ± 2.1
670	1.212	0.0082	1.660	11.6	10.8	55.3	0.6749	8.7 ± 0.4
740	0.832	0.0073	0.3208	30.8	34.9	82.7	0.6912	9.0 ± 0.2
800	0.789	0.0138	0.2084	19.7	50.2	85.8	0.6818	8.8 ± 0.1
850	1.037	0.0362	1.216	6.44	55.3	60.2	0.6334	8.2 ± 0.8
900	1.102	0.0499	1.716	4.22	58.6	48.9	0.5507	7.1 ± 0.7
950	1.590	0.0320	2.712	1.47	59.7	44.9	0.7439	9.6 ± 1.2
1030	1.122	0.0093	1.338	3.57	62.5	59.1	0.6798	8.8 ± 0.7
1100	0.815	0.0059	0.2541	20.6	78.5	84.6	0.6930	9.0 ± 0.1
1200	0.804	0.0234	0.1610	25.3	98.3	88.0	0.7108	9.2 ± 0.1
1350	1.123	0.0218	1.167	2.17	100	62.7	0.7330	9.5 ± 1.0
87H21D KSPAR (J=0.007006;wt.=0.15196g)								
450	272.1	0.1868	346.5	0.048	0.049	61.9	169.7	1413 ± 58.4
500	37.60	0.0187	34.30	0.588	0.650	72.6	27.42	317.0 ± 5.1
550	10.51	0.0272	3.916	0.842	1.51	87.6	9.304	113.9 ± 4.4
580	2.134	0.0087	0.3902	2.60	4.17	90.8	1.972	24.8 ± 0.7
610	1.403	0.0056	0.8971	3.93	8.19	76.4	1.091	13.7 ± 0.3
640	1.176	0.0061	0.8379	5.51	13.8	73.8	0.8816	11.1 ± 0.3
670	0.818	0.0068	0.8895	5.76	19.7	60.9	0.5086	6.4 ± 0.4
700	0.806	0.0048	0.0904	5.85	25.7	89.0	0.7329	9.2 ± 0.2
750	1.327	0.0061	0.9239	5.22	31.0	74.8	1.007	12.7 ± 0.3
820	1.378	0.0097	0.9568	8.48	39.7	75.5	1.049	13.2 ± 0.3
890	1.487	0.0114	1.161	7.98	47.9	73.2	1.098	13.8 ± 0.5
950	2.749	0.0101	1.454	5.82	53.8	82.2	2.273	28.5 ± 0.2
1020	3.355	0.0079	0.6714	21.4	75.7	92.6	3.110	38.9 ± 0.2
1100	6.005	0.0100	4.917	1.95	77.7	74.4	4.506	56.1 ± 1.3
1200	5.692	0.0126	2.237	16.2	94.3	87.5	4.985	61.9 ± 0.3
1250	5.125	0.0106	6.404	1.72	96.1	61.5	3.187	39.8 ± 1.6
1300	3.466	0.0206	2.607	1.83	98.0	75.3	2.650	33.2 ± 0.5
1350	4.435	0.0701	4.564	1.42	99.4	67.6	3.044	38.1 ± 1.8
1550	14.51	0.0475	32.47	0.553	100	33.2	4.876	60.6 ± 4.6
87H21D BIOTITE (J=0.007101;wt.=0.09584g)								
600	23.33	0.0318	75.06	3.97	3.52	4.75	1.110	14.2 ± 0.7
670	4.876	0.0086	13.78	19.9	21.2	15.5	0.7566	9.7 ± 0.3
740	2.177	0.0069	5.123	33.8	51.1	28.3	0.6163	7.9 ± 0.1
800	1.375	0.0135	2.595	18.5	67.5	40.7	0.5620	7.2 ± 0.1
850	1.244	0.0270	1.874	6.98	73.7	51.3	0.6454	8.2 ± 0.5
900	1.482	0.0231	2.751	6.28	79.2	41.6	0.6231	8.0 ± 0.5
950	3.739	0.0121	10.09	4.12	82.9	18.9	0.7112	9.1 ± 1.0
1030	2.676	0.0044	6.150	5.55	87.8	30.1	0.8115	10.4 ± 0.7
1100	1.369	0.0020	1.618	3.55	91.0	60.4	0.8444	10.8 ± 0.4
1200	0.802	0.0054	0.5275	8.65	98.6	73.7	0.5993	7.7 ± 0.3
1350	1.545	0.0152	2.306	1.55	100	50.8	0.8177	10.4 ± 1.8

TEMP C	$^{40}Ar/^{39}Ar$	$^{37}Ar/^{39}Ar$	$^{36}Ar/^{39}Ar$ (E-3)	^{39}Ar (E-13 mol)	$\%^{39}Ar$ released	$^{40}Ar^*$ %	$^{40}Ar^*/^{39}Ar_K$	AGE ± 1 s.d. Ma
87H21D MUSCOVITE (J=0.007132;wt.=0.04838g)								
650	31.43	0.0330	102.8	1.79	2.33	3.17	0.9967	12.8 ± 2.4
730	1.407	0.0256	2.673	3.62	7.05	39.8	0.5714	7.3 ± 1.0
800	1.297	0.0232	2.268	6.42	15.4	44.3	0.5809	7.5 ± 0.3
880	1.429	0.0104	2.615	22.9	45.2	42.6	0.6104	7.8 ± 0.2
950	0.902	0.0082	0.9666	15.6	65.5	62.7	0.5695	7.3 ± 0.3
1030	1.471	0.0045	1.793	1.52	67.5	58.2	0.8943	11.5 ± 1.5
1100	0.926	0.0066	0.7696	9.99	80.5	69.7	0.6521	8.4 ± 0.3
1200	0.829	0.0081	0.1785	14.3	99.1	87.3	0.7302	9.4 ± 0.1
1350	3.593	0.0706	1.509	0.689	100	83.1	3.105	39.5 ± 1.6

NA

87H19A HORNBLENDE (J=.007104;wt.=.35455)								
700	136.0	2.192	171.0	0.810	1.92	62.9	85.73	858.1 ± 4.7
800	35.06	0.8142	63.42	0.866	3.96	46.4	16.34	198.1 ± 3.2
900	6.784	1.576	8.184	1.13	6.65	64.4	4.429	55.9 ± 2.6
950	4.681	5.704	9.359	0.591	8.04	46.4	2.260	28.7 ± 2.4
990	4.467	7.846	10.73	0.578	9.41	38.2	1.784	22.7 ± 2.2
1020	4.163	7.515	7.492	1.08	12.0	56.5	2.419	30.7 ± 3.0
1040	4.143	7.204	6.451	1.12	14.6	63.1	2.687	34.1 ± 2.4
1060	3.372	6.952	3.643	2.13	19.7	79.3	2.728	34.6 ± 0.6
1080	3.493	6.516	4.607	1.58	23.4	70.9	2.533	32.2 ± 1.3
1100	3.861	6.447	4.763	2.14	28.5	72.6	2.852	36.2 ± 1.0
1130	4.551	6.548	3.979	7.54	46.3	82.5	3.786	47.9 ± 0.2
1160	4.332	6.218	3.574	14.6	80.7	84.0	3.663	46.3 ± 0.2
1200	4.009	6.384	3.527	6.44	96.0	83.1	3.363	42.6 ± 0.4
1450	4.420	6.963	4.220	1.70	100	80.2	3.611	45.7 ± 0.6
87H19B (J=.007182; wt.=.10536g)								
600	9.958	0.0178	28.21	1.14	0.576	15.7	1.578	20.3 ± 3.3
670	2.846	0.0056	4.462	9.97	5.62	51.8	1.481	19.1 ± 0.2
740	2.033	0.0026	1.363	31.9	21.8	77.8	1.583	20.4 ± 0.1
800	2.329	0.0029	2.237	17.3	30.5	69.4	1.622	20.9 ± 0.1
850	3.653	0.0059	6.810	7.90	34.5	43.5	1.594	20.5 ± 0.3
900	2.177	0.0065	2.066	6.06	37.6	69.3	1.520	19.6 ± 0.5
1030	1.644	0.0036	0.1966	57.1	66.5	93.5	1.539	19.8 ± 0.1
1100	1.657	0.0031	0.1081	40.6	87.0	95.1	1.578	20.3 ± 0.1
1200	1.717	0.0040	0.3478	25.3	99.8	91.1	1.567	20.2 ± 0.1
1350	17.86	2.092	%-1018.6940	0.391	100	%1760.9	319.5	2151 ± 699

NGOZUMBA

TEMP C	$^{40}Ar/^{39}Ar$	$^{37}Ar/^{39}Ar$	$^{36}Ar/^{39}Ar$ (E-3)	^{39}Ar (E-13 mol)	$\%^{39}Ar$ released	$^{40}Ar^*$ %	$^{40}Ar^*/^{39}Ar_K$	AGE ± 1 s.d. Ma
87H18A K-SPAR (J=0.007039;wt.=0.15232g)								
450	255.0	0.0408	223.3	0.760	0.340	74.1	189.0	1526 ± 13.1
500	17.81	0.0198	18.16	0.774	0.686	69.1	12.39	150.9 ± 3.7
550	6.376	0.0091	3.048	1.67	1.43	84.4	5.429	67.7 ± 1.8
580	2.605	0.0108	1.996	2.30	2.46	74.3	1.969	24.8 ± 0.7
610	3.180	0.0084	1.624	2.55	3.60	82.4	2.654	33.4 ± 0.8
640	2.513	0.0105	0.9040	4.02	5.40	86.7	2.199	27.7 ± 0.8
670	2.053	0.0149	0.1401	2.88	6.69	94.2	1.966	24.8 ± 0.6
700	1.854	0.0188	0.0828	2.94	8.01	94.5	1.784	22.5 ± 0.7
750	2.755	0.0246	1.076	2.74	9.23	85.7	2.392	30.1 ± 1.1
820	2.471	0.0433	0.7414	7.57	12.6	88.9	2.208	27.8 ± 0.6
880	1.668	0.0763	0.2563	8.00	16.2	92.3	1.551	19.6 ± 0.2
940	1.636	0.0740	0.3812	8.66	20.1	89.9	1.481	18.7 ± 0.4
1000	1.979	0.0474	0.7395	8.17	23.7	86.2	1.717	21.7 ± 0.5
1050	2.659	0.0205	0.6895	9.40	27.9	90.3	2.409	30.3 ± 0.3
1100	2.910	0.0133	0.6309	13.4	33.9	91.8	2.677	33.7 ± 0.1
1150	2.924	0.0184	0.6600	19.5	42.7	91.6	2.683	33.8 ± 0.1
1200	2.662	0.0100	0.4244	59.7	69.4	93.5	2.490	31.3 ± 0.1
1250	2.425	0.0051	0.4386	54.5	93.8	92.7	2.248	28.3 ± 0.1
1300	2.439	0.0092	1.008	2.94	95.1	84.7	2.094	26.4 ± 0.3
1350	2.709	0.0217	0.9897	1.25	95.7	85.0	2.371	29.9 ± 1.6
1550	2.155	0.0114	0.7352	9.71	100	87.4	1.892	23.9 ± 0.2
87H18a biotite (J=0.007188; wt.=0.09614 g)								
600	16.85	0.0302	54.69	3.62	3.04	3.80	0.6409	8.3 ± 2.9
670	3.064	0.0046	5.846	10.2	11.6	42.0	1.290	16.6 ± 0.3
740	1.976	0.0020	1.958	31.9	38.4	68.2	1.351	17.4 ± 0.1
800	1.979	0.0015	2.016	29.3	63.0	67.4	1.337	17.3 ± 0.1
850	2.251	0.0037	3.094	9.75	71.1	57.0	1.290	16.6 ± 0.3
900	2.264	0.0063	2.791	4.99	75.3	61.0	1.392	18.0 ± 0.6
950	1.924	0.0081	1.909	4.76	79.3	67.5	1.314	17.0 ± 0.3
1030	2.556	0.0039	3.768	15.3	92.1	54.5	1.396	18.0 ± 0.2
1100	3.670	0.0057	6.872	4.02	95.5	43.1	1.593	20.5 ± 1.1
1200	1.665	0.0095	1.070	5.18	99.8	77.3	1.302	16.8 ± 0.4
1350	1.935	0.0093	-.9375	0.186	100	87.6	2.166	27.9 ± 11.3
87H18B BIOTITE (J=0.007154;wt.=0.09772)								
600	33.53	0.0548	109.1	4.00	3.54	3.73	1.252	16.1 ± 1.9
670	5.591	0.0079	14.53	8.69	11.2	22.3	1.250	16.1 ± 0.3
720	8.523	0.0051	23.29	19.2	28.2	18.7	1.595	20.5 ± 0.2
780	9.578	0.0049	26.44	20.1	46.0	17.9	1.718	22.0 ± 0.2
840	2.510	0.0050	3.931	11.1	55.8	51.7	1.301	16.7 ± 0.2
900	3.145	0.0075	6.071	8.41	63.3	41.3	1.305	16.8 ± 0.3
1000	3.384	0.0141	6.435	11.9	73.8	42.3	1.437	18.4 ± 0.6
1070	1.746	0.0081	1.265	23.5	94.6	75.7	1.325	17.0 ± 0.1
1130	5.354	0.0216	14.04	0.922	95.4	21.2	1.159	14.9 ± 3.8
1200	1.665	0.0122	0.9784	4.41	99.3	78.8	1.330	17.1 ± 0.6
1350	3.789	0.0097	7.114	0.773	100	41.9	1.640	21.0 ± 4.4

TEMP C	$^{40}Ar/^{39}Ar$	$^{37}Ar/^{39}Ar$	$^{36}Ar/^{39}Ar$ (E-3)	^{39}Ar (E-13 mol)	$\%^{39}Ar$ released	$^{40}Ar^{*}$ %	$^{40}Ar^{*}/^{39}Ar_K$	AGE ± 1 s.d. Ma
87H18B K-SPAR (J=0.007049;wt.=0.15046g)								
450	180.7	0.0117	125.4	1.61	1.93	79.4	143.6	1262 ± 4.8
500	9.513	0.0058	4.586	3.12	5.66	85.0	8.111	100.3 ± 0.6
550	2.157	0.0056	0.9422	2.13	8.21	83.1	1.832	23.1 ± 0.8
580	2.298	0.0049	0.9993	2.47	11.2	83.6	1.956	24.7 ± 1.0
610	2.819	0.0039	1.347	2.89	14.6	83.2	2.374	29.9 ± 0.4
640	2.727	0.0046	1.560	3.97	19.4	80.6	2.220	28.0 ± 0.7
670	3.266	0.0121	3.285	1.46	21.1	67.5	2.249	28.4 ± 3.1
700	3.591	0.0054	1.454	2.49	24.1	85.8	3.115	39.2 ± 1.2
750	3.351	0.0121	3.346	1.95	26.4	68.1	2.317	29.2 ± 1.0
800	2.294	0.0142	0.8539	3.85	31.0	86.0	1.995	25.2 ± 0.7
870	2.478	0.0179	0.5208	5.97	38.1	91.3	2.279	28.7 ± 0.6
930	1.814	0.0164	0.1880	6.63	46.1	93.6	1.712	21.6 ± 0.4
980	2.080	0.0111	0.8573	3.98	50.8	84.6	1.781	22.5 ± 0.7
1030	2.836	0.0089	1.301	8.12	60.5	84.4	2.405	30.3 ± 0.6
1080	3.773	0.0064	1.596	6.04	67.7	85.9	3.255	40.9 ± 0.6
1130	5.630	0.0112	6.699	1.27	69.3	63.1	3.604	45.3 ± 2.2
1190	4.525	0.0062	4.185	5.37	75.7	71.3	3.242	40.8 ± 0.6
1250	3.454	0.0033	1.674	7.58	84.7	84.0	2.913	36.7 ± 0.4
1350	3.060	0.0051	0.7985	8.88	95.3	90.4	2.778	35.0 ± 0.2
1550	3.694	0.0083	1.843	3.91	100	83.4	3.102	39.0 ± 0.5
87H18B MUSCOVITE (J=0.007132;wt.=0.10003g)								
650	8.953	0.0101	23.62	3.79	2.97	21.5	1.928	24.6 ± 0.8
720	1.991	0.0087	2.217	6.16	7.81	64.2	1.289	16.5 ± 0.7
780	1.838	0.0064	1.628	10.0	15.7	70.9	1.311	16.8 ± 0.2
820	1.920	0.0039	1.838	15.8	28.0	69.0	1.330	17.0 ± 0.2
860	1.625	0.0023	0.9100	30.8	52.2	80.4	1.309	16.8 ± 0.1
900	2.081	0.0027	2.115	3.83	55.2	66.9	1.410	18.0 ± 0.6
970	1.749	0.0038	1.206	4.33	58.6	76.0	1.346	17.2 ± 0.3
1050	1.815	0.0043	1.800	2.29	60.4	66.5	1.237	15.8 ± 1.4
1120	1.480	0.0032	0.3244	38.8	90.9	90.2	1.337	17.1 ± 0.1
1200	1.602	0.0127	0.5072	9.35	98.2	87.2	1.406	18.0 ± 0.3
1350	2.505	0.0553	2.006	2.25	100	73.3	1.869	23.9 ± 1.7

TEMP C	$^{40}Ar/^{39}Ar$	$^{37}Ar/^{39}Ar$	$^{36}Ar/^{39}Ar$ (E-3)	^{39}Ar (E-13 mol)	$\%^{39}Ar$ released	$^{40}Ar^*$ %	$^{40}Ar^*/^{39}Ar_K$	AGE ± 1 s.d. Ma
87H18C KSPAR (J=0.007084;wt.=0.15261g)								
450	131.5	0.0164	145.2	1.39	1.02	67.3	88.53	878.3 ± 3.8
500	9.481	0.0085	5.721	2.70	3.01	81.4	7.744	96.4 ± 1.8
550	2.617	0.0061	0.8150	9.01	9.64	88.6	2.330	29.5 ± 0.2
580	2.275	0.0108	2.388	0.708	10.2	63.0	1.523	19.4 ± 3.5
610	1.873	0.0060	0.9096	4.98	13.8	82.3	1.558	19.8 ± 0.6
640	1.866	0.0096	1.925	2.25	15.5	65.5	1.250	15.9 ± 0.7
670	1.711	0.0076	1.524	2.66	17.4	69.4	1.214	15.4 ± 0.9
700	1.632	0.0069	0.5678	2.89	19.6	85.1	1.417	18.0 ± 0.5
750	1.999	0.0121	1.611	2.45	21.4	72.4	1.477	18.8 ± 1.1
820	1.933	0.0085	0.3996	6.06	25.8	90.7	1.769	22.5 ± 0.5
880	1.623	0.0121	0.8201	3.72	28.6	80.9	1.335	17.0 ± 0.5
940	1.481	0.0099	0.3844	9.35	35.5	88.6	1.321	16.8 ± 0.4
1000	1.679	0.0087	0.5636	7.88	41.3	86.7	1.466	18.6 ± 0.5
1060	2.264	0.0087	0.6864	8.52	47.5	88.5	2.015	25.6 ± 0.3
1120	2.674	0.0094	0.7820	7.78	53.2	89.2	2.397	30.4 ± 0.2
1180	2.998	0.0068	0.9215	14.6	64.0	89.2	2.680	33.9 ± 0.2
1210	2.854	0.0020	0.7776	23.7	81.4	90.2	2.577	32.6 ± 0.2
1240	2.758	0.0019	0.6231	20.2	96.2	91.5	2.527	32.0 ± 0.1
1280	2.773	0.0039	1.175	3.17	98.6	84.8	2.379	30.2 ± 0.6
1350	3.356	0.0204	5.935	0.671	99.1	44.4	1.557	19.8 ± 4.5
1550	3.668	0.0038	2.871	1.27	100	74.0	2.772	35.1 ± 2.7
87H18C MUSCOVITE (J=.007113;wt.=0.10238g)								
650	8.283	0.0194	22.75	3.81	2.43	18.2	1.514	19.3 ± 0.8
720	1.915	0.0117	1.743	7.77	7.37	70.2	1.354	17.3 ± 0.4
780	2.519	0.0071	3.739	9.88	13.7	54.1	1.367	17.5 ± 0.4
820	1.999	0.0057	2.137	10.8	20.5	65.8	1.321	16.9 ± 0.3
860	1.799	0.0029	1.548	28.6	38.7	71.8	1.295	16.5 ± 0.0
890	1.654	0.0026	1.074	22.7	53.2	77.8	1.290	16.5 ± 0.2
920	1.967	0.0028	2.015	14.6	62.5	67.1	1.325	16.9 ± 0.2
1000	1.553	0.0033	0.6772	24.9	78.3	83.9	1.306	16.7 ± 0.1
1050	1.596	0.0035	0.7438	17.0	89.1	83.0	1.330	17.0 ± 0.2
1100	2.711	0.0032	4.281	1.54	90.1	50.4	1.399	17.9 ± 3.3
1160	1.461	0.0089	0.3328	15.6	100	89.7	1.316	16.8 ± 0.4

Correction Factors:

	$(^{39}Ar/^{37}Ar)_{Ca}$ x 10^{-4}	$(^{36}Ar/^{37}Ar)_{Ca}$ x 10^{-4}	$(^{40}Ar/^{39}Ar)_K$ x 10^{-2}	system blank x 10^{-14} mol ^{40}Ar
all samples	8.05	2.26	4.7	1.0

REFERENCES

Acharyya, S.K., 1978, Stratigraphy and tectonic features of the eastern Himalaya: In: Tectonic Geology of the Himalaya, P.S. Saklani (ed.), 243-268.

Andrieux, J., Brunel, M., and Hamet, J., 1977, Metamorphism, granitization and relation with the Main Central Thrust in central Nepal, Rb/Sr age determination and discussion: In: Colloq. Int. 268, Ecologie et géologie de l'Himalaya, Paris, ed. Cent. Natl. Rech. Sci., Sci. de la Terre, 31-40.

Arita, K., 1983, Origin of the inverted metamorphism of the Lower Himalayas, central Nepal: Tectonophysics, 95, 43-60.

Berthé, D., Choukroune, P., and Jegouzo, P., 1979, Orthogneiss, mylonite and non coaxial deformation of granites: the example of the South Armorican Shear zone: J. of Struct. Geol., 1, 1, 31-42.

Bhattacharya, S.C., and Niyogi, D., 1971, Geologic evolution of the Krol Belt in Simla Hills, H.P.: Himal. Geol., 1, 178-212.

Bolhen, S.R., Wall, V.J., and Boettcher, A.L., 1983, Experimental investigations and geological applications of equilibria in the FeO-TiO_2-Al_2O_3-SiO_2-H_2O: American Mineralogist, 68, 1049-1058.

Bordet, P., 1961, Recherches géologiques dans l'Himalaya du Népal, région du Makalu: (ed.) Cent. Natl. Rech. Sci, Paris, 275p.

Bordet, P., 1973, On the position of the Himalayan Main Central Thrust within Nepal Himalaya: In: Seminar on Geodynamics Himal. région, Natl. Geophy. Res. Inst., Hyderabad, 148-155.

Bordet, P.,Colchen, M., Le Fort, P., and Pêcher, A., 1981, The geodynamic evolution of the Himalaya - ten years of research in central Nepal Himalaya and some other regions: In: Zagros, Hindu Kush, Himalaya Geodynamic Evolution, H.K. Gupta and F.M. Delany (eds.), Am. Geophys. Union, Washington DC, Geodyn. Ser., 3, 149-168.

Bortolami, G.C., Lombardo, B., and Polino, R., 1983, The granites of the upper Imja Khola (Everest region), eastern Nepal: In: Granites of Himalaya, Karakorum and Hindu-Kush, F.A. Shams (ed.), Punjab University, Lahore, 257-270.

Brewer, J., 1981, Thermal effects of thrust faulting: Earth Planet Sci. Lett., 56, 233-244.

Brunel, M., 1983, Etude pétro-structurale des chevauchements ductiles en Himalaya (Népal oriental et Himalaya du Nord-Ouest): Thèse Doct. Etat, Univ. Paris VII, 395p.

Brunel, M., and Andrieux, J., 1977, Déformations superposées et mécanismes associés au chevauchement central Himalayan "M.C.T.": In: Colloq. Int. 268, Ecologie et géologie de l'Himalaya, Paris, ed. Cent. Natl. Rech. Sci., Sci. de la Terre, 69-84.

Brunel, M., and Kienast, J.R., 1986, Étude pétro-structurale des chevauchements ductile himalayens sur la transversale de L'Everest-Makalu (Népal oriental). Can. J. Earth Sci., 23, 1117-1137.

Burchfiel, B.C., and Royden, L.H., 1985, North-south extension within the convergent Himalayan region: Geology, 13, 679-682.

Burg, J.P., Brunel, M., Gapais, D., Chen, G.M., and Liu, G.H., 1984, Deformation of leucogranites of the crystalline Main Central Thrust sheet in southern Tibet (China): J. of Struct. Geol., 6(5), 535-542.

Caby, R., Pêcher, A., and Le Fort, P., 1983, Le grand chevauchement central himalayan; nouvelles données sur le metamorphisme inverse à la base de la Dalle du Tibet: Rev. Géol. Dynamique Géogr. Phys., 24, 89-100.

Colchen, M., Le Fort, P., and Pêcher, A., 1986, Notice explicative de la carte géologique Annapurna-Manaslu-Ganesh (Himalaya du Népal) au 1/200.000è: (bilinque: français-english), ed. Cent. Natl. Rech. Sci., Paris, 136 p.

Copeland, P., Harrison, T.M., Parrish, R., Burchfiel, B.C., and Hodges, K.V., 1987, Constraints on the age of normal faulting, north face of Mt. Everest:

Implications for Oligo-Miocene uplift: EOS, 68(44), 1444.

Copeland, P., Parrish, R., and Harrison, T.M., (in press), Identification of inherited radiogenic Pb in monazite and its implications for U-Pb systematics: Nature.

Das, B.K., and Pande, I.C., 1973, Zones of progressive regional metamorphism in Dudatoli syncline, Garhwal Himalaya: Himal. Geol., 3, 190-208.

Deniel, C., Vidal, P., Fernandez, A., Le Fort, P., and Peucat, J., 1987, Isotopic study of the Manaslu granite (Himalaya, Nepal): inferences on the age and source of Himalayan leucogranites: Contrib. Mineral. Petrol., 96,78-92.

Dewey, J.F., and Bird, J.M., 1970, Mountain belts and the new Global tectonics: J. Geophys. Res., 75(14), 2625-2647.

Ferrara, G., Lombardo, B., and Tonarini, S., 1983, Rb/Sr geochronology of granites and gneisses from the Mount Everest region, Nepal Himalaya: Geol. Rdsch., 72(1), 119-136.

Ferry, J., and Spear, F.S., 1978, Experimental calibration of the partitioning of Fe and Mg between garnet and biotite: Contrib. Miner. Petrol., 66, 113-117.

France-Lanord, C., 1987, Chevauchement, métamorphisme et magmatisme en Himalaya du Népal Central étude isotopique H,C, O: PhD thesis, l'Institut National Polytechnique de Lorraine, France, 202p.

Fuchs, G., 1981, Outline of the geology of the Himalaya: Mitt. Osterr. geol. Ges., 74(75), 101-127.

Fuchs, G., and Frank, W., 1970, The geology of west Nepal between the rivers Kali Gandaki and Thulo Bheri: Jb. Geol., B-A, Wien, 18, 103 p.

Fuchs, G., and Sinha, A.K., 1978, The tectonics of the Garhwal-Kumaun Lesser Himalaya: Jb. Geol. B.-A., 121(2), 219-241.

Gansser, A., 1964, Geology of the Himalayas: Wiley Interscience, London, 289

p.

Gansser, A., 1966, The Indian Ocean and the Himalaya: a geologic interpretation: Eclog. Geol. Helv., 59, 832-848.

Gansser, A., 1981, The geodynamic history of the Himalaya: In: Zagros, Hindu Kush, Himalaya Geodynamic Evolution, H.K. Gupta and F.M. Delany (eds.), Am. Geophys. Union, Washington DC, Geodyn. Ser., 3, 111-121.

Graham, C.M., and England, P.C., 1976, Thermal regimes and regional metamorphism in the vicinity of overthrust faults: an example of shear heating and inverted metamorphic zonation from southern California: Earth Planet. Sci. Lett., 31, 142-152.

Hagen, T., 1969, Report on the geological survey of Nepal, Vol. 1: Denkschr. Schweiz. Naturf. Gesell., 86(1), 185p.

Harrison, T.M., and J.D. FitzGerald, 1986, Exsolution in hornblende and its consequences for $^{40}Ar/^{39}Ar$ age spectra and closure temperature: Geochim. Cosmochim. Acta, 50, 247-253.

Harrison, T.M., and McDougall, I., 1982, The thermal significance of potassium feldspar K-Ar ages inferred from $^{40}Ar/^{39}Ar$ age spectrum results: Geochim. Cosmochim. Acta, 46, 1811-1820.

Hashimoto, S., Ohta, Y. and Akiba, C. (eds.), 1973, Geology of the Nepal Himalaya: Hokkaido University, Sapporo, 286 p.

Heim, A., and Gansser, A., 1939, Central Himalaya. Geological observations of the Swiss expedition 1936: Mem. Soc. Helv. Sci. Nat., Zürich, 73(1), 245 p.

Heizler, M., and Harrison, T.M., in press, Multiple trapped argon isotope components revealed by $^{40}Ar/^{39}Ar$ isochron analysis: Geochim. Cosmochim. Acta.

Herren, E., 1987, Zanskar shear zone: northeast-southwest extension within the Higher Himalayas (Ladakh, India): Geology, 15, 409-413.

Hodges, K.V., and Crowley, P.D., 1985, Error estimation and empirical geothermobarometry for pelitic systems: American Mineralogist, 70, 702-709.

Hodges, K.V., and McKenna, L.W., 1987, Realistic propagation of uncertainties in geologic thermobarometry: American Mineralogist, 72, 673-682.

Hodges, K.V. , and Royden, L.H., 1984, Geothermometry and geobarometry of retrograded metamorphic rocks: and indication of the uplift trajectory of a portion of the northern Scandinavian Caledonides: J. Geophys. Res., 89, 7077-7090.

Hodges, K.V., and D. S. Silverberg, (in press), Thermal evolution of the greater Himalaya, Garhwal, India: Tectonics.

Hodges, K.V., Hubbard, M.S., and Silverberg, D.S., (in press), Metamorphic constraints on the thermal evolution of the central Himalayan orogen: Phil. Trans. Roy. Soc. London.

Honegger, K., 1983, Strukturen und Metamorphose im Zanskar Kristallin (Ladakh - Kashmir, Indien): Ph. D. Thesis, ETH, Zürich, No. 7456, 117p.

Hubbard, M., 1986, Thermal structure of the Main Central Thrust zone, eastern Nepal, from mineral rim thermobarometry (abstract): Geological Society of America Abstracts with Programs, 18, 642.

Hubbard, M., (in press), Thermobarometric constraints on the thermal history of the Main Central Thrust Zone and Tibetan Slab, Eastern Nepal: J. Metam. Geol.

Hubbard, M., Harrison, T.M., and Hodges, K., 1988, $^{40}Ar/^{39}Ar$ timing constraints for deformation along the Main Central Thrust and leucogranitic intrusion, eastern Nepal Himalaya (abstract): EOS, 69(16), 520.

Ishida, T., 1969, Petrography and structure of the area between the Dudh Kosi and Tamba Kosi, East Nepal: J. Geol. Soc. Japan, 75,.115-125.

Jaros J., and Kalvoda, J., 1976, Geological results of the Czechoslovak Makalu Expedition: Himal. Geol. 6, 176-196.

Krummenacher, D., 1956a, Contribution à l'étude pétrographique de l'Himalaya du Népal. 1: Sur quelques roches de la région de Namche Bazar: Arch. Sci., Genève, 9(1), 111-114.

Krummenacher, D., 1956b, Contribution à l'étude géologique et pétrographique de l'Himalaya du Népal. 2: Sur les roches du Bassin supérieur de la Dudh Kosi, de l'Imja Khola et de la Bhote Kosi: Arch. Sci., Genève, 9(3),263-281.

Krummenacher, D., Bassett, A.M, Kingery, F.A., and Layne, H.F., 1978, Metamorphism and K-Ar age determinations in eastern Nepal: In: Tectonic Geology of the Himalaya, P.S. Saklani (ed.), Today and Tomorrow's print. and publ., New Delhi, 151-166.

La Tour, T.E., 1987, Geochemical model for the symplectic formation of myrmekite during amphibolite-grade progressive mylonitization of granite: Geological Society of America Abstracts with Programs, 19(7), 741.

Le Fort, P., 1975, Himalayas: the collided range. Present knowledge of the continental arc: American Journal of Science, 275-A, 1-44.

Le Fort, P., 1981, Manaslu leucogranite: a collision signature of the Himalaya, A model for its genesis and emplacement: J. Geophys. Res., 86, B11, 10545-10568.

Le Fort, P., Pêcher, A., and Upreti, B.N., 1986, A section through the Tibetan Slab in central Nepal (Kali Gandaki Valley): mineral chemistry and thermobarometry of the Main Central Thrust zone: In: Sciences de la Terre, P. Le Fort, M. Colchen, and C. Montenat (eds), Memoire 47, 211-228.

Le Fort, P., Cuney, M., Deniel, C., France-Lanord, C., Sheppard, S.M.F., Upreti, B.N., and Vidal, P., 1987, Crystal generation of the Himalayan leucogranites: Tectonophysics, 134, 39-57.

Lombard, A., 1953, Les grandes lignes de la Géologie du Népal oriental: Bull. Soc. belge Géol. Pal. Hydr., 41(3), 260-264.

Lombard, A., 1958, Un itinéraire géologique dans l'Est du Népal (Massif du Mont Everest): Mém. Soc. Helv. Sci. nat., 82, 107p.

Maluski, H., Matte, P., and Brunel, M., 1988, Argon 39 - Argon 40 dating of metamorphic and plutonic events in the North and High Himalaya belts (southern Tibet - China): Tectonics, 7(2), 299-326.

Mc Dougall, I., and Harrison, T.M., 1988, Geochronology and thermochronology by the $^{40}Ar/^{39}Ar$ method: Oxford, New York, 208p.

Maruo, Y. and Kizaki, K., 1981, Structure and metamorphis m in eastern Nepal: In: Metamorphic Tectonites of the Himalaya, P.S. Saklani (ed.), Today and Tomorrow's Printers and Publ., New Delhi, 175-230.

Maruo, Y. and Kizaki, K., 1983, Thermal structure in the nappes of the eastern Nepal Himalayas: In: Granites of Himalaya, Karakorum and Hindu-Kush, F.A. Shams (ed.), Punjab University, Lahore, Pakistan, 271-286.

Maruo, Y., Pradhan, B.M., and Kizaki, K., 1979, Geology of eastern Nepal: between Dudh Kosi and Arun: Bull. College of Science, Univ. Ryukyus, 28, 155-191.

Mattauer, M., 1975, Sur le mécanisme de formation de la schistosité dans l'Himalaya: Earth Planet. Sci. Lett., 28, 144-154.

Medlicott, H.B., 1864, On the geological structure and relations of the southern portion of the Himalayan ranges between the rivers Ganges and the Ravee: Mem. geol. Surv. India, 3(2), 1-212.

Molnar, P., 1984, Structure and tectonics of the Himalaya: constraints and implications of geophysical data: Annu. Rev. Earth Planet. Sci., 12, 489-518.

Molnar, P., Chen, W.P., and Padovani, E., 1983, Calculated temperatures in overthrust terrains and possible combinations of heat sources responsible for the Tertiary granites in the Greater Himalaya: J. Geophys. Res., 88, 6415-6429.

Newton, R.C., and Haselton, H.T., 1981, Thermodynamics of the garnet-

plagiocase-Al_2SiO_5-quartz geobarometer: In: Thermodynamics of Minerals and Melts, R.C. Newton, A. Navrotsky, and B.J. Wood, (eds.), Springer-Verlag, New York, 131-147.

Nicolas, A., Girardeau, J., Marcoux, J., Dupre, B., Wang, X., et al., 1981, The Xigaze ophiolite (Tibet): a peculiar oceanic lithosphere: Nature, 294, 414-417.

Norton, I.O., and Sclater, J.G., 1979, A model for the evolution of the Indian Ocean and the breakup of Gondwanaland: J. Geophys. Res., 84(12), 6803-6830.

Oldham, R.D., 1883, Notes on a traverse between Almora and Mussooree in October 1882: Geological Survey of India Reconnaissance, 16(3),162-164.

Palivcova, M., Kalvoda, and J., Minarik, L., 1982, Petrology of the Makalu Massif, Nepal Himalayas: Rozpravy Ceskoslovenske Akademie Ved, Praha, 92(2), 3-101.

Pêcher, A., 1977, Geology of the Nepal Himalaya: deformation and petrography in the Main Central Thrust zone: In: Colloq. Int. 268, Ecologie et géologie de l'Himalaya, Paris, ed. Cent. Natl. Rech. Sci., Sci. de la Terre, 301-318.

Royden, L.H., and Burchfiel, B.C., 1987, Thin-skinned N-S extension within the convergent Himalayan region: gravitational collapse of a Miocene topographic front: In: Continental Extensional Tectonics, M.P. Coward, J.F. Dewey, and P.L. Hancock, (eds.), Geol Soc. Spec. Publ., 28, 611-619.

Schärer, U., 1984, The effect of initial ^{230}Th disequilibrium an young U-Pb ages: the Makalu case, Himalaya: Earth Planet. Sci. Lett., 67, 191-204.

Schärer, U., Xu, R.H., and Allègre, C.J., 1986, U-(Th)-Pb systematics and ages of Himalayan leucogranites, South Tibet: Earth Planet. Sci. Lett. 77, 35-48.

Schelling, D., 1987, The geology of the Rolwaling-Lapchi Kang Himalayas,

east-central Nepal: preliminary findings: J. of Nepal Geol. Soc., 4, 1&2, 1-19.

Scholz, C.H., 1980, Shear heating and the state of stress on faults: J. Geophys. Res., 85, 6174-6184.

Searle, M., 1986, Structural evolution and sequence of thrusting in the High Himalayan, Tibetan-Tethys and Indus suture zones of Zanskar and Ladakh, western Himalaya: J. Struc. Geol., 8(8), 923-936.

Sengör, A.M.C., 1984, The Cimmeridge orogenic system and the tectonics of Eurasia: Geol., Soc. of America, spec. paper, 195, 82p.

Shah, S.K., and Sinha, A.K., 1974, Stratigraphy and tectonics of the "Tethyan" zone in a part of western Kumaun Himalaya: Himal. Geol., 4, 1-27.

Silverberg, D.S., and Hodges, K.V., 1986, Pressure-temperature constraints on metamorphism and tectonism in the Tibetan Slab, Kumaun Himalaya, north India: Geological Society of America Abstracts with Programs, 18, 750.

Sinha, A.K., 1981, Geology and tectonics of the Himalayan region of Ladakh, Himachal, Garwhal-Kumaun and Arunachal Pradish: a review: In: Zagros, Hindu Kush, Himalaya Geodynamic Evolution, H.K. Gupta and F.M. Delany (eds.), Am. Geophys. Union, Washington DC, Geodyn. Ser., 3, 122-148.

Spear, F.S., and Selverstone, J., 1983, Quantitative P-T paths from zoned minerals: theory and tectonic applications: Contrib. Miner. Petrol., 83, 348-357.

Spry, P., 1969, Metamorphic Textures: Pergamon Press, Oxford, 350 p.

St. Onge, M.R., 1987, Zoned poikoloblastic garnets: P-T paths and synmetamorphic uplift through 30km of structural depth, Wopmay Orogen, Canada: J. Petrol., 28, 1-27.

Stöcklin, J., 1980, Geology of Nepal and its regional frame: J. Geol. Soc. London, 137, 1-34.

Thakur, V.C., and Choudhury, B.K., 1983, Deformation, metamorphism and tectonic relations of Central Crystallines and Main Central Thrust in eastern Kumaun Himalaya: In: Himalayan Shears, P.S. Saklani (ed.), Today and Tomorrow's Printers and Publ., 45-57.

Valdiya, K.S., 1980, The two intracrustal boundary thrusts of the Himalaya: Tectonophysics, 66, 323-348.

Valdiya, K.S., 1981, Tectonics of the central sector of the Himalaya: In: Zagros, Hindu Kush, Himalaya Geodynamic Evolution, H.K. Gupta and F.M. Delany (eds.), Am. Geophys. Union, Washington DC, Geodyn. Ser., 3, 87-110.

Vidal, P., 1978, Rb-Sr systematics in granite from Central Nepal (Manaslu): significance of the Oligocene age and high $^{87}Sr/^{86}Sr$ ratio in Himalayan orogeny: comment. Geology, 6, 196.

Vidal, Ph., Bernhard-Griffiths, J., Cocheril, A., Le Fort, P., Peucat, J.J., and Sheppard, S.M.F., 1984, Geochemical comparison between Himalayan and Hercynian leucogranites: Phys. Earth Planet. Inter., 35 (spec. Issue), 179-190.

BIOGRAPHICAL INFORMATION

Year	Relevant Event	Location
1958	born	Evanston, IL
1961	got small rock stuck in nose, taken to doctor, reprimanded	Northbrook, IL
1961	family outing to collect garnets from schist, but we were unable to calculate pressures and temperatures	Black Hills, S.D.
1964	geode hunt with family, smashed thumb with hammer	Southern Illinois
1966-1968	extensive studies in experimental sedimentology in stream table at father's office and sandbox at home - study ended when hose was left on and sand was all washed from the box (results unpublished)	Northbrook, IL
1972	8th grade GPA sufficient to skip Earth Science class in 9th grade (school counselor advised that Earth Science is for dummies and one is better off to move on to Chemistry, Biology, and Physics)	Northbrook, IL
1974	transferred secondary school systems and took Earth Science with a minor in skiing	Aspen, CO
1977	decided geology was not practical, enrolled in Chemistry and Biology	Middlebury, VT
1978	declared geology as a major, who cares about practicality, geologists sure beat pre-med students	Boulder, CO
1981	in an effort to work for a living, took a job as a mud-logger	WY, UT, CO

1982	started grad school, met an enthusiastic professor who swore that metamorphic rocks are the greatest things and that geothermobarometry can solve the problems of the world	Laramie, WY
1984	was gullible enough to follow this enthusiastic man across the country to a place where life is hectic and housing is expensive	Cambridge, MA
1985-87	early exposure to the word "boondoggle" resulted in three trips to Nepal	Solu-Khumbu
1988-?	real life? I hope to continue geology while keeping rocks out of my nose and my thumb away from the hammer head	The World

"Thanks for waiting for me, PJ, but I still can't play. I've decided to go for a ~~Ph.D.~~ post-doc.

PLATE 1

GEOLOGY OF AN AREA SURROUNDING THE DUDH KOSI, HINKU, AND HONGU DRAINAGES, EASTERN NEPAL

M.S. Hubbard 1988

TIBETAN SLAB
- bs — biotite schist
- lg — leucogranite
- gg — granitic gneiss
- ag — augen gneiss
- cs — calc silicate rock
- bg — biotite gneiss

MCT ZONE
- bg — biotite schist
- m — marble
- ag — augen gneiss
- qmq — quartzite/micaceous quartzite
- m — marble
- gms2 — garnet mica schist 2
- gs — graphitic schist
- ps — psammite
- m — marble
- amp — amphibolite
- gms1 — garnet mica schist 1
- pag — Phaplu augen gneiss

LESSER HIMALAYA
- ok — Okhaldhunga Unit (chlorite schist/quartzite)

- lithologic contact (dashed where inferred)
- approximate boundary of MCT zone
- minor shear zone
- 30 — dominant schistosity
- 10 — lineation
- antiform (dashed where inferred)
- synform (dashed where inferred)

Khumbu Himal, Shorong/Hinku, and Dudh Kosi maps from E. Schneider series used as topographic base.

N

2 km

LOCATION

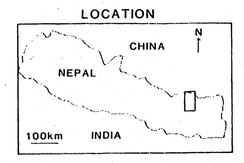

PLATE 2: CROSS SECTIONS FROM THE EVEREST REGION, EASTERN NEPAL

no vertical exaggeration

vertical scale: meters above sea level

M.S. Hubbard 1988

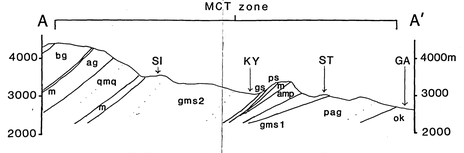

isograds: SI-sillimanite, KY-kyanite, ST-staurolite, GA-garnet